ENHANCEMENT OF ULTRAVIOLET RESISTANCE OF POLYASPARTICS

A Thesis Submitted to
the Graduate School of
İzmir Institute of Technology
in Partial Fulfillment of the Requirements for the Degree of

Master of Science

in Polymer Science and Engineering

by
Bahar DEMİRTAŞ KARABACAK

July 2024
İZMİR

We approve the thesis of **Bahar DEMİRTAŞ KARABACAK**

Examining committee members:

Prof. Dr. Mustafa Muammer Demir
Department of Material Science and Engineering, İzmir Institute of Technology

Assoc. Prof. Seda Kehr
Department of Chemistry, İzmir Institute of Technology

Assoc. Prof. Aylin Ziylan
Department of Metallurgy and Materials Engineering, Dokuz Eylül University

08 July 2024

Prof. Dr. Mustafa Muammer Demir
Supervisor, Department of Material Science and Engineering,

Prof. Dr. Ekrem Özdemir
Head of the Department of Polymer Science and Engineering

Prof. Dr. Mehtap EANES
Dean of the Graduate School

ACKNOWLEDGEMENTS

Firstly, I would like to express my deep gratitude to my advisor, Prof. Dr. Mustafa M. DEMİR, for his expert guidance, valuable recommendations, motivation, friendliness, and patience. Additionally, I would like to express my gratitude to Dr. Merve DEMİRKURT AKBAL for her invaluable assistance concerning my thesis.

Also, I would like to thank all the members of DEMİR Lab for their lovely companionship and support.

I am thankful to my lovely husband Soner KARABACAK for his precious support and inspiration all the time. I am grateful to my lovely family Nevin DEMİRTAŞ, Ş. Ahmet DEMİRTAŞ and Yağmur DEMİRTAŞ for their support, being with me and cherish me all the time.

ABSTRACT

ENHANCEMENT OF ULTRAVIOLET RESISTANCE OF POLYASPARTICS

The degradation of polyaspartic ester (PAE) resins under ultraviolet (UV) exposure poses significant challenges for their long-term use in outdoor applications. This study investigates the enhancement of UV resistance of PAE resins through the incorporation of metal oxide particles as UV absorbers. The research aims to determine the efficacy of metal oxide particles in improving the UV protective properties of PAE resins. Experimental results demonstrate that the UV absorption values of resin dispersions containing metal oxide particles significantly increased compared to pure PAE resin. This enhancement may be attributed to the metal oxides' ability to absorb and scatter UV light, thereby reducing the transmission of harmful UV rays through the resin matrix. Various concentrations of metal oxide particles were tested, and the findings underscore the importance of achieving a homogeneous dispersion within the resin for optimal UV protection. The study concludes that the incorporation of metal oxide particles into PAE resins can remarkably enhance the UV resistance of PAE. The improved UV absorption characteristics make these modified resins more suitable for applications exposed to prolonged UV radiation. This research provides a foundation for further exploration into optimizing particle concentrations and dispersion techniques to maximize the UV resistance of polyaspartic ester resins while maintaining their transparency over visible region of the optical spectrum.

ÖZET

POLİASPARTİKLERİN ULTRAVİYOLE DİRENCİNİN ARTTIRILMASI

Poliaspartik ester (PAE) reçinelerinin ultraviyole (UV) ışınlarına maruz kalması, açık hava uygulamalarında uzun ömürlü kullanımlarında önemli zorluklar yaratmaktadır. Bu çalışma, UV soğurucu olarak metal oksit tanecikleri eklenerek PAE reçinelerinin UV direncinin artırılmasını araştırmaktadır. Araştırmanın amacı, metal oksit taneciklerin PAE reçinelerinin UV koruma özelliklerini iyileştirmedeki etkinliğini belirlemektir. Deneysel sonuçlar, metal oksit tanecikleri içeren reçine dispersiyonlarının UV absorpsiyon değerlerinin saf PAE reçinesine kıyasla önemli ölçüde arttığını göstermektedir. Bu iyileşme, metal oksitlerin UV ışığını absorbe etme ve saçma yeteneklerine bağlanmaktadır; böylece zararlı UV ışınlarının reçine matrisi içinden geçişi azalır. Çeşitli metal oksit tanecik konsantrasyonları test edilmiş ve optimal UV koruması için reçine içinde homojen bir dağılımın önemini vurgulamaktadır. Çalışma, metal oksit taneciklerinin PAE reçinelerine eklenmesinin, reçinelerin UV direncini etkili bir şekilde artırdığını sonucuna varmıştır. Gelişmiş UV absorpsiyon özellikleri, bu modifiye edilmiş reçineleri, uzun süreli UV ışınımına maruz kalan uygulamalar için daha uygun hale getirmektedir. Bu araştırma, poliaspartik ester reçinelerinin UV direncini maksimize etmek ve görünüt bölgede saydamlığını korumak için tanecik derişimini ve dispersiyon tekniklerinin optimize edilmesine yönelik çalışmalara temel oluşturmaktadır.

TABLE OF CONTENTS

LIST OF FIGURES

Figure **Page**

Figure **Page**

Figure **Page**

Figure **Page**

LIST OF TABLES

Table **Page**

CHAPTER 1

INTRODUCTION

1.1. General Information about Paints

Paint is a liquid substance applied to surfaces to add color, protection, or decoration. It typically consists of a pigment (the colorant), a binder (which holds the pigment particles together and adheres them to the surface), a solvent (which keeps the paint in a liquid form until it's applied), and additives (which can modify the paint's properties like drying time, durability, or sheen). There are various types of paint, including water-based (like acrylic or latex), oil-based, enamel, and others, each with its own characteristics and suitable applications. The properties of paint can vary depending on its composition, intended use, and the specific requirements of the application.[1] However, some common properties of paint include:

- Opacity/Transparency: Paint can be opaque or transparent/translucent, allowing some of the underlying surface to show through.[2]
- Sheen: Paint can have different levels of glossiness or sheen, ranging from high-gloss to matte. The choice of sheen can affect the appearance and durability of the painted surface.[3]
- Color: Paint provides color to surfaces, allowing for decoration and aesthetic enhancement.[3]
- Coverage: Paint should have adequate coverage, meaning it can effectively cover the surface with the desired color and finish in a reasonable number of coats.[3]
- Adhesion: Good paint should adhere well to the surface it is applied to, forming a strong bond that resists peeling, chipping, or flaking.[3,4]
- Drying Time: The time it takes paint to dry, and cure can vary depending on its composition. Faster drying times may be desirable for efficiency, while slower drying times can allow for better leveling and smoother finishes.

- Durability: Paint should withstand environmental factors like sunlight, moisture, heat, and abrasion, remaining intact and retaining its color and finish over time.[3–6]
- Flexibility: Some paints need to be flexible to accommodate expansion and contraction of the substrate without cracking or peeling. This is especially important for surfaces like wood or metal that may experience dimensional changes due to temperature or moisture.
- Cleanability: Paint should be easy to clean, especially for surfaces that may be exposed to dirt, grease, or other contaminants.
- Toxicity and Environmental Impact: Depending on its ingredients, paint can have varying levels of toxicity and environmental impact. Water-based paints, for example, are generally less toxic and have lower VOC (volatile organic compound) emissions compared to oil-based paints.[7,8]

These properties can be adjusted and optimized by formulating the paint with different types and amounts of pigments, binders, solvents, and additives. Paint typically consists of several key components:

- Binders: They are also known as resins or polymers that hold the pigment particles together and adhere them to the surface after the paint has dried. Coatings and paints are generally categorized according to major type of resins it contains. They can be acrylic, alkyd, epoxy, polyester, silicone, etc.[3–5] Binders are polymer components of coatings. They supply a continuous film that can be thought of as the backbone of the coating. These polymers hold all the ingredients together and supply most of the characteristic properties of coatings like adhesion to substrate, chemical resistance, elasticity, etc. In addition, coating's mechanical and thermal properties, chemical reactivities, gloss, durability in environmental stress depends on the polymer/resin.[1]
- Pigments: Pigments are insoluble materials that are generally used to provide color and opacity to coating. They also supply gloss and rheology control and different functions like corrosion inhibition. There are two main types of pigments that are inorganic (metal oxides or combinations of oxides) and organic (phthalocyanurates or quinacridones).[1] The selection of the pigment can be

complicated. In order to give a coating desired properties, the pH stability, UV resistance, particle size (generally 0.01 to 100 micrometers) and oil absorption of the pigments should be considered. If pigment selection is made without taking into account environmental factors (like acid rain, sunlight or heat) that the coating will experience throughout its service life, the results may be the degradation and change of its color.[1]

- Fillers: They are chemically inert materials. They are used to supply hardness, mar resistance, abrasion resistance, strength, non-skid properties or gloss control. In addition to all these, the morphology of the used fillers may supply different properties. For example, flake type aluminum or mica supply a horizontal barrier against atmosphere. Also, flexibility may be supplied by using fibers in the paint system.[6]
- Solvents: Solvents are liquids that keep the paint in a liquid form until it is applied to the surface. They help to dissolve or disperse the pigments and binders evenly, making the paint easier to apply.[7] Solvents evaporate as the paint dries, leaving behind a solid film of pigment and binder.[3,5] Water is the primary solvent in water-based paints, while oil-based paints use organic solvents such as mineral spirits or turpentine. In addition, the synthesis of resins (polymers), as a backbone of the coating structure, is generally achieved in organic solvents. The formulators chose the proper solvent(s) by considering the compatibility with especially resins, boiling point, evaporation rate, reactivity and toxicity. While the compatibility is very important, the others are also important to prevent paint defects like pinhole, wrinkling, etc. With the Volatile Organic Compound (VOC) regulations the amount of solvent per gallon of paint has been important. Local laws determine the ranges.[3,5,7] Also, the flash point, a safety and shipping concern, determined mainly by solvent compositions in paint.[1]

The types of solvents that are used in paint formulation can be classified by their molecular structure. In a general way, these are aliphatic and aromatic hydrocarbons, alcohols, esters, ethers, ketones. The most widely used solvents in formulations are toluene, xylene, mineral spirits, methyl ethyl ketone and ethylene glycol.[6] Thinners are also solvent mixtures. It should be formulated again by considering the above-mentioned subjects.

- Additives: Additives are additional ingredients added to paint to modify or enhance its properties.[9] They are added to the coating mixture in very small amounts (weight or volume percentages of 1 percent or less). These small amounts have a great impact on coatings performance. Common additives include:

1. Thickeners: Adjust viscosity for better application control.[5]
2. Antifoaming agents: Prevent foaming during mixing and application.[8]
3. Antimicrobial agents: Inhibit the growth of mold, mildew, and bacteria.
4. Drying agents: Accelerate drying time.[10]
5. UV stabilizers: Protect against fading and degradation caused by exposure to sunlight.[11]
6. Rheology modifiers: Control the flow and leveling characteristics of the paint.[8]
7. Anti-settling agents: Prevent settling of pigments during storage.
8. Plasticizers: Increase flexibility and durability of the dried paint film.[11]

These components are carefully formulated and balanced to achieve the desired performance characteristics of the paint, such as color, durability, adhesion, and ease of application.[9] The specific formulation of paint can vary depending on its intended use, substrate, environmental conditions, and regulations.[1]

1.2.General Information about Resin

In the paint industry, resin refers to a key component of paint formulations, also known as binders or polymers. Resins are responsible for binding together the pigment particles and adhering them to the surface as the paint dries and cures.[3] Resins are typically film-forming materials that provide several important functions in paint:

- Gloss and Sheen: Resins can influence the glossiness or sheen of the paint film, with different types of resins producing different levels of shine from high gloss to matte.[6]
- Adhesion: Resins adhere the pigment particles to the surface being painted, creating a strong bond that prevents the paint from easily peeling, flaking, or chipping off.[2]

- Durability: Resins contribute to the durability and longevity of the paint film by providing resistance to environmental factors such as moisture, sunlight, heat, and abrasion.[2,3]
- Flexibility: Some resins are formulated to be flexible, allowing the paint film to expand and contract with changes in temperature and humidity without cracking or peeling.[5]
- Chemical Resistance: Certain resins offer resistance to chemicals, stains, and other substances, making the painted surface easier to clean and maintain.[2,3,5]

Binders/resins can be classified as thermoset and thermoplastics. Thermoset coatings applied in liquid form, cures in a chemical reaction pathway that become insoluble in coating mixture.[8] This chemical reaction can be defined as also crosslinking. By this way small molecules are converted to larger molecules. In other words, low molecular weight materials converted to high molecular weight materials. Thermoplastic coatings are generally cure by solvent evaporation and remain soluble in solvent(s). This coating type can be softened by heat or re-dissolved by particular solvent(s).[1,1]

The choice of resin depends on factors such as the type of paint (water-based or oil-based), the substrate being painted, the desired performance characteristics, and regulatory considerations.

Common types of resins used in paints include:

- Acrylic: Acrylic resins generally based on acrylate and methacrylate monomers. They offer good weather resistance, resistance to hydrolysis, gloss and color retention in outdoor use. Acrylic resins can be employed in organic solvent-borne, waterborne, powder and radiation-curable paints/coatings. They can be thermoplastic or thermosets.[2,3,5,10]
- Latex: Latex resins are a type of acrylic resin dispersed in water. They are known for their fast-drying time, low odor, and easy cleanup.
- Alkyd: Alkyd resins are oil-based binders derived from vegetable oils or synthetic sources. They provide excellent adhesion and durability, especially in solvent-based paints.[10]
- Epoxy: Epoxy resins are highly durable and resistant to chemicals, making them suitable for industrial and marine applications. There are numerous thermosetting

structures and curing agent variations for epoxy resins. As a result, a broad range of rigidity and flexibility can be achieved in physical attributes. Epoxies often have good heat resistance, good colourability, and high mechanical and electrical qualities.[2,5,8]

- Polyurethane: The broad family of polymers known as polyurethanes (PUs) is based on the product of the reaction between an organic isocyanate and substances with a hydroxyl group. The primary repeating unit in polyurethane is the urethane group, which is obtained when alcohol (-OH) and isocyanate (NCO) react.[12] The PU macromolecule is composed of two alternating non-polar units: the hard segment, which is obtained from an isocyanate (aliphatic or aromatic); and the soft segment, which is derived from a nonpolar macrodiol, primarily polyester, polyether, and polycarbonate-based.[11,13,14] The polymer receives distinct properties from each of the segments. Generally, the polymer's stiffness, film-forming ability, and resistance to abrasion are attributed to the hard segment; the soft segment contributes to the elastomeric qualities. Polyurethane resins offer exceptional durability, UV resistance, and abrasion resistance. They are often used in high-performance coatings for floors, furniture, and automotive applications.[15]
- Polyurea: It is described as a coating substance that is produced when amine-terminated resins react with isocyanates. Aspartic esters may be a component of polyurea coatings that can offer also amine functionality. An amine bond-containing chemical backbone is provided by a polyurea. With its strong chemical resistance to hydrocarbons and hydrogen sulfide gas, polyurea is frequently employed as an industrial coating in tough locations, including submerged sewers.[16] Amines and aromatic methylene diisocyanate (MDI) are used to make conventional polyurea polymers.[11,12,17] The mainstay of two-component polyurea technology has been aromatic-based two-component systems. Conventional polyurea, which are aromatic chemicals, can yellow or deteriorate when exposed to ultraviolet light for a variety of reasons.[11–14]

Three distinct generations of polyurea have emerged because of the substantial evolution of the compound throughout time: aromatic polyurea (first generation), aliphatic polyurea (second generation), and polyaspartic polyurea (third generation). Aromatic polyurea, as first generation, is an economical choice for waterproofing and anti-corrosive material.[15,16,18] This generation is not suitable for outdoor applications due

to its low UV-stability. Also, a nearly 7-second cure time reduces total adhesion and complicates application. Aliphatic polyurea is more suitable compared to aromatic polyurea for outdoor applications in terms of UV-stability. However, it is not suitable for use in humid conditions or at cold temperatures (3°C). Polyaspartic polyurea, as the third generation, has several advantages compared to first and second generations. It supplies extended gel time providing a variety of application methods, such as high pressure, brushing, etc.[18]

Polyaspartic esters (Figure 1.1) are a relatively new and advanced type of resin used in the paint and coatings industry. It belongs to the polyurea family of polymers and is characterized by its fast-curing time, excellent durability, and versatility in various applications.[1,16,19] One of the most significant advantages of polyaspartic ester resin is its relatively rapid curing time. Unlike traditional coatings that may take hours or even days to cure, polyaspartic coatings can cure in a matter of minutes to a few hours. This fast cure time allows for quicker turnaround times in projects, reducing downtime and increasing productivity. Polyaspartic ester polyureas are highly durable and offer excellent resistance to abrasion, chemicals, UV radiation, and weathering. This makes them suitable for demanding environments such as industrial floors, automotive coatings, bridges, and marine applications.[1,9] They exhibit strong adhesion to a wide variety of substrates, including concrete, metal, wood, and existing coatings. This ensures a long-lasting bond between the coating and the substrate, minimizing the risk of delamination or peeling.[18]

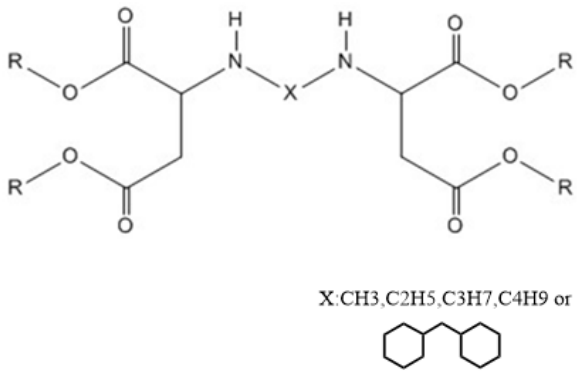

Figure 1.1. Polyaspartic ester structure.

Despite their exceptional durability, polyaspartic ester polyureas remain flexible even after curing. This flexibility allows them to withstand substrate movement, thermal expansion and contraction, and other stresses without cracking or delaminating.[1,9,16,18] Many polyaspartic ester polyurea formulations have low volatile organic compound (VOC) emissions, making them environmentally friendly and compliant with regulatory standards for air quality and emissions. Polyaspartic ester polyureas can be formulated with various additives to achieve specific performance characteristics such as slip resistance, chemical resistance, or decorative effects.[16] They can also be tinted in a wide range of colors to meet aesthetic requirements. These coatings can be applied in a wide range of temperatures and humidity levels, making them suitable for both indoor and outdoor applications. They can be spray-applied, roller-applied, or trowel-applied, depending on the specific requirements of the project. Overall, polyaspartic ester polyureas offer a combination of fast curing, durability, adhesion, and flexibility that make them an attractive option for a variety of coating applications in industries such as construction, automotive, aerospace, and marine.[1,15,16]

Polyaspartic ester polyurea is typically synthesized through a chemical reaction between an aliphatic polyisocyanate and a polyaspartic ester.[1,16,18] The process involves several steps and specialized equipment, and it is typically carried out in a controlled laboratory or industrial setting. Here's a simplified overview of the synthesis process:

- Preparation of Polyaspartic Ester: It is typically obtained by reacting maleic anhydride with an amine compound, such as ammonia or a primary amine. This reaction results in the formation of polyaspartic ester, which is a linear polymer containing repeating aspartic ester units (Figure 1.2a).
- Additives and Formulation: Various additives, such as catalysts, solvents, plasticizers, and UV stabilizers, may be incorporated into the resin formulation to modify its properties or improve performance characteristics. These additives are typically added during or after the polymerization process.[1,4,9]
- Reaction with Polyisocyanate (Polymerization): The polyaspartic ester is then reacted with an aliphatic polyisocyanate compound, such as hexamethylene diisocyanate (HDI) or isophorone diisocyanate (IPDI) (Figure 1.2b). This reaction is typically carried out under controlled conditions, such as elevated temperature and pressure, to facilitate the formation of polyaspartic ester polyurea. The reaction between the

polyaspartic ester and polyisocyanate leads to the formation of polyurea linkages, resulting in the polymerization of the resin. This process is exothermic, meaning it generates heat, so cooling equipment may be used to maintain the desired reaction temperature.

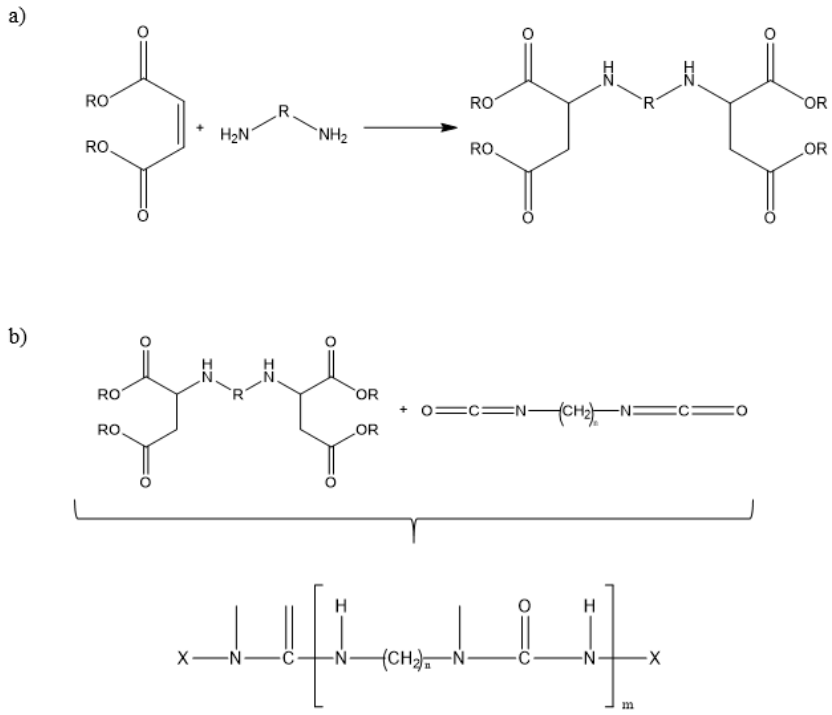

Figure 1.2. a) Synthesis of polyaspartic ester b) Synthesis of polyaspartic ester polyurea resin.

1.3.UV Degradation

UV stands for ultraviolet radiation. It's a type of electromagnetic radiation that has shorter wavelengths and higher frequencies than visible light but longer wavelengths and lower frequencies than X-rays. UV radiation is naturally emitted by the sun and can also be produced artificially by certain light sources, such as UV lamps. UV radiation is categorized into three main types based on its wavelength: Ultraviolet A (UVA), Ultraviolet B (UVB), Ultraviolet C (UVC).[19,20]

UVA radiation has the longest wavelength among the three types of UV radiation, ranging from 320 to 400 nanometers (nm). It is the least energetic form of UV radiation

but is the most prevalent in sunlight. UVA rays can penetrate deep into the skin's layers and are primarily responsible for tanning, skin aging, and wrinkling. UVB radiation has shorter wavelengths, ranging from 280 to 320 nm.[21] It is more energetic than UVA radiation and is partially absorbed by the Earth's atmosphere, although some UVB rays still reach the Earth's surface. UVB rays are the primary cause of sunburn, skin damage, and contribute to the development of skin cancer. UVC radiation has the shortest wavelengths, ranging from 100 to 280 nm.[19,20,22] It is the most energetic form of UV radiation but is largely absorbed by the Earth's atmosphere and does not reach the Earth's surface in significant amounts.[21] UVC radiation is commonly used for disinfection purposes, such as sterilizing water, air, and surfaces, due to its ability to destroy microorganisms.[21] Exposure to UV radiation can have both beneficial and harmful effects on living organisms. Moderate exposure to sunlight is necessary for the production of vitamin D in the skin and can have positive effects on mood and circadian rhythm.[21] However, excessive exposure to UV radiation, especially from sunlight, can lead to sunburn, premature aging of the skin, eye damage (such as cataracts), and an increased risk of skin cancer. To protect against the harmful effects of UV radiation, it's important to take precautions such as wearing sunscreen, protective clothing, and sunglasses, seeking shade during peak sunlight hours, and avoiding artificial tanning devices that emit UV radiation.[21,23,24]

UV degradation refers to the process by which materials undergo deterioration or damage when exposed to ultraviolet (UV) radiation from the sun. UV radiation is a type of electromagnetic radiation with wavelengths shorter than visible light but longer than X-rays, falling within the range of 10 to 400 nm.[22] When materials are exposed to UV radiation, especially over prolonged periods, several mechanisms can lead to degradation:

- Photodegradation: UV radiation can break chemical bonds within the molecular structure of materials, leading to the formation of free radicals or other reactive species. These reactive species can initiate chain reactions, resulting in the degradation of polymers, discoloration, embrittlement, or loss of mechanical properties.[19,20]
- Crosslinking: UV radiation can also induce crosslinking reactions, where polymer chains become interconnected through chemical bonds. While crosslinking can

sometimes enhance the mechanical properties of materials, excessive crosslinking can lead to brittleness and loss of flexibility.[18,20,21]

- Discoloration: UV radiation can cause materials to undergo color changes, typically through the formation of chromophores or chemical groups that absorb visible light. This can result in fading, yellowing, or darkening of the material's appearance.
- Surface Erosion: UV radiation can contribute to the physical erosion of materials by promoting the degradation of surface layers. This can manifest as cracking, chalking, or flaking of the material's surface.[1,16,19–21]
- Loss of Performance: UV degradation can compromise the performance characteristics of materials, such as reduced strength, stiffness, or impact resistance. This can be particularly problematic for outdoor applications where materials are exposed to sunlight for extended periods.[19–21]

UV degradation is a common concern for a wide range of materials, including polymers (plastics and rubbers), paints, coatings, textiles, wood, and composites. To mitigate UV degradation, various strategies can be employed, such as incorporating UV stabilizers or inhibitors into materials, using protective coatings or films, selecting UV-resistant materials, and minimizing exposure to sunlight through shading or protective barriers. Additionally, proper design, maintenance, and material selection can help extend the service life of outdoor structures and products.[19–21,25]

Photodegradation of polyaspartic ester resin refers to the process by which the resin undergoes deterioration or damage when exposed to ultraviolet (UV) radiation from sunlight or other sources of UV light. Polyaspartic ester resin, like many other polymers, is susceptible to photodegradation due to the energy carried by UV radiation. [11,14,19,20,25]

The photodegradation mechanism of polyaspartic ester resin involves a series of complex chemical reactions initiated by the absorption of ultraviolet (UV) radiation from sunlight or other sources (Table 1.1). While the specific details may vary depending on the resin's composition and environmental conditions, the general photodegradation mechanism of polyaspartic ester polyurea can be described as follows:

- Absorption of UV Radiation: Polyaspartic ester polyurea contains chemical groups, such as carbonyl (C=O) or aromatic groups, that can absorb UV radiation. When

exposed to sunlight, these groups absorb photons of UV light, becoming excited to higher energy states.[23,24,26]

- Formation of Excited States: After absorbing UV radiation, the chemical groups within the resin molecules undergo a transition to excited electronic states. These excited states are less stable than the ground state, making them prone to undergoing chemical reactions.[24,27]
- Photochemical Reactions: The excited resin molecules can undergo various photochemical reactions, including:
- Photolysis: Some chemical bonds within the resin molecules may break, leading to the formation of free radicals or other reactive species. For example, UV radiation can cause cleavage of carbon-carbon bonds or carbon-oxygen bonds, resulting in the formation of radical species.[23,24,27]
- Oxygen Activation: UV radiation can also activate molecular oxygen (O_2) to form reactive oxygen species (ROS) such as singlet oxygen ($^1O_2$) or superoxide radicals (O_2^-). These ROS can initiate oxidation reactions in the resin, leading to the formation of oxidized products and degradation of the polymer backbone.[2,5,21]
- Crosslinking: In addition to bond cleavage, UV radiation can induce crosslinking reactions in the resin molecules. Radical species generated by photolysis or oxygen activation can react with nearby polymer chains, forming covalent bonds and increasing the degree of crosslinking in the resin network.[6,12,14,28]
- Propagation of Degradation Reactions: Once initiated, the degradation reactions can propagate through the polymer matrix, leading to the fragmentation of polymer chains, loss of molecular weight, and changes in the material's mechanical and chemical properties.
- Formation of Degradation Products: As photodegradation progresses, various degradation products may form, including carbonyl groups, hydroperoxides, ketones, aldehydes, and other reactive species. These degradation products can contribute to discoloration, loss of clarity, and deterioration of the resin's physical properties.

Overall, the photodegradation mechanism of polyaspartic ester polyurea involves a combination of photochemical and oxidative processes that result in the degradation of the polymer matrix. To mitigate photodegradation, UV stabilizers or inhibitors are often added to resin formulations to absorb or block UV radiation and prevent the initiation of

degradation reactions.[21,23,24] Additionally, proper design, formulation, and maintenance practices can help minimize the effects of UV exposure and extend the service life of polyaspartic ester resin coatings.

UV radiation, whether natural or manufactured, degrades organic compounds, discolors dyes and pigments, and reduces mechanical qualities and gloss in polymers and plastics. A photochemical reaction happens when light activates a molecule or polymer into excited singlet (S*) or triplet (T*) states.[20] Polymers and other organic compounds undergo photo-oxidative degradation in the presence of air, but pure degradation (chain scission and crosslinking) happens exclusively in an inert environment.[21] In the literature there is a few possible photodegredation mechanisms of polyurethane/urea.

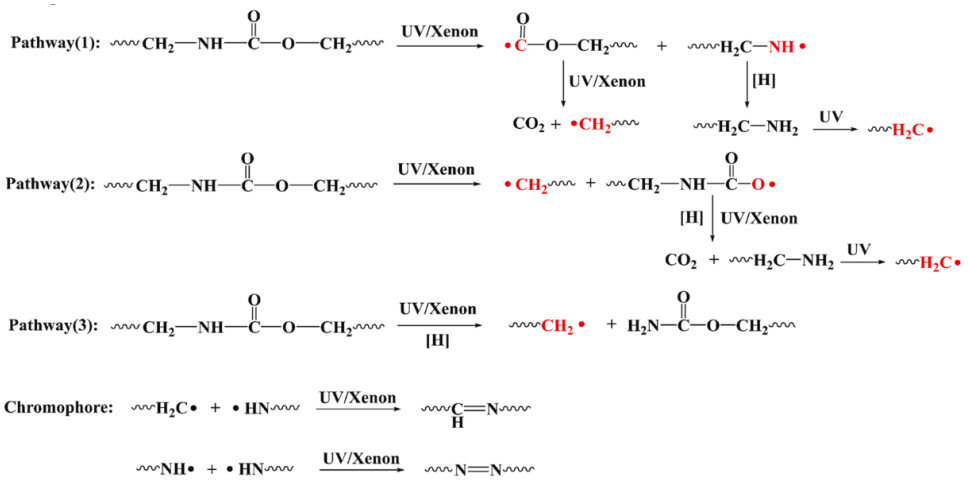

Figure 1.3. Photodegradation mechanism of Polyurethane/Polyurea.[20]

In Figure 1.3, for the urethane bond, three potential routes exist, including homolytic breakage of C-N and C-O bonds. Initially, urethane bond breakage produced active chain-free radicals such as amines and alkyls. UV irradiation causes the major degradation products to disintegrate further. Chain radicals combine to form chromophore -C=N- and -N=N- linkages, causing yellowing of PU.[20] Carboxyl radicals are transformed to CO_2. As deterioration continued, the number of N-H and C-N bonds reduced. The chromophores cause the UV degradation (yellowing) of polyaspartic ester.[20]

Table 1.1. Main reactions of the photo oxidative degradation of polymers.[21]

Initiation (UV light)	$R–H \rightarrow R^{\bullet} + H^{\bullet}$
Propagation	$R^{\bullet} + O_2 \rightarrow R–O–O^{\bullet}$
	$R–O–O^{\bullet} + R–H \rightarrow R–O–OH + R^{\bullet}$
	$R–O–OH \rightarrow R–O^{\bullet} + OH^{\bullet}$
Termination	$R^{\bullet} + R^{\bullet} \rightarrow R–R$
	$R^{\bullet} + R–O–O^{\bullet} \rightarrow R–O–O–R$
	$R–O–O^{\bullet} + R–O–O^{\bullet} \rightarrow$
	R–O–O–R + nonradical products

1.4.Photostabilization of Coatings

Photostabilization of coatings refers to the process of enhancing a coating's resistance to degradation caused by exposure to light, particularly ultraviolet (UV) radiation. The goal is to prolong the life and maintain the appearance and performance of the coating by preventing or minimizing the harmful effects of UV exposure. There are several ways for photostabilization of coatings:

- UV Absorbers: UV absorbers are compounds added to coatings formulations that absorb UV radiation and convert it into harmless heat. These compounds typically contain chromophores that absorb UV light, preventing it from reaching the underlying coating or substrate. UV absorbers are effective at protecting coatings from UV-induced degradation and can be used in various types of coatings, including paints, varnishes, and plastics.[21,24]
- UV Scavengers: UV scavengers, also known as free radical scavengers or antioxidants, are compounds that neutralize reactive oxygen species (ROS) generated by UV radiation. These ROS can initiate oxidation reactions in coatings, leading to degradation of polymer chains and loss of mechanical properties. UV scavengers intercept these ROS, preventing them from propagating degradation reactions and preserving the integrity of the coating.[19]
- Hindered Amine Light Stabilizers (HALS): HALS are a class of compounds that inhibit degradation of coatings by UV radiation. They act by scavenging free radicals generated during photodegradation reactions, thereby preventing chain scission and crosslinking of polymer chains. HALS are particularly effective in polymeric

coatings, such as paints and varnishes, and can significantly extend the service life of coatings exposed to outdoor environments. [19–21]

- Antioxidants: Antioxidants are compounds that inhibit oxidation reactions in coatings caused by UV radiation. They work by donating hydrogen atoms to reactive oxygen species, thereby neutralizing them and preventing further degradation of the coating. Antioxidants are commonly used in combination with UV absorbers and HALS to provide comprehensive protection against photodegradation.[19–21,25]
- Synergistic Formulations: Photostabilization of coatings often involves formulating combinations of photostabilizers to achieve synergistic effects. By combining different types of photostabilizers, coatings manufacturers can enhance the overall resistance of coatings to UV-induced degradation and optimize performance under specific environmental conditions.[19]

Overall, photostabilization of coatings is essential for maintaining the aesthetic appearance, durability, and performance of coated surfaces exposed to UV radiation. By incorporating appropriate photostabilizers into coatings formulations, manufacturers can ensure that coatings maintain their properties and functionality over extended periods of outdoor exposure.

UV absorbers, also known as UV filters or UV blockers, are chemical compounds that are added to coatings, plastics, textiles, and other materials to absorb ultraviolet (UV) radiation and prevent it from reaching underlying substrates.[19–22] UV absorbers are an essential component of photostabilization strategies, as they help protect materials from UV-induced degradation and damage. There are several types of UV absorbers commonly used in various applications:

- Benzophenones: Benzophenone-based UV absorbers are among the most widely used types of UV absorbers. They are effective at absorbing UV radiation in the range of 280 to 350 nanometers (nm) and are commonly used in coatings, plastics, and personal care products.[21]
- Benzotriazoles: Benzotriazole-based UV absorbers are another common type of UV absorber. They absorb UV radiation in the range of 300 to 400 nm and are particularly effective at protecting polymers from degradation caused by long-wavelength UVB

and UVA radiation. Benzotriazole UV absorbers are often used in outdoor applications such as automotive coatings, architectural coatings, and plastics.[20,21]

- Triazines: Triazine-based UV absorbers are highly efficient at absorbing UV radiation in the range of 300 to 400 nm. They are commonly used in coatings, plastics, and textiles to provide protection against UV-induced degradation and fading.[19–22]
- Salicylates: Salicylate-based UV absorbers are effective at absorbing UV radiation in the range of 290 to 340 nm. They are often used in sunscreen formulations to provide broad-spectrum UV protection.[19–21]
- Anthranilates: Anthranilate-based UV absorbers absorb UV radiation in the range of 320 to 400 nm. They are commonly used in sunscreen formulations and other cosmetic products to provide protection against UVA and UVB radiation.[19–21]
- Benzimidazoles: Benzimidazole-based UV absorbers absorb UV radiation in the range of 280 to 350 nm. They are often used in coatings and plastics to provide protection against UV-induced degradation and discoloration.[19,21]

UV absorbers work by absorbing UV radiation and converting it into harmless heat, preventing it from reaching the underlying substrate and causing degradation. They are often used in combination with other photostabilizers, such as antioxidants and hindered amine light stabilizers (HALS), to provide comprehensive protection against UV-induced degradation and extend the service life of materials exposed to outdoor environments.

Also, metal oxide particles can act as effective UV absorbers or blockers when incorporated into coatings, plastics, textiles, and other materials. These metal oxides, particularly zinc oxide (ZnO) and titanium dioxide (TiO_2), are widely used for their ability to absorb or scatter UV radiation, thereby providing protection against UV-induced degradation and damage.[29–33]

In this study, metal oxide nanoparticles are used as UV absorbers. The experiments were conducted with the TiO_2, CeO_2 and γ-MnO_2 as metal oxide nanoparticles in this thesis. The crystal structures of the metal oxide nanoparticles aregiven in Figure 1.4.

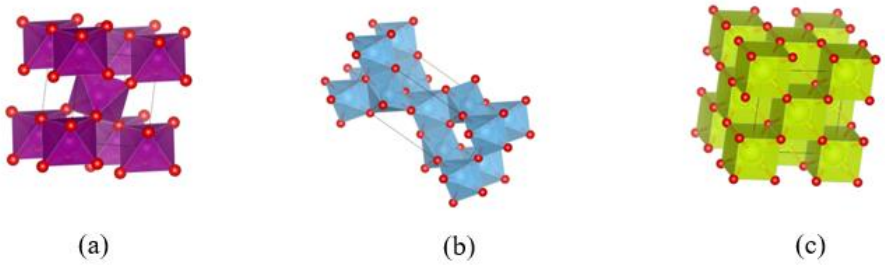

Figure 1.4.a) γ-Manganese (IV) oxide, b) Titanium (IV)oxide (anatase), c) Cerium (IV)oxide.

Cerium oxide nanoparticles, also known as ceria nanoparticles, have emerged as a promising material for various applications, including as UV absorbers. Cerium oxide (CeO_2) nanoparticles exhibit unique optical and catalytic properties, making them suitable for use in UV protection and other photostabilization applications.[29]

- UV Absorption Properties: Cerium oxide nanoparticles have been shown to absorb UV radiation, particularly in the UVB (280-320 nm) and UVA (320-400 nm) regions of the electromagnetic spectrum.[34] The UV absorption properties of cerium oxide nanoparticles are attributed to the electronic transitions between the valence and conduction bands, which occur due to the presence of oxygen vacancies and defects in the nanoparticle structure.
- Photocatalytic Activity: In addition to absorbing UV radiation, cerium oxide nanoparticles exhibit photocatalytic activity, meaning they can facilitate chemical reactions under UV light. This photocatalytic activity can contribute to the degradation of organic pollutants and the neutralization of reactive oxygen species (ROS) generated by UV radiation, thereby providing additional photoprotection to materials.[29,34,35]
- UV Protection in Coatings and Films: Cerium oxide nanoparticles have been incorporated into coatings, films, and other materials to provide UV protection. When dispersed in a matrix material, cerium oxide nanoparticles can effectively absorb and scatter UV radiation, reducing its penetration into the underlying substrate and preventing photodegradation.[29]

Cerium oxide nanoparticles have shown promise for applications in coatings, plastics, textiles, and other materials where UV protection and photostability are desired.

Overall, cerium oxide nanoparticles offer a promising avenue for enhancing UV protection and photostability in a variety of materials. Ongoing research and development in this area are expected to further elucidate the potential of cerium oxide nanoparticles as UV absorbers and their applications in UV-protective coatings, films, and other photostabilization applications.[34]

Titanium dioxide (TiO_2) nanoparticles are widely used as UV absorbers and blockers due to their excellent UV absorption properties, high refractive index, and photostability.[31,36,37]

- UV Absorption Properties: Titanium dioxide nanoparticles are highly effective at absorbing and scattering UV radiation, particularly in the UVB (280-320 nm) and UVA (320-400 nm) regions of the electromagnetic spectrum. The UV absorption properties of titanium dioxide nanoparticles are primarily attributed to their wide bandgap energy (~3.0 eV for anatase phase), which allows them to absorb UV radiation and generate electron-hole pairs via photoexcitation.[19,20,31,36]
- Photocatalytic Activity: In addition to their UV absorption properties, titanium dioxide nanoparticles exhibit photocatalytic activity, meaning they can initiate chemical reactions under UV light.[19,31,36] This photocatalytic activity can be harnessed for applications such as air and water purification, self-cleaning surfaces, and degradation of organic pollutants.
- Particle Size and Morphology: The UV absorption and scattering properties of titanium dioxide nanoparticles depend on factors such as particle size, morphology, crystalline phase, and surface characteristics. Nanoscale titanium dioxide particles (<100 nm) exhibit enhanced UV absorption and scattering efficiency compared to larger particles, due to their larger surface area-to-volume ratio and quantum size effects.[36,37]
- Dispersion and Stability: Proper dispersion of titanium dioxide nanoparticles within a matrix material is crucial for maximizing UV protection and photostability. Surface modification techniques, such as coating nanoparticles with organic or inorganic compounds, can improve their dispersion and stability in various solvent systems and matrix materials.

The photostabilization mechanism of titanium dioxide (TiO_2) involves its ability to absorb and scatter ultraviolet (UV) radiation, thereby preventing UV-induced degradation of materials. Titanium dioxide acts as a UV absorber and blocker, particularly in the UVB (280-320 nm) and UVA (320-400 nm) regions of the electromagnetic spectrum.[19,22,31,36] Titanium dioxide nanoparticles absorb UV radiation when exposed to sunlight. The energy from the absorbed UV photons excites electrons within the titanium dioxide nanoparticles, leading to the formation of electron-hole pairs. In addition to absorbing UV radiation, titanium dioxide nanoparticles scatter and reflect a significant portion of the incident UV light. This scattering effect redirects UV radiation away from the surface of the material, reducing its penetration depth and decreasing the exposure of the underlying substrate to UV radiation.[19–21,31,36] Titanium dioxide nanoparticles exhibit photocatalytic activity suggesting thatthey can initiate chemical reactions under UV light. This property can be harnessed to degrade organic pollutants, neutralize reactive oxygen species (ROS), and inhibit the formation of harmful photochemical products that contribute to material degradation. Titanium dioxide nanoparticles can quench reactive oxygen species (ROS) generated by UV radiation through photocatalytic reactions. ROS, such as singlet oxygen ($^1O_2$) and superoxide radicals (O_2^-), are highly reactive and can contribute to oxidative degradation of materials.[19,31,36] By quenching ROS, titanium dioxide nanoparticles help prevent oxidative damage and maintain the stability of materials exposed to UV radiation. These nanoparticles can form a physical barrier on the surface of materials, providing additional protection against UV radiation. [19,31,34,36,37]This barrier helps shield the underlying substrate from direct exposure to UV light and reduces the risk of UV-induced degradation. Overall, the photostabilization mechanism of titanium dioxide involves a combination of UV absorption, scattering, reflection, photocatalytic activity, and ROS quenching. By harnessing these properties, titanium dioxide nanoparticles can effectively protect materials from UV-induced degradation, extend their service life, and maintain their aesthetic and functional properties when exposed to sunlight or other sources of UV radiation.

Overall, titanium dioxide nanoparticles are highly versatile and effective UV absorbers, making them invaluable for enhancing UV protection and photostability in a wide range of materials and applications. Continued research activity on this chemistry for nanoparticle synthesis, dispersion, and application methods are expected to further

expand the utility of titanium dioxide nanoparticles in UV protection and photostabilization technologies.

Manganese dioxide (MnO_2) nanoparticles have attracted interest as UV absorbers due to their unique chemical and physical properties.[33] While not as commonly used as titanium dioxide (TiO_2) or zinc oxide (ZnO) for this purpose, MnO_2 nanoparticles still offer valuable benefits in specific applications. Here's a detailed overview of manganese dioxide nanoparticles as UV absorbers:

- Chemical Composition: Manganese dioxide exists in several polymorphs, including α-MnO_2, β-MnO_2, γ-MnO_2, and δ-MnO_2. The polymorph can influence its optical and UV absorption properties. MnO_2 is an inorganic compound composed of manganese and oxygen with the chemical formula MnO_2.[38]
- Optical Properties: MnO_2 nanoparticles have strong UV absorption capabilities due to their electronic structure, which allows them to absorb UV light and convert it [38–41]into other forms of energy, such as heat. The absorption of UV radiation helps protect underlying materials from UV-induced degradation.
- Photocatalytic Activity: MnO_2 nanoparticles exhibit photocatalytic properties, enabling them to degrade organic pollutants and other contaminants upon UV light exposure. This makes them useful in environmental applications such as water and air purification. The photocatalytic activity also helps in the breakdown of reactive oxygen species (ROS), reducing oxidative stress on materials.[40]
- Size and Morphology: The size and morphology of MnO_2 nanoparticles can significantly affect their UV absorption efficiency. Smaller nanoparticles have a higher surface area-to-volume ratio, which enhances their interaction with UV light. Morphological variations (e.g., nanorods, nanospheres, nanowires) can also influence the UV absorption and photocatalytic properties.[38–41]
- Coatings and Paints: MnO_2 nanoparticles can be incorporated into coatings and paints to provide UV protection. This helps in extending the lifespan and maintaining the aesthetic quality of surfaces exposed to sunlight. The nanoparticles can be mixed with traditional coatings to enhance UV resistance without significantly altering the coating's appearance.[38,42]
- Plastics and Polymers: Adding MnO_2 nanoparticles to plastics and polymers improves their UV resistance, preventing discoloration, degradation, and loss of mechanical

properties. This application is particularly valuable in outdoor plastic products, automotive parts, and packaging materials.[38–40]

- Textiles: MnO_2 nanoparticles can be embedded in textile fibers to impart UV-blocking properties, protecting fabrics and reducing UV exposure to the skin. Such treated textiles are useful for outdoor clothing, tents, and other sun-exposed fabric products.

Manganese dioxide nanoparticles have a broad absorption spectrum, including the UV region. They can absorb both UVA (320-400 nm) and UVB (280-320 nm) radiation. [40] Upon absorbing UV photons, MnO_2 nanoparticles become excited to higher electronic states. This prevents the UV radiation from penetrating deeper into the material and causing degradation. The absorbed UV energy is dissipated as heat or through non-radiative relaxation processes. This conversion of harmful UV radiation into less harmful forms of energy helps protect the underlying materials from photodegradation. MnO_2 nanoparticles exhibit photocatalytic properties, meaning they can catalyze reactions under UV light. This includes the degradation of organic pollutants and contaminants on the material's surface. This photocatalytic activity can help in self-cleaning applications, where the degradation of organic matter on surfaces is beneficial. UV radiation can generate reactive oxygen species (ROS) such as superoxide radicals (O_2^-), hydroxyl radicals (OH•), and singlet oxygen ($^1O_2$).[38,41] These ROS can cause oxidative stress and damage to materials. MnO_2 nanoparticles can help neutralize these ROS, either by acting as catalysts for their breakdown or by participating in redox reactions that mitigate their harmful effects.

1.5. Literature Works

Surface modification of metal oxide nanoparticles involves altering or adding to the outer layer of nanoparticles to enhance their stability, functionality, or compatibility with specific applications. This modification can be achieved through various chemical, physical, or biological methods. This involves attaching functional groups or molecules onto the surface of metal oxide nanoparticles (Figure 1.5). Common functional groups include amino (-NH_2), carboxyl (-COOH), thiol (-SH), and hydroxyl (-OH) groups. These

functional groups can enhance the stability, solubility, or reactivity of the nanoparticles. Silica coating is a widely used method to modify metal oxide nanoparticles' surfaces. It involves depositing a layer of silica (SiO_2) onto the metal oxide nanoparticles, which can improve their stability, biocompatibility, and dispersibility in various solvents.

As an example of metal oxide nanoparticle, it is commonly known that ZnO have a hydrophilic surface and that their practical uses are thus restricted to a wide range of specialized disciplines. Furthermore, the active surface of nanoparticles causes them to clump together readily. Therefore, it is crucial to select the right modifying agent and to modify the highly distributed ZnO nanoparticles' surface in this way. MA Shu-rui et al. reports that in this study the effective treatment of ZnO nanoparticles in a mixed solvent of water and alcohol using 3-methacryloxypropyltrimethoxysilane, also known as KH570 silane coupling agent. The findings show that a chemical reaction between KH570 and the hydroxylic groups on the surface of ZnO nanoparticles produced the covalent bonds. As a result, ZnO nanoparticles' surface transitioned from hydrophilic to hydrophobic, and their dispersion was enhanced at the same time. They followed the procedure, a suitable quantity of KH570 was added to 100 milliliters of water-alcohol (v:v, 1:1) mixed solvent, and the mixture was stirred while maintained at 60°C for 30 min. After adding 10.0 g of ZnO nanoparticles, the mixture was continuously agitated at a speed of 5,000 r/s for one hour. Filtration was used to gather the precipitates, which were then routinely cleaned with acetone. The finished goods were then vacuum-dried for 12 hours at 80°C.[30] Initially, KH570's alkoxy groups hydrolyze to produce new, functional silanol groups. Secondly, silane's silanol groups have the potential to form hydrogen bonds with the hydroxyl groups on the nanoscale ZnO surface. Third, the final products are obtained by dehydrating the reaction products that are just beginning to form in the second procedure. As a result, the KH570 is successfully grafted onto ZnO nanoparticle surfaces (Figure 1.6).

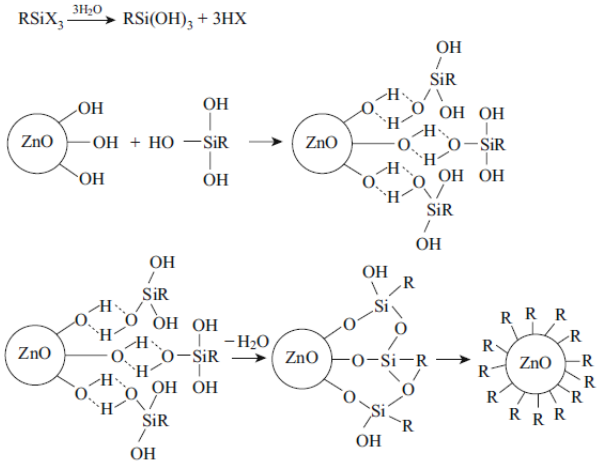

Figure 1.5. Schematic process for graft of silane coupling agent onto ZnO nanoparticles.[30]

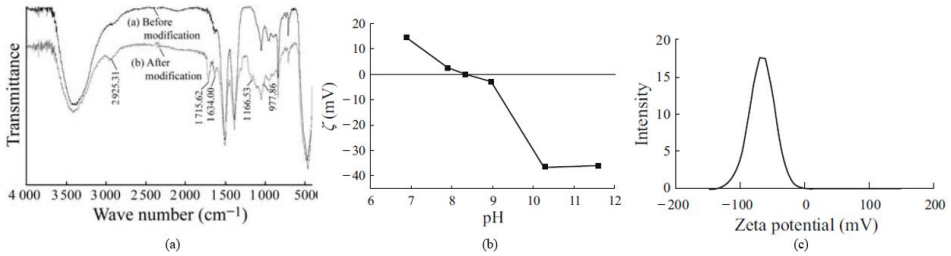

Figure 1.6. (a) FTIR spectra of ZnO nanoparticles before and after modification (b) Zeta potentials of ZnO nanoparticles before modification (c) after modification.[30]

In the following study example, effectively modified nano-TiO_2 particles using a 3-(trimethoxysilyl) propyl methacrylate silane coupling agent in an alcohol solvent. Ammonia was used as a catalyst for the silane hydrolysis reaction. TMSPM was successfully grafted onto nano-TiO_2 with a maximum efficiency of 97.7% at 3% concentration /(Figure 1.7). Nano-TiO_2's crystal structure and particle size remained unchanged following alteration (Figure 1.8).[31]

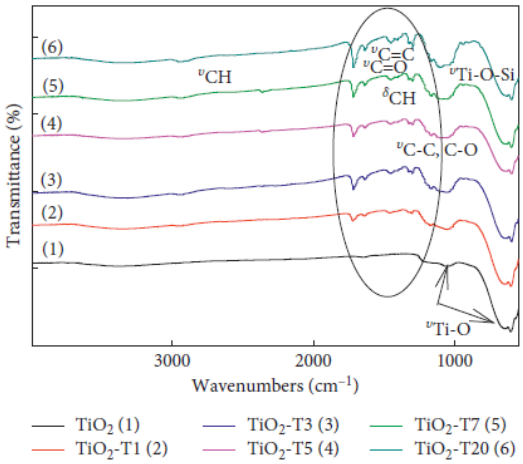

Figure 1.7. FTIR spectra of nano-TiO_2 and nano-TiO_2 modified with different volumes of TMSPM.[31]

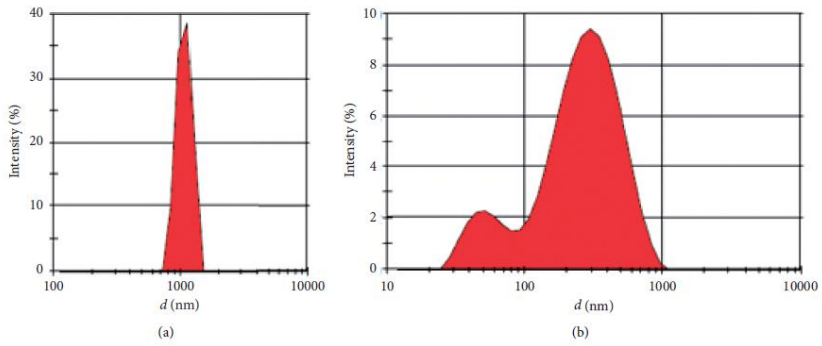

Figure 1.8. Size distribution diagrams of nano-TiO_2 (a) and TiO_2-T3 (b).[31]

Another in literature study, tetraethyl silicate, which was utilized as UV-shielding filler to manufacture UV-curable coatings, was hydrolyzed in-situ to deposit a SiO_2 layer on the surface of TiO_2 particles, yielding a series of SiO_2 coated TiO_2 particles (TiO_2@SiO_2). While the transmittance of TiO_2 coating was approximately 30% and 3.2% in the visible range (400–800 nm) and the UV region (300–400 nm), respectively, the transmittance of pure resin coating was approximately 84% in the visible region (400–800 nm) and more than 50% in the UV area (300–400nm) (Figure 1.9a). The outcome indicates that TiO_2 might considerably improve the coating's ability to filter UV rays by decreasing its transmittance, which was linked to TiO_2's exceptional UV-shielding capabilities. The pure resin showed the biggest color change (ΔE = 21.7) after 1000 h of

aging, suggesting that it lacked inadequate weather resilience. The TiO_2 coating exhibited the least amount of color change (ΔE = 7.5) following 1000 h of UV aging (Figure 1.9b). This can be attributed to TiO_2's exceptional ability to shield molecules from UV degradation, protecting the functional groups inside the coating. Thus, the TiO_2@SiO_2 coating's color change was somewhat greater than that of the TiO_2 coating but still far less than that of the pure resin coating, indicating that the addition of TiO_2@SiO_2 might still lessen the UV-cured coating's color change and improve its weather resistance.[36]

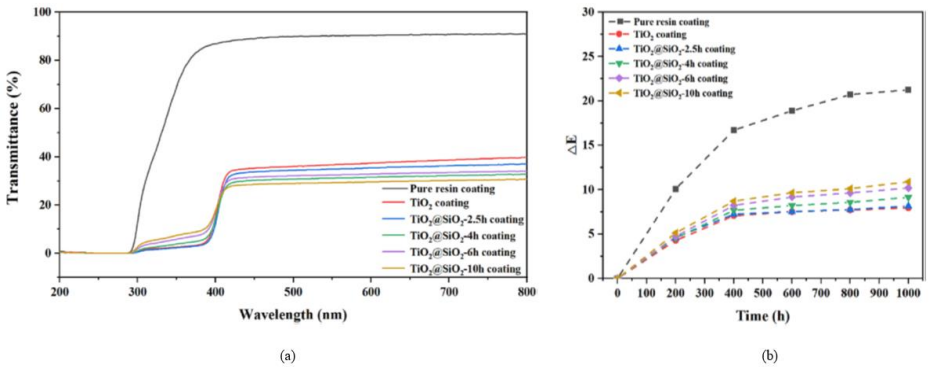

Figure 1.9. a) The UV−Vis transmittance spectra of UV-cured coatings. b) ΔE of the UV-cured coatings after different UV accelerated aging time.[36]

The following literature work explains MnO_2 is an n-type semiconductor that is capable of strongly absorbing UV light up to 400 nm. There are many polymorph phases of MnO_2, including α-, β-, δ-, and γ-MnO_2. Although MnO_2 NPs have a good UV-shielding capacity, their use as UV-shielding materials has been restricted because of their particle nature and aggregation. To get around this, MnO_2 NPs can be simply incorporated into a polymer matrix through solution casting, creating polymer nanocomposites in the form of films (Figure 1.10). Solution casting was used to create pure PVA and PVA–MnO_2 nanocomposite films. In deionized water, a 2% (w/w) PVA solution was made in order to create composite films. At 80 °C, PVA was gradually added to water with after two hours of constant stirring, it was cooled to 25 °C without further stirring. Next, PVA–MnO_2 nanocomposites with MnO_2 NPs in solution at 0.5, 1.0, 1.5, 2.0, and 4.0 weight percent were made.[33]

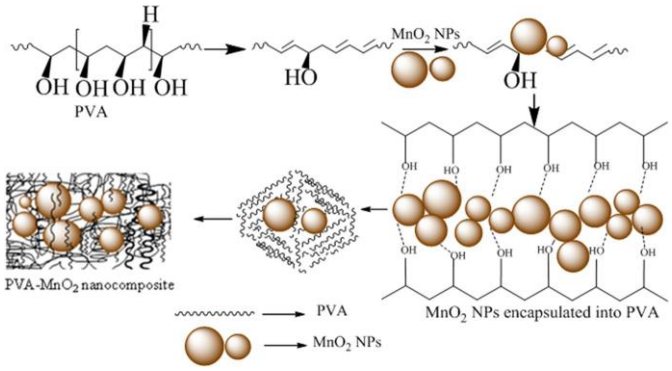

Figure 1.10. Schematic representation of PVA and MnO_2 NPs in PVA–MnO_2 nanocomposites.[33]

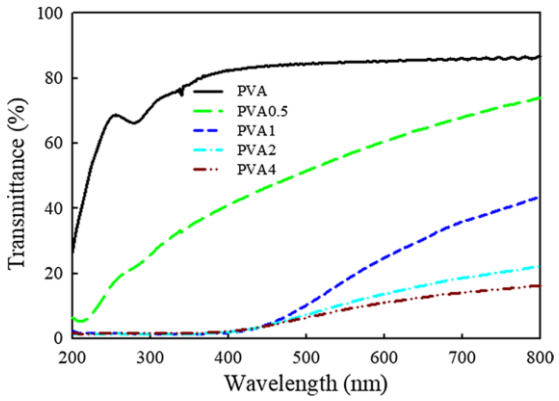

Figure 1.11. UV–Vis transmittance spectra of PVA, PVA0.5, PVA1, PVA2, and PVA4 nanocomposite films.[33]

PVA film is transparent in the visible range (400-800 nm). As MnO_2 levels rise, transmittance typically decreases. Increasing the concentration of MnO_2 NPs affects the optical transparency of films to visible light. Films with more than 1 wt% of MnO_2 NPs totally absorb UV light, making them suitable for UV-shielding applications. Increasing the amount of MnO_2 NPs from 1 to 4 wt.% improves UV shielding effectiveness (Figure 1.11). The nanocomposites' UV-shielding property is due to the development of a complex between MnO_2 NPs and pendant -O-H groups in the PVA matrix, which helps absorb UV rays.[33]

CHAPTER 2

MATERIALS AND METHODS

2.1. Materials

Titanium(IV) oxide (anatase, powder, 99.8% trace metals basis, Sigma Aldrich), Cerium(IV) oxide (powder,<5 μm, 99.9% trace metals basis), Gamma Manganese dioxide (powder, China) 3-methacryloxypropyltrimethoxysilane (KH 570) (Ataman Chemicals), Ethanol (absolute for analysis, Sigma Aldrich), Chloroform-d (99.8%, Merck), Desmophen NH 1420 (Aminofunctional co-reactant for polyisocyanates, Covestro), Tolonate XF 450 (aliphatic polyisocyanate based on Hexamethylene Diisocyanate, Vencorex).

2.2.Methods

2.2.1. Surface Modification

3-(methacryloxy)propyltrimethoxy silane (KH 570) were hydrolyzed with ethanol/water (1:1) (v:v) solution at 50 ℃ to obtain hydroxyl end groups. Metal oxide nanoparticles then added into the solution stirred in ultrasonic bath (Figure 2.1). In order to get rid of the unreacted silane, the mixture is centrifuged and washed twice with ethanol/water solution. The precipitate was put into the oven at 50 ℃ for a day to dry the particles (Figure 2.2).

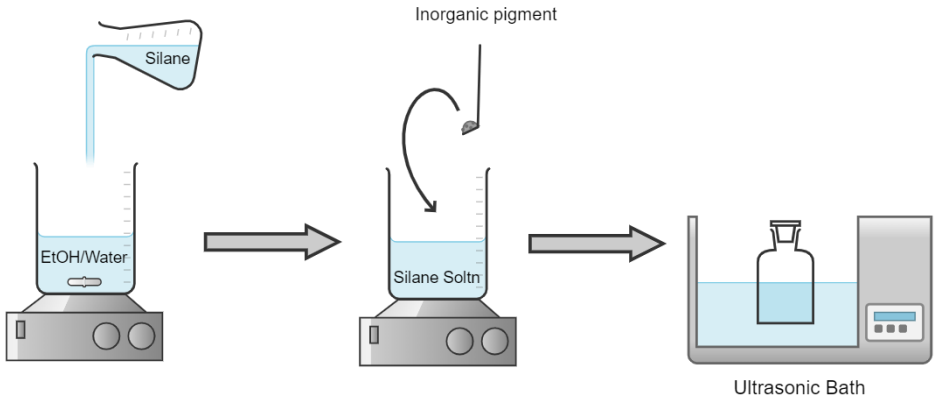

Figure 2.1. Procedure of surface modification of the particles.

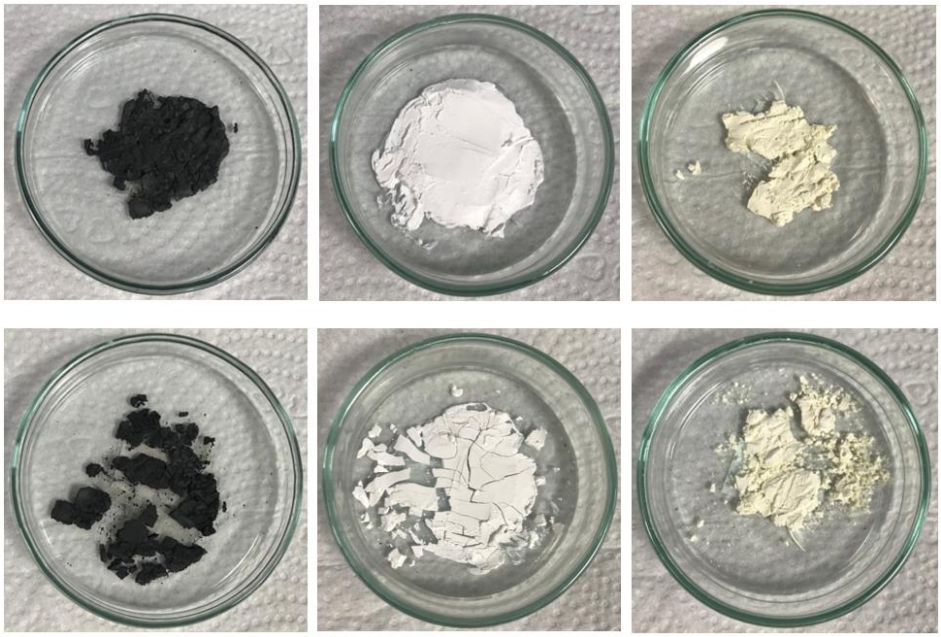

Figure 2.2. Silane-modified metal oxides (above: before drying, below: after drying).

2.2.2. Integration of Metal Oxides in Polyaspartic Ester Resin

The silane modified metal oxides was added into the polyaspartic ester resin (Desmophen 1420) (Figure 2.3). The mixture, firstly, stirred by stirrer. Then mixture was located in an ultrasonic bath and sonicated for 30 min.

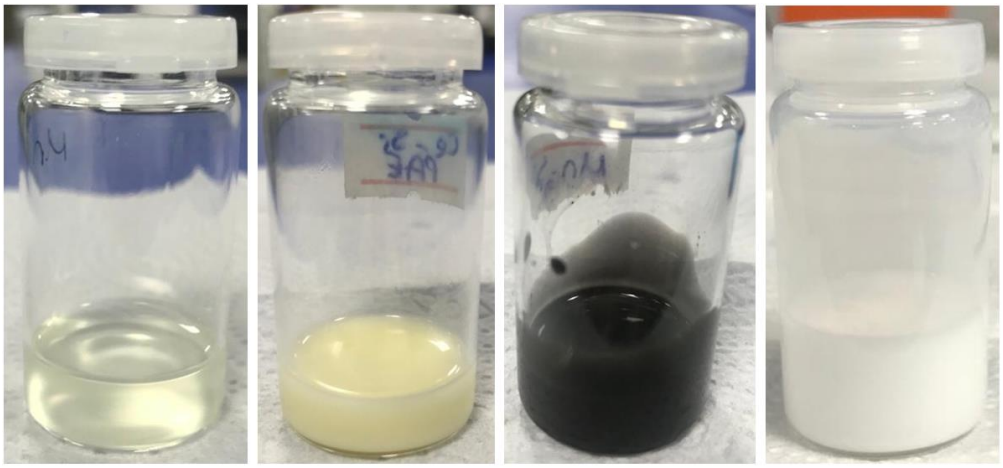

Figure 2.3. PAE Resin included metal oxide particles (from left to right: PAE Resin, CeO_2, MnO_2, TiO_2).

2.2.3. Preparation of Metal Oxide Included Polyaspartic Ester Polyurea Film

The isocyanate was mixed with the dispersed PAE resin mixture. The mixture was stirred fast. Right after the stirring, the mixture was casted on the plate (Figure 2.4). The PAE resin film was prepared with casting, Dr. Blade and spin coating method. The Dr. Blade coating method, also known as knife coating, is a process used to apply a thin, uniform layer of a material (1% metal oxide amount) onto a flat substrate (Figure 2.5a). The applied thickness values were 30, 60 and 120 μm. The different amount of metal oxide (10 % 5% 3%) including PAEPU films were prepared with Dr. Blade method too (Figure 2.6). Also, the spin coating method was used to obtain uniformly thinner films than the Dr. Blade method (Figure 2.5b). The used substrate was the glass slide. A small amount of the sample was poured onto the center of the substrate. Spin speed was 6000 revolutions per minute (rpm) and duration was 60 sec.

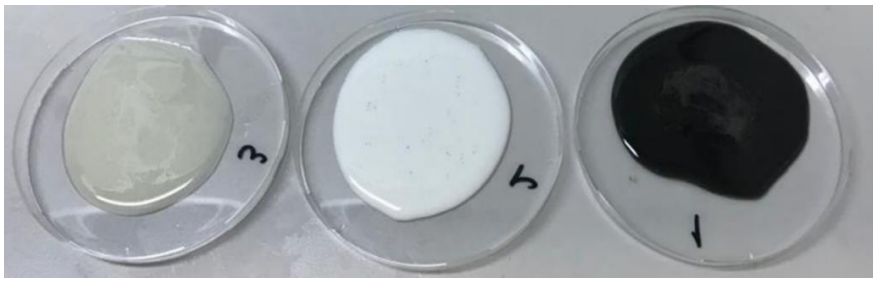

Figure 2.4. PAEPU Resin films includes metal oxides via casting method (from left to right: CeO_2, TiO_2, MnO_2).

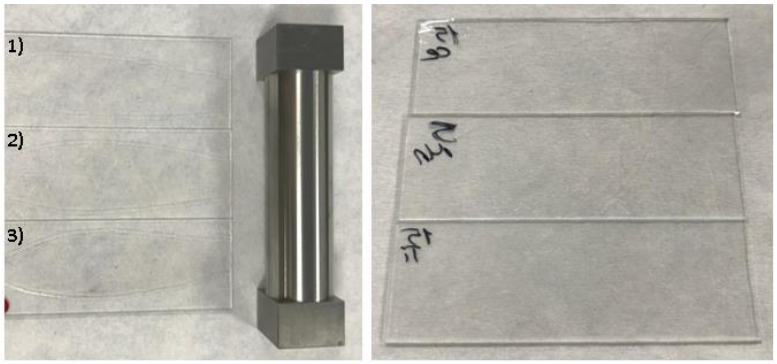

Figure 2.5. PAEPU Resin films includes metal oxides prepared with a) Dr. Blade method 0.2 % metal oxide (from up to down: 30, 60, 120 μm) b) Spin coating method.

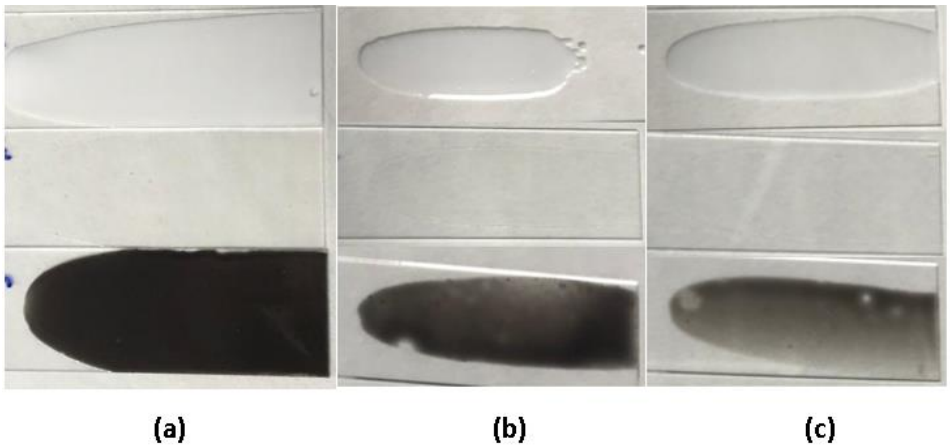

Figure 2.6. PAEPU Resin films includes metal oxides prepared by Dr. Blade method with a metal oxide oxide content of a) 10 % b) 5% c) 3%

2.3. Characterization Tests

The products were characterized with below techniques. In this thesis, there are many characterization methods were used in order to reach to detailed information about the products. Also, some technique information was given about characterization tests in subtitles.

2.3.1. Scanning Electron Microscopy (SEM)

SEM images provided detailed information about the surface topography and morphology of the sample. Features such as texture, roughness, cracks, pores, grains, and surface contaminants can be observed. These features can provide insights into the composition, structure, and properties of the sample. A good imaging requires coating the sample with a thin layer of conductive material, which is gold to improve image quality and reduce charging effects. The SEM analysis was done with FEI QUANTA 250 FEG. It can image the structures of materials at micro and nano dimensions. SEM images can also be used to analyze the elemental composition of the sample through techniques such as energy-dispersive X-ray spectroscopy (EDS). EDS detects characteristic X-ray emissions from the sample when it is bombarded with electrons, allowing for the identification and mapping of elements present in the sample.

2.3.2.UV-Visible Spectrophotometer Analysis (UV-Vis)

The UV absorbance spectrum of metal oxide nanoparticles involves considering the specific characteristics of the nanoparticles and understanding how they interact with light in the UV-visible range. UV-Visible spectral analysis was carried out with using a Shimadzu UV-2550 UV-VIS spectrophotometer. Quartz cuvette was used for all spectral analysis which have light path 1 mm with width 1 cm. Also, range of 200-800 nm was used for scanning. Generally, water and acetone was used as solvent for all analysis.

2.3.3.FTIR-Attenuated Total Reflectance Analysis (FTIR)

FTIR spectra provide information about the vibrational modes of chemical bonds within the nanoparticles. Signals in the spectrum correspond to specific functional groups present in the material. The intensity of absorption peaks may correlate with the concentration or abundance of the corresponding functional groups in the sample. Fourier Transform Infrared-Attenuated Total Reflectance (FTIR-ATR) (Perkin Elmer) was used in order to analyze.

2.3.4. Energy Dispersive X-Ray Fluorescence (EDXRF)

Energy Dispersive X-ray Fluorescence (EDXRF) analysis provides qualitative and quantitative information about the elemental composition of the nanoparticles. The results typically include the presence and concentration of major elements as well as trace elements present in the sample. EDXRF spectra display characteristic signals corresponding to the X-ray fluorescence emitted by different elements in the sample. Each signal is associated with a specific element, and its energy corresponds to the characteristic X-ray emission energy of that element. Spectro IQ II was used to perform elemental analysis of samples.

2.3.5. Dynamic Light Scattering Analysis (DLS)

The size intensity distribution (DLS) graph of metal oxide nanoparticles obtained from (DLS) involves understanding the relationship between the intensity of scattered light and the size distribution of the nanoparticles. DLS is a technique used to measure the size distribution of particles in a suspension by analyzing the fluctuations in the intensity of light scattered by the particles as they undergo Brownian motion. The analysis were done with ultrapure water and acetone as a solvent. Zeta sizer Nano ZS, Malvern instrument was used in order to determine average size and zeta potential of the products. Quartz cuvettes and disposable cuvettes were used in size measurements, and folded capillary cell was used in zeta potential measurements.

2.3.6. Nuclear Magnetic Resonance Analysis (NMR)

Nuclear Magnetic Resonance (NMR) spectrum involves understanding how different nuclei within a molecule respond to a magnetic field and radiofrequency radiation. NMR spectroscopy relies on the interaction of atomic nuclei with a strong magnetic field and radiofrequency (RF) radiation. Products were analyzed with ^{1}H NMR (400 MHz) with using $CDCl_3$ as deuterium solvent.

2.3.7.Atomic Force Microscopy (AFM)

AFM images provide high-resolution information about the surface morphology of the nanoparticles. The image displays variations in height (or depth) across the surface, revealing features such as nanoparticles, aggregates, pores, and surface roughness. By analyzing AFM images, it can be can measured the size and distribution of the metal oxide nanoparticles. AFM images can also revealed information about the shape of the nanoparticles, whether they are spherical, rod-shaped, or irregular. AFM analysis was done with Bruker-MMSPM Nanoscope 8.

2.3.8.Brunauer-Emmett-Teller Surface Area Analysis (BET)

BET (Brunauer-Emmett-Teller) analysis of metal oxide nanoparticles involves understanding the specific surface area, pore size distribution, and pore volume of the nanoparticles. BET analysis provides information about the specific surface area of the nanoparticles, which is a measure of the total surface area per unit mass of the material. The surface area of metal oxide nanoparticles and products were analyzed with Micromeritics 3Flex at 90 °C.

2.3.9. X-Ray Diffraction (XRD)

X-ray diffraction (XRD) of metal oxide particles involves understanding the crystalline structure, phase composition, crystallographic orientation, and particle size of

the nanoparticles. The diffractogram displays reflections corresponding to the crystallographic planes of the material. Each reflection represents the constructive interference of X-rays scattered by the crystal lattice planes. The position of diffraction peaks 2θ in the XRD corresponds to the spacing between crystal lattice planes, which is determined by Bragg's law: $n\lambda = 2d \sin\theta$, where λ is the wavelength of the X-rays, d is the interplanar spacing, θ is the diffraction angle, and n is the order of diffraction. Philips X'Pert Pro was used for the XRD analysis.

2.3.10.UV-Weathering Test

UV weathering test, the "delta *E*" (ΔE) value refers to the change in color (or color difference) of a material before and after exposure to ultraviolet (UV) radiation. It is a measure of the extent of color change or fading that occurs because of UV exposure. UV weathering test results involve assessing the changes in material properties, performance, and appearance of a sample after exposure to simulated or real-world UV radiation. In this test, the QUV accelerated tester was used.

CHAPTER 3

RESULTS AND DISCUSSIONS

3.1. Characterization of Metal Oxide Nanoparticles

Elemental, spectroscopic and microscopic characterizations of the metal oxides were done by XRD, XRF, UV-Vis and SEM methods.

3.1.1. EDXRF Analysis

The material characterizations were performed to identify impurities and chemical composition present in the nanoparticles (Table 3.1,Table 3.2,Table 3.3). The results came out as expected. The presence of aluminum could be due to contamination from the sample preparation process or the environment. Aluminum is a common element that can be introduced from laboratory equipment, sample holders, or even airborne particles. Tantalum contamination is less common. It could occur if there is contact with tantalum-containing equipment or if the sample has been in an environment where tantalum is present.

Table 3.1. Elemental analysis of MnO_2.

Element	(w/w) %	Oxide	(w/w) %
Mn	65.3	MnO	84.3
Al	6.3	Al_2O_3	12.0
Ta	1.9	Ta_2O_5	2.3

Table 3.2. Elemental analysis of TiO_2.

Element	(w/w) %	Oxide	(w/w) %
Ti	54.2	TiO	84.3
Al	4.0	Al_2O_3	7.6
Ta	1.0	Ta_2O_5	1.3

Table 3.3. Elemental analysis of CeO_2.

Element	(w/w) %	Oxide	(w/w) %
Ce	85.3	Ce	85.3
Al	6.4	Al_2O_3	12.0
Ta	2.0	Ta_2O_5	2.4

3.1.2. XRD

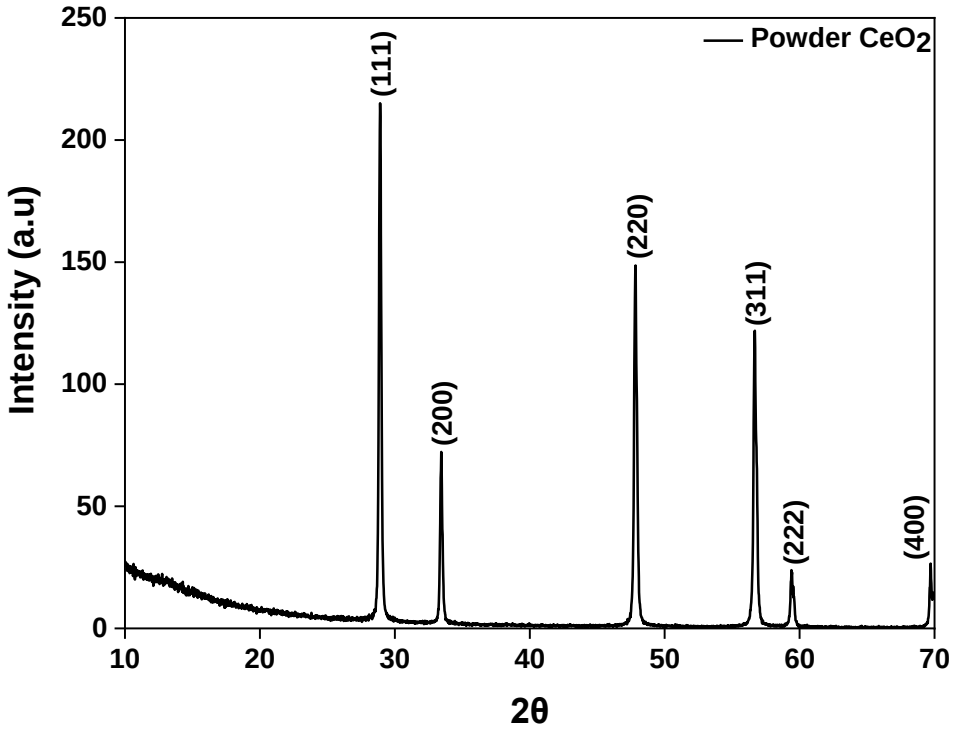

Figure 3.1. XRD of Powder CeO_2.

Figure 3.1 shows the powder XRD pattern of the cerium oxide nanoparticle. The characteristic signals are located at 2ϑ = 28.5, 33.9, 47.8, 56.2, 58.5 and 69.10 and they correspond to (111), (200), (220), (311), (222) and (400) lattice planes, respectively, which are typical of face-centered cubic fluorite structure of CeO_2 (space group: F*m*3*m*) with lattice constant a = 5.4 Å, which is in agreement with the JCPDS file no 75-0076 for CeO_2 .[43,44] (96-156-2990)

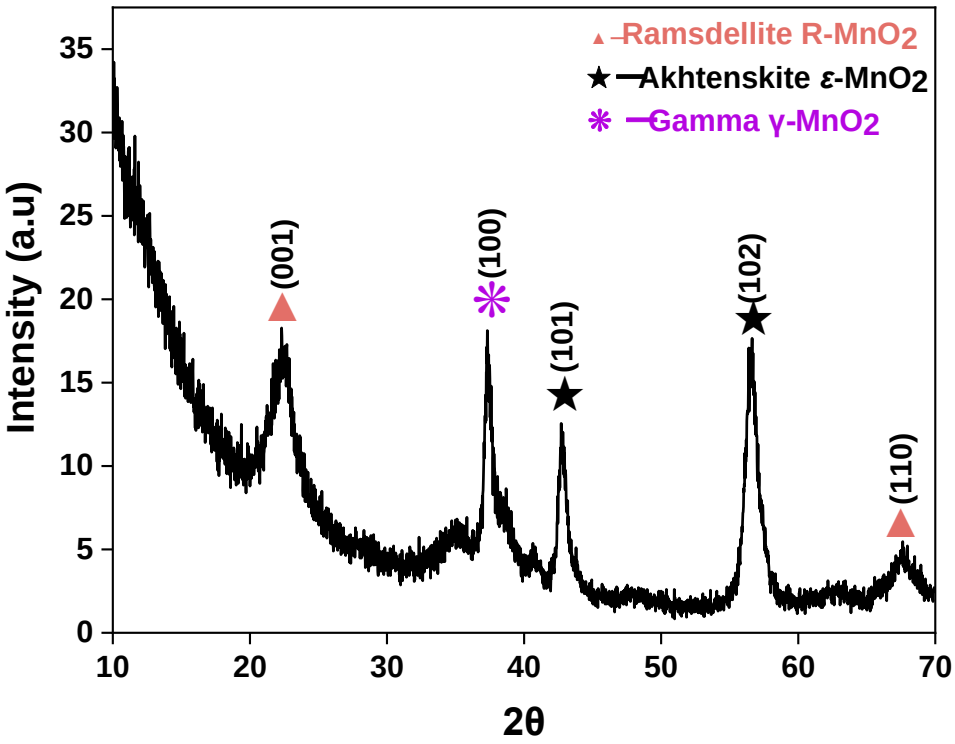

Figure 3.2. XRD of Powder γ-MnO_2.

For γ-MnO_2 (gamma manganese dioxide), the XRD reflections correspond to its disordered and mixed-phase structure, which includes both tunneled and layered arrangements. Typical XRD reflections for γ-MnO_2 include a series of broad signals, indicative of its less crystalline nature compared to other polymorphs. Figure 3.2 shows the XRD signals indicate a mixture of three phases of: akhtenskite (ε-MnO_2), ramsdellite (R-MnO_2) and gamma (γ-MnO_2) polymorphs of MnO_2. The broad reflection at 2θ angle of 22.1° corresponds to the (001) and 66.3° (110) plane of ramsdellite (R-MnO_2) phase. Ramsdellite (R-MnO_2) has an orthorhombic structure. The gamma manganese dioxide has reflection at 37.5° (2θ) with a *d*-spacing of approximately 2.4 Å. The diffraction signals found at angles of 42.6° and 56.4° are presumably from the akhtenskite (ε-MnO_2) phase with (101) and (102) planes, respectively. Akhtenskite (ε-MnO_2) is a metastable polymorph of MnO_2 with hexagonal structures.[42]

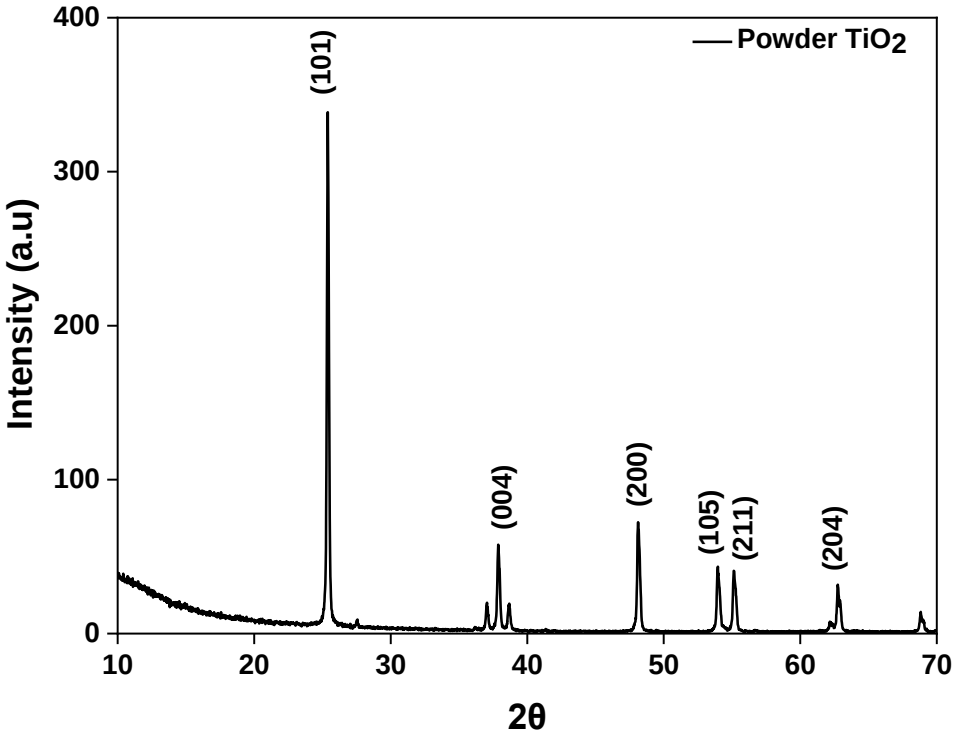

Figure 3.3. XRD of Powder TiO_2.

The characteristic XRD signals of anatase emerged with the 2ϑ values centered at 25.31°, 37.80°, 48.04°, 53.89°, 55.06°, and 62.69°, which corresponded to the crystal planes (101), (004), (200), (105), (211), and (204), respectively.[37] The result indicated the presence of the anatase phase (Figure 3.3. XRD of Powder TiO_2..

3.1.3. UV-Vis Spectroscopy Analysis

Metal oxide nanoparticles can exhibit unique electronic properties due to quantum confinement effects, surface plasmon resonance, or bandgap transitions, depending on their size, shape, and composition. The position (wavelength) and intensity (absorbance) of these peaks provide information about the electronic transitions occurring within the nanoparticles. Metal oxide nanoparticles, especially those with sizes on the order of a few nanometers, may exhibit quantum size effects. These effects can lead to shifts in the absorption spectrum compared to bulk materials. Smaller nanoparticles generally have higher energy bandgaps and exhibit absorption in the UV region. Metal oxide

nanoparticles with semiconductor properties, titanium dioxide (TiO_2), cerium oxide (CeO_2) and manganese dioxide (MnO_2), may exhibit absorption due to bandgap transitions. The absorption edge of these materials typically occurs in the UV region and is associated with electron transitions from the valence band to the conduction band. If the metal oxide nanoparticles are surface-functionalized or coated with ligands, organic molecules, or other materials, additional absorption features may be observed in the spectrum due to the electronic transitions associated with these surface modifications. According to the UV absorbance spectra of metal oxides, the max wavelength value of CeO_2 is 820 nm with very low intensity (Figure 3.4), MnO_2 has max absorbance value at 581 nm (Figure 3.5), and TiO_2 has 435 nm (Figure 3.6). The UV absorbance was examined with the water as a solvent.

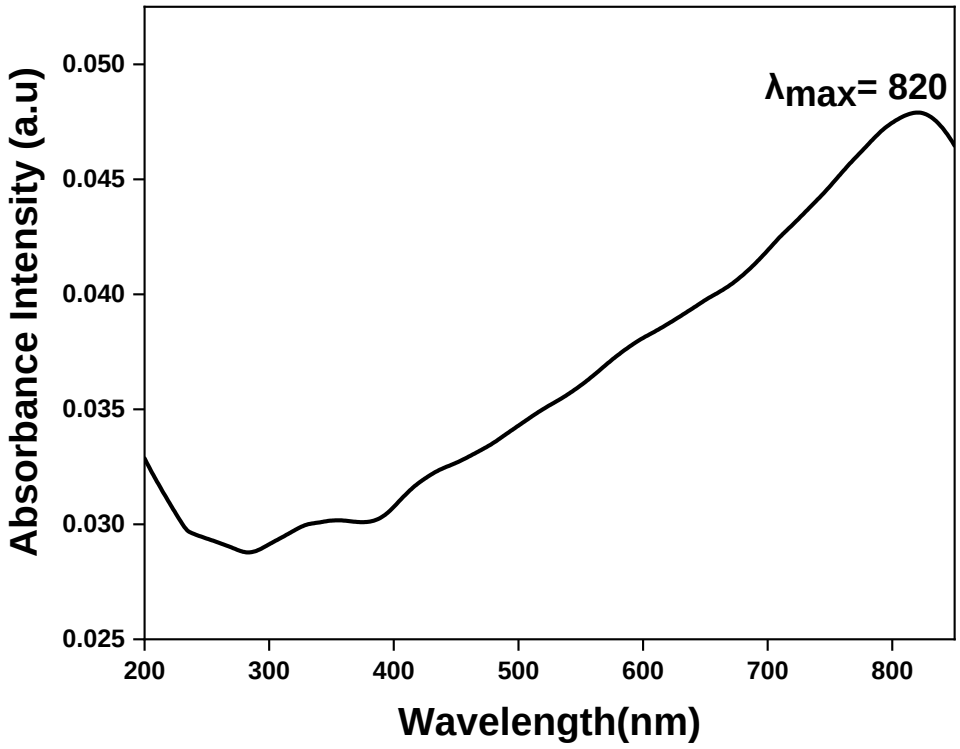

Figure 3.4. The UV absorbance spectrum of CeO_2 (1.4×10^{-3} M).

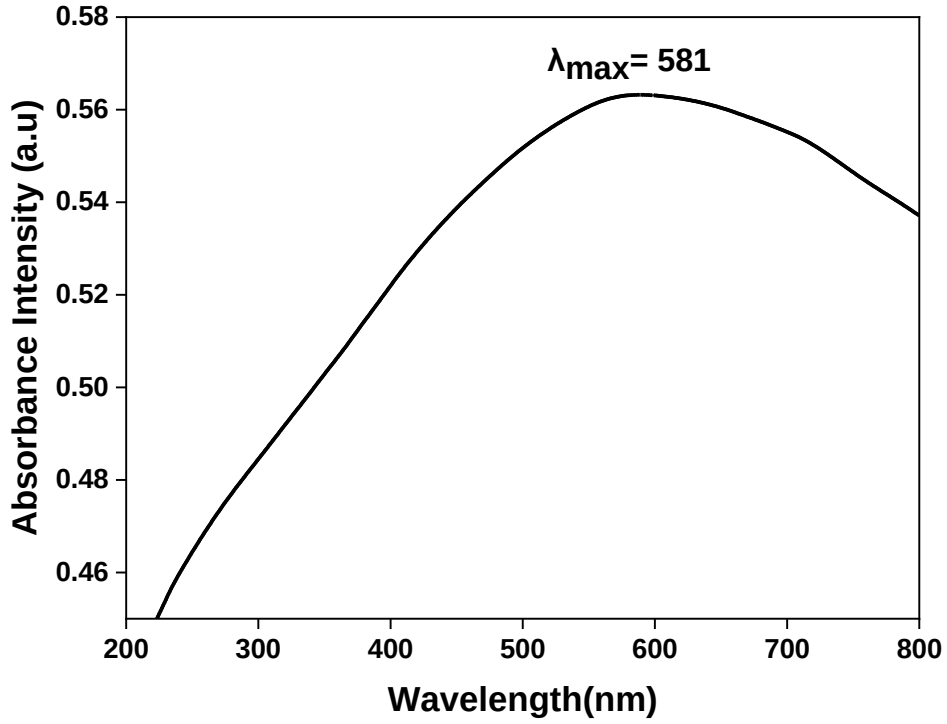

Figure 3.5. The UV absorbance spectrum of MnO_2 (1.6×10^{-3} M).

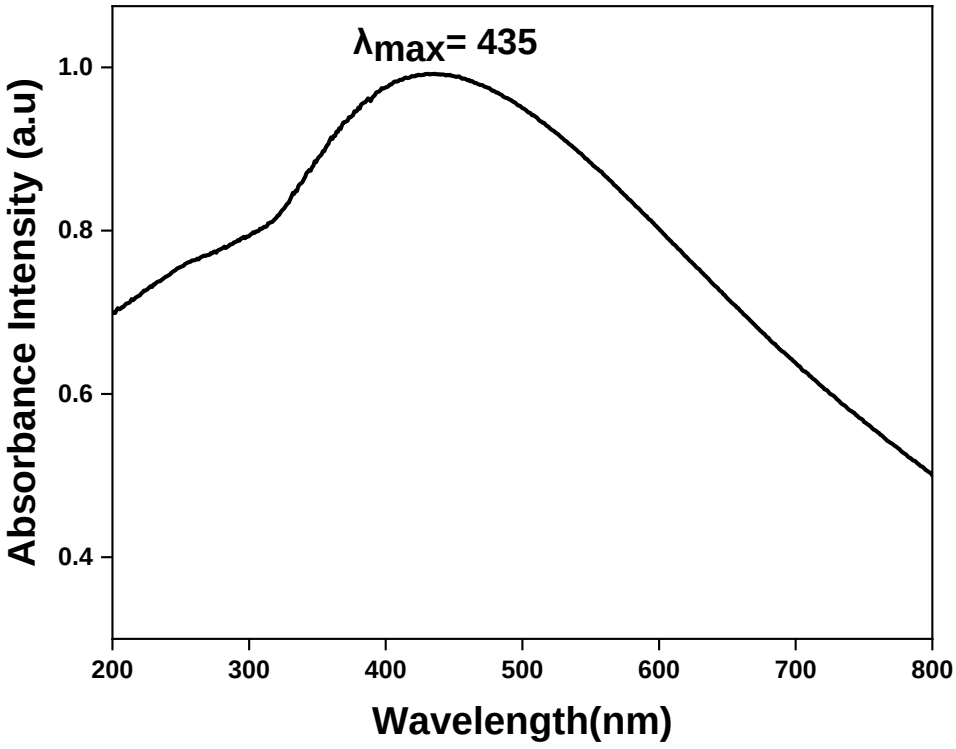

Figure 3.6. The UV absorbance spectrum of TiO_2 (7.5×10^{-3} M).

3.1.4. BET Analysis

BET analysis can provide information about the distribution of pore sizes within the nanoparticles. The pore volume represents the total volume of void space within the nanoparticles and is related to the porosity and pore structure of the material. By analyzing the results of BET analysis, it gave valuable insights into the surface area, pore structure, and porosity of metal oxide nanoparticles. The powder titanium dioxide has higher surface area, nearly 10 m^2/g and pore size was 61 Å (Table 3.4). The cerium oxide's surface area was 3 m^2/g and the pore size was measured as 84 Å (Table 3.4). The manganese dioxide has lowest surface area and pore size, which are 1 m^2/g and 38 Å, respectively (Table 3.4).

Table 3.4. BET surface area, pore volume and pore size values of powder metal oxides

Sample	**BET Surface Area (m^2 /g)**	**Pore Size (Å)**
Powder TiO_2	10	61
Powder CeO_2	3	84
Powder MnO_2	1	38

3.1.5. DLS/Size Analysis

The *y*-axis of the DLS graph represents the intensity of scattered light detected by the instrument. This intensity is proportional to the number of particles contributing to the scattering signal. The *x*-axis of the DLS graph represents the hydrodynamic diameter of the particles in the suspension. The hydrodynamic diameter is a measure of the effective size of the particles in solution, taking into account their Brownian motion and interactions with the surrounding solvent molecules. The signals in the DLS result

correspond to particle size populations within the suspension. The position of each peak on the *x*-axis indicates the average hydrodynamic diameter of particles in that size range, while the height or area of the peak reflects the relative abundance or intensity of particles of that size. The width of the peaks in the DLS graph reflects the polydispersity of the nanoparticle sample, which is a measure of the distribution of particle sizes. A narrow distribution suggests a presence of more monodisperse sample with particles of similar sizes, while a broad peak suggests a more polydisperse sample with a wider range of particle sizes. In some cases, particularly for metal oxide nanoparticles, aggregates or agglomerates of particles may form in solution due to van der Waals forces or electrostatic interactions. These aggregates/agglomerates may appear as larger peaks or shoulders in the DLS graph at sizes larger than the individual nanoparticles (Figure 3.7). The analysis was done with ultra pure water as a solvent for the metal oxide nanoparticle analysis.

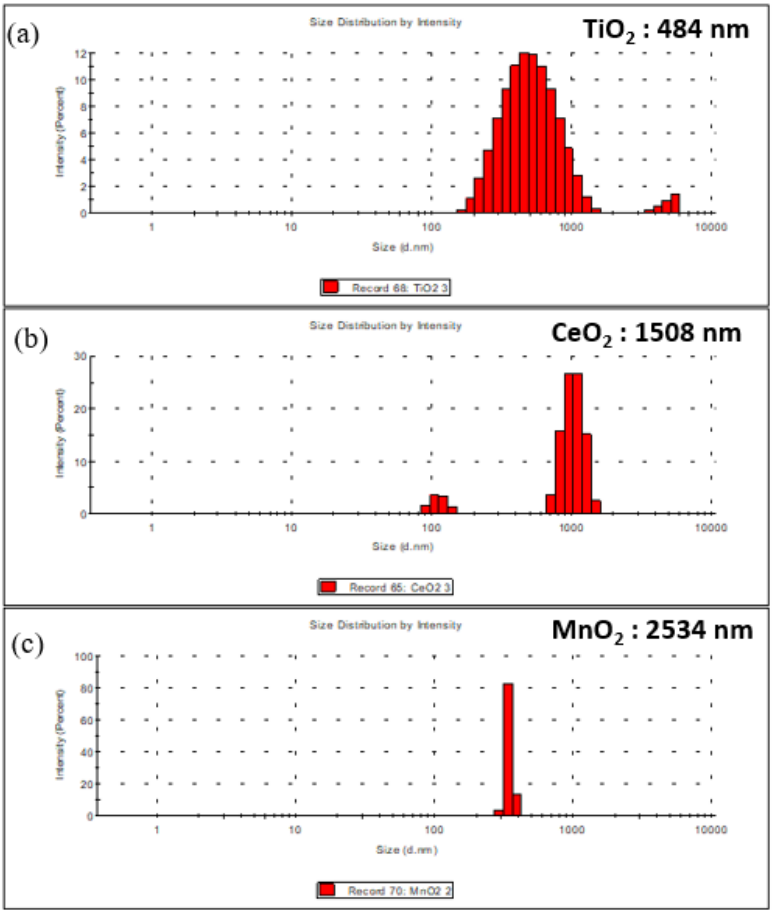

Figure 3.7. Intensity size distributions of metal oxides a) TiO_2 b) CeO_2 c) MnO_2.

3.1.6. SEM Images

Figure 3.8 shows the images of titanium dioxide nanoparticles, Figure 3.9 represents the manganese dioxide nanoparticle images and Figure 3.10 shows the cerium oxide nanoparticles.

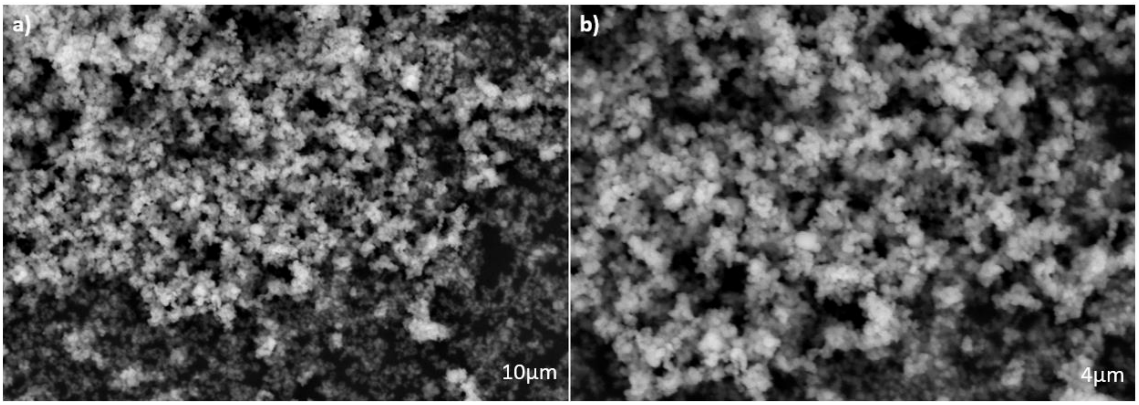

Figure 3.8. SEM images of the TiO_2 powder at a) 15k × and b) 25k × magnification.

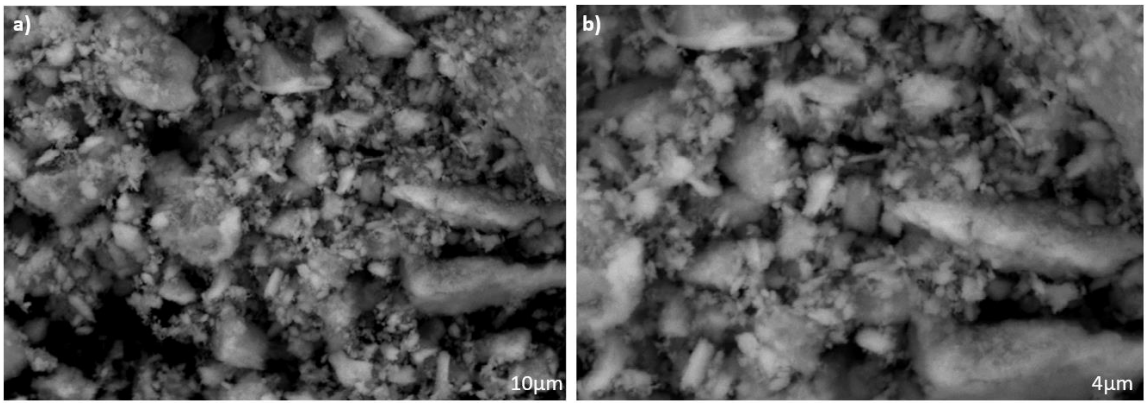

Figure 3.9. SEM images of the MnO_2 powder at a) 15k × and b) 25k × magnification.

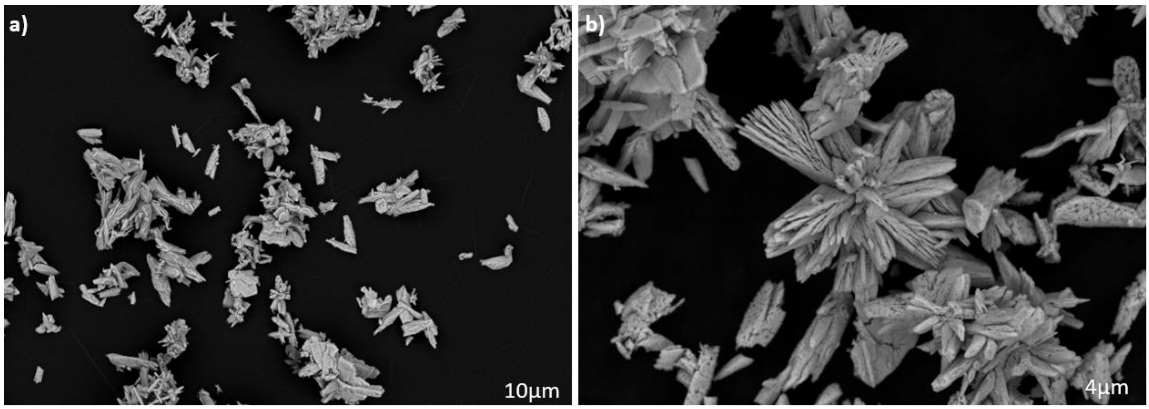

Figure 3.10. SEM images of the CeO_2 powder at a) 50k × and b) 5k × magnification.

3.1.7. EDS

EDS detects characteristic X-rays emitted by the sample when it is bombarded with electrons, allowing for the identification and mapping of elements present in the sample (Figure 3.11,Figure 3.12,Figure 3.13). The analysis approved the elemental content of the used metal oxide particles.

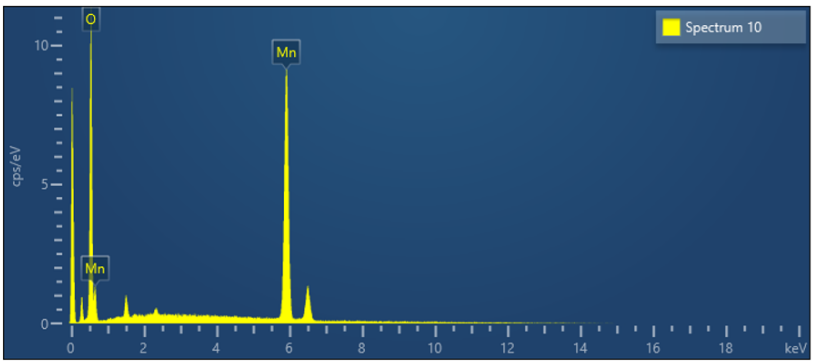

Spectrum 10							
Element	Line Type	Weight %	Weight % Sigma	Atomic %	Oxide	Oxide %	Oxide % Sigma
O	K series	22.55	0.19	50.00			
Mn	K series	77.45	0.19	50.00	MnO	100.00	0.24
Total		100.00		100.00		100.00	

Figure 3.11. The EDS graph of MnO_2.

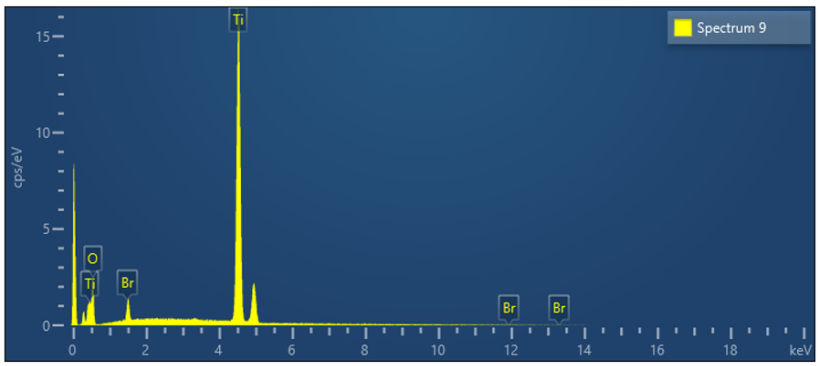

Spectrum 9							
Element	**Line Type**	**Weight %**	**Weight % Sigma**	**Atomic %**	**Oxide**	**Oxide %**	**Oxide % Sigma**
O	K series	38.88	0.21	66.01			
Ti	K series	58.20	0.22	33.00	TiO2	97.08	0.36
Br	L series	2.92	0.12	0.99		0.00	0.12
Total		100.00		100.00		97.08	

Figure 3.12. The EDS graph of TiO_2.

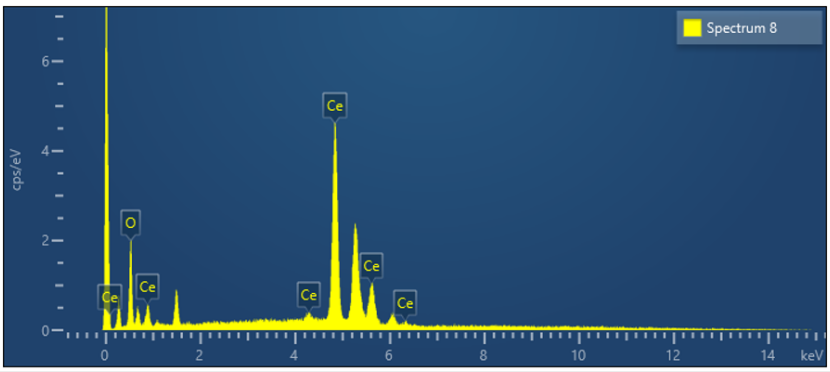

Spectrum 8							
Element	**Line Type**	**Weight %**	**Weight % Sigma**	**Atomic %**	**Oxide**	**Oxide %**	**Oxide % Sigma**
O	K series	14.62	0.20	60.00			
Ce	L series	85.38	0.20	40.00	Ce2O3	100.00	0.23
Total		100.00		100.00		100.00	

Figure 3.13. The EDS graph of CeO_2.

3.2.Characterizations of Silane Modified Metal Oxides and PAE Resin

3.2.1. FTIR Analysis

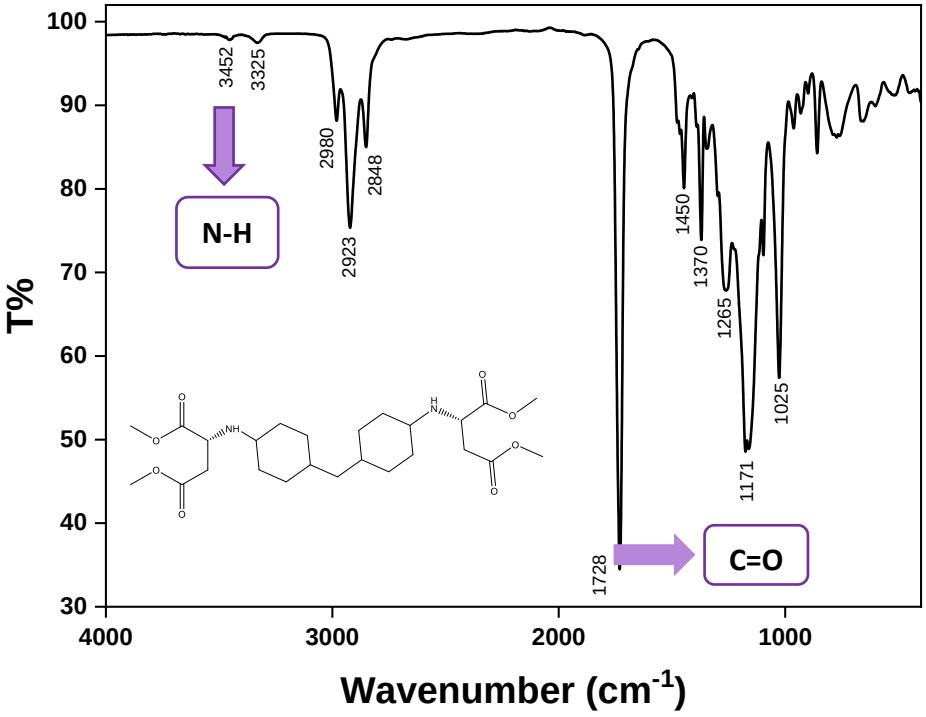

Figure 3.14. FTIR transmittance spectrum of PAE Resin (Desmophen1420).

3452 cm^{-1}: N-H stretching, primary amine, 3325 cm^{-1}: N-H stretching, secondary amine, 2980-2848 cm^{-1}: C-H stretching, alkane, 1728 cm^{-1}: C=O stretching, ester, 1450 cm^{-1}: C-H bending, alkane (methyl group), 1370 cm^{-1}: C-H bending, methylene group, 1265 cm^{-1}: C-N stretching, amine, 1171 cm^{-1}: C-O stretching, ester, 1025 cm^{-1}: C-O-C stretching, ester. These signals confirm the chemical structure of Desmophen 1420, as expected (Figure 3.14).

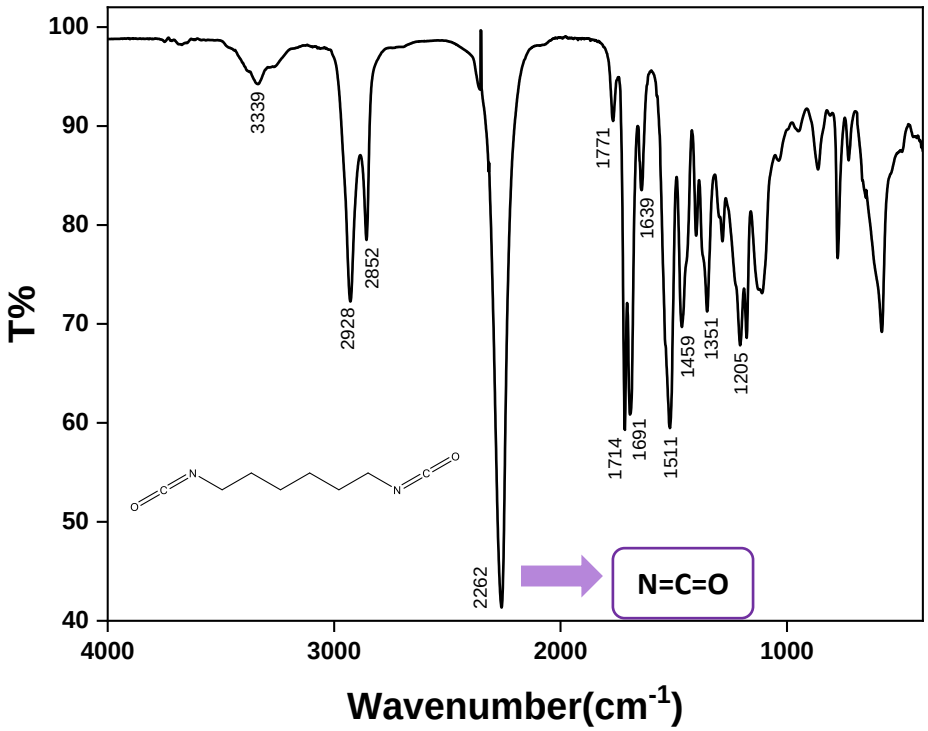

Figure 3.15. FTIR transmittance spectrum of isocyanate (Tolonate XF 450).

There are signals at the 3339 cm^{-1}: N-H stretching, secondary amine, 2928-2852 cm^{-1}: C-H stretching, alkane, 2262 cm^{-1}: N=C=O stretching, isocyanate, 1771 cm^{-1}: C=O, conjugated anhydride, vinyl or phenyl ester, 1714 cm-1: C=O stretching, ester, 1691 cm^{-1}: C-N stretching, imine, 1639 cm^{-1}: N-H bending, amine group (urea), 1511 cm^{-1}: N-O stretching, nitro, 1459 cm^{-1}: C-H bending, alkane (methyl group), 1351 cm^{-1}: C-H bending, methylene group, 1205 cm^{-1}: C-O-C stretching. These signals match the functional groups within the Tolonate XF 450. Especially, the N=C=O (isocyanate) signal at the 2262 cm^{-1} is significant for the Tolonate XF 450 (Figure 3.15).

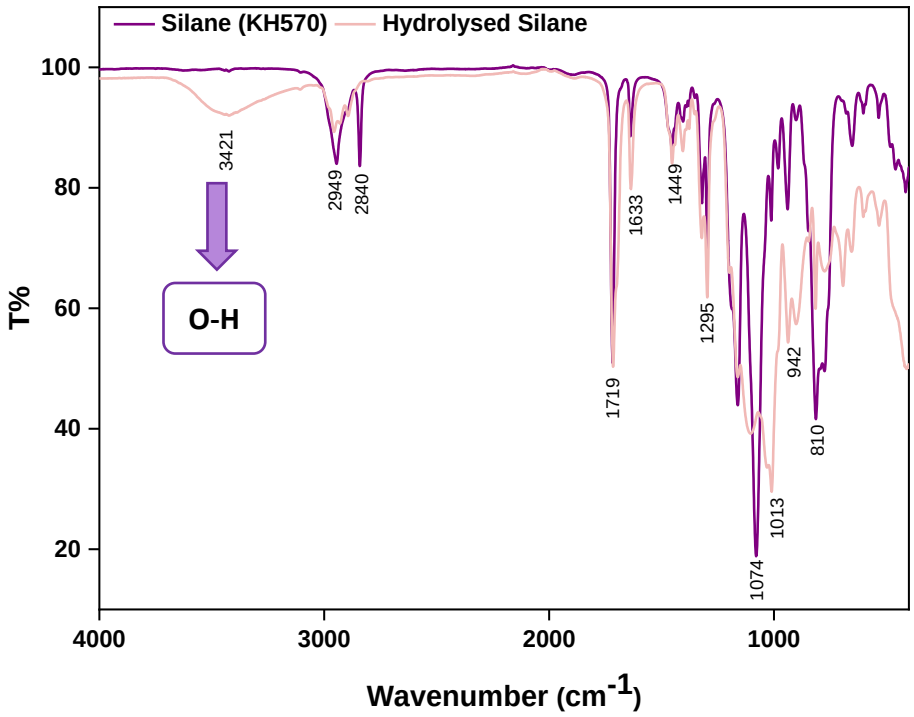

Figure 3.16. FTIR transmittance spectra of Silane (KH570) and Hydrolyzed Silane.

The signals at the 3427 cm^{-1}: O-H, alcohol, 2949-2840 cm^{-1}: C-H, alkane, alkene ,1719 cm^{-1}: C=O stretching, ester, 1633 cm^{-1}: C-H bending, alkane (methyl group), 1449 cm^{-1}: C-H bending, methylene group, 1295 cm^{-1}: stretching C-O, ether, 1074 cm^{-1}: Si-O-C, 1013 cm^{-1}: Si-O-CH_3, 810 cm^{-1}: Si-H represented. The O-H signal at the 3421 cm^{-1} shows that the hydrolysis of the silane was carried out (Figure 3.16).

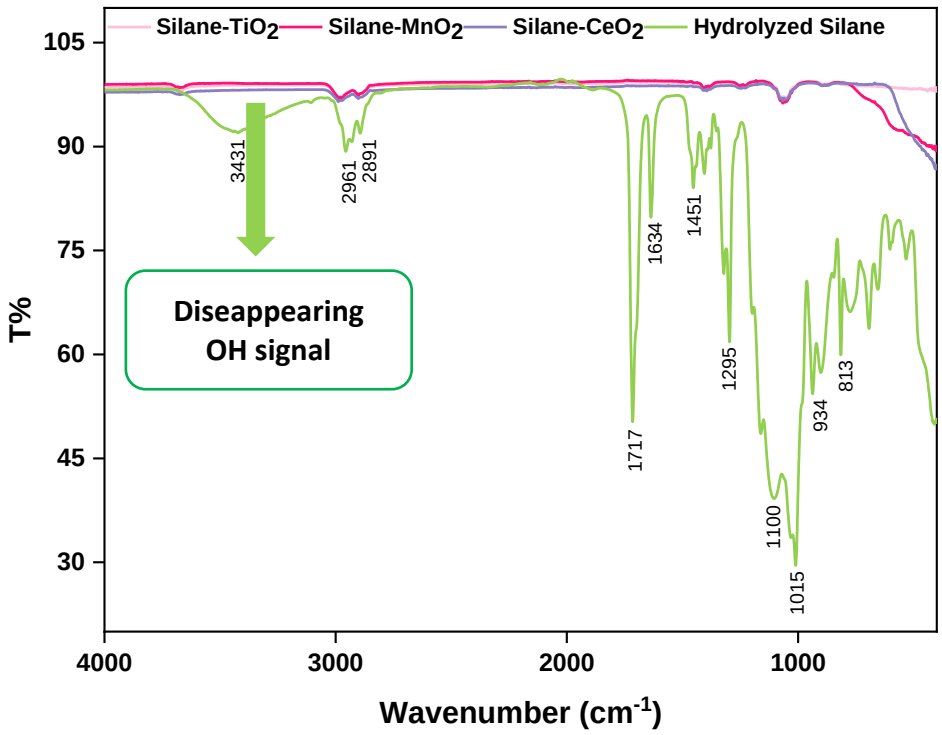

Figure 3.17. FTIR transmittance spectra of Hydrolyzed silane, silane-modified TiO_2, silane-modified MnO_2, silane-modified CeO_2.

3431 cm^{-1}: O-H stretching, alcohol, 2968,2908 cm^{-1}: C-H stretching, alkane and alkene, 1396 cm^{-1}: C-H bending, alkane (methyl group), 1237 cm^{-1}: C-O stretching, ether, 1051 cm^{-1}: Si-O-CH_3. The broad OH signal at 3431 cm^{-1} has decreased, that means the OH bonding to the surface of the metal oxide particles (Figure 3.17).

3.2.2. NMR Analysis

The Figure 3.18 shows the ^1H NMR spectrum of PAE resin (Desmophen1420). According to the spectrum, the signals at the 3.7 ppm and 3.8 ppm, referred to the 1,31,11 and 35 numbered hydrogens which are, neighboring the Oxygen. The peaks at the 2.7 ppm represents the 7 and 27 numbered hydrogens, which are near the (O=C) carboxyl groups. The peaks at the 2.6 ppm represents the 12 and 22 numbered hydrogens, which are near the (NH) amine groups. At 1.3 ppm, there are ethyl ester groups. The hydrogens between the oxygen and amine groups, were shown at the 4.2 ppm.

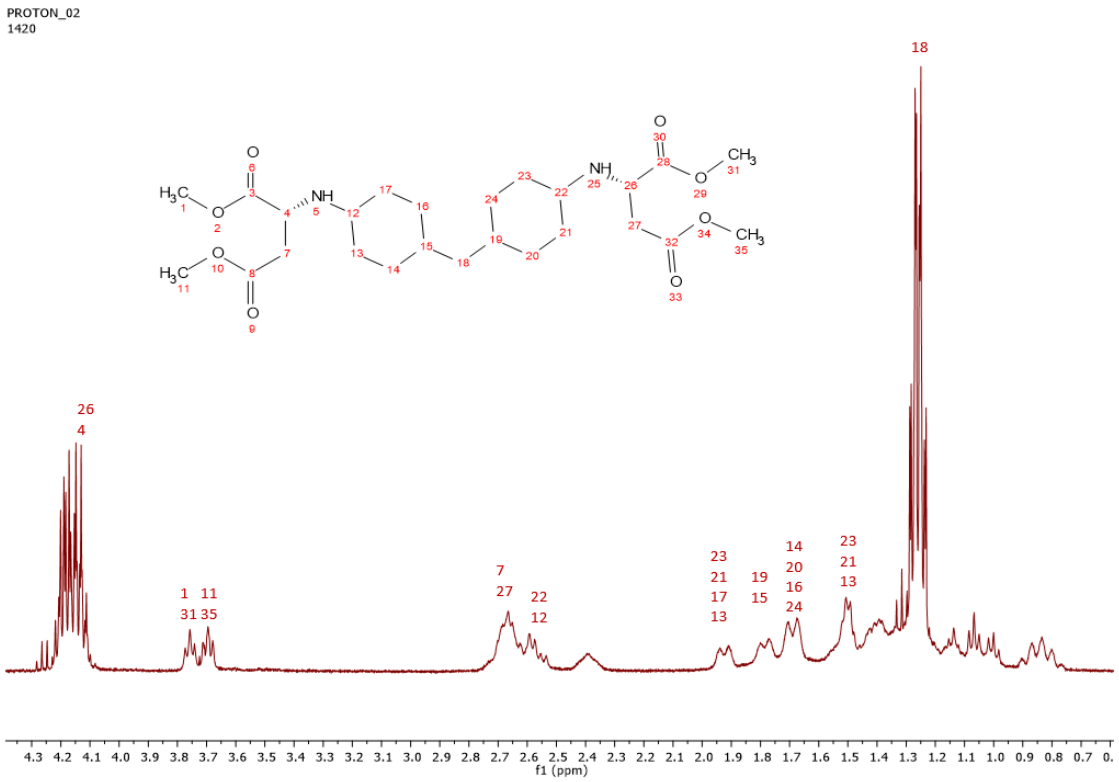

Figure 3.18.NMR spectrum of PAE resin.

3.2.3. BET Analysis

According to the Table 3.5. BET surface area, pore volume and pore size values of silane modified metal oxide particles, the surface area of powder TiO_2 and CeO_2 have remained same. Several factors may be explained by these results: The silane molecules might form a monolayer or a thin coating on the surface of the titanium dioxide particles. This thin layer would not significantly add to the overall surface area since it is just covering the existing surface rather than creating new surface area. If the surface is fully saturated with silane molecules, the overall surface area available for nitrogen adsorption during BET analysis remains unchanged. Silane modification could cause the existing pores to widen. This can happen if silane molecules attach to the inner walls of the pores, causing the pores to expand in diameter. This would explain the increase in pore size from 61 Å to 88 Å. The interaction between silane molecules and the titanium dioxide surface might lead to structural rearrangements that expand the pore size without creating new

pores or additional surface area. Silane molecules are relatively small compared to the dimensions of the pores. When these molecules attach to the pore walls, they can increase the effective diameter of the pores by adding a thin layer to the walls. On the contrary, the silane-modified MnO_2 has bigger surface area, pore size and pore volume than the powder MnO_2. There may be some explanations of this phenomenon: The introduction of silane molecules onto the surface of MnO_2 can create additional surface roughness. This increased roughness can provide more surface area for adsorption, thus increasing the BET surface area measurement. Silane modification may result in the formation of a more nanostructured or fractal-like surface, which inherently has a higher surface area compared to the relatively smooth, unmodified MnO_2. The chemical interaction between silane molecules and the MnO_2 surface can lead to the formation of new pores or the expansion of existing pores. This process can occur if silane molecules penetrate the surface and cause structural changes at the nanoscale, thereby increasing the overall pore volume. Silane molecules could potentially act as spacers between MnO_2 particles or agglomerates, leading to the widening of existing pores. The result is an increase in both the average pore size and the total surface area accessible to nitrogen gas during BET analysis. Silane modification can improve the dispersion of MnO_2 particles by reducing particle agglomeration. Better dispersion results in more exposed surface area, contributing to a higher BET surface area measurement.

Table 3.5. BET surface area, pore volume and pore size values of silane modified metal oxide particles

Sample	**BET Surface Area (m^2 /g)**	**Pore Size (Å)**
Silane-TiO_2	10	62
Silane-CeO_2	3	77
Silane-MnO_2	29	54

3.2.4. DLS/Size Analysis

The Figure 3.19 represents the size intensity distribution graphs of silane modified TiO_2, CeO_2 and MnO_2, respectively. For the analysis of silane modified nanoparticles the acetone was used as dispersing medium. Non-modified metal oxide particles often have a tendency to aggregate due to high surface energy and interparticle attractive forces (such as van der Waals forces). This can result in a broader size distribution, larger apparent particle sizes due to aggregation and potential presence of multiple peaks in the size distribution, indicating polydispersity. Silane modification can lead to: Narrower size distributions due to reduced aggregation, smaller apparent particle sizes as the particles are better dispersed and exist more as individual entities rather than aggregates and more monodisperse distributions with single, sharper peaks in the size intensity distribution. In summary, DLS analysis, silane-modified metal oxide particles typically exhibit a narrower, more monomodal size intensity distribution with smaller apparent particle sizes and greater colloidal stability compared to non-modified metal oxide particles. This behavior can be attributed to the reduction in aggregation and improved dispersion stability provided by the surface modification with silane agents.

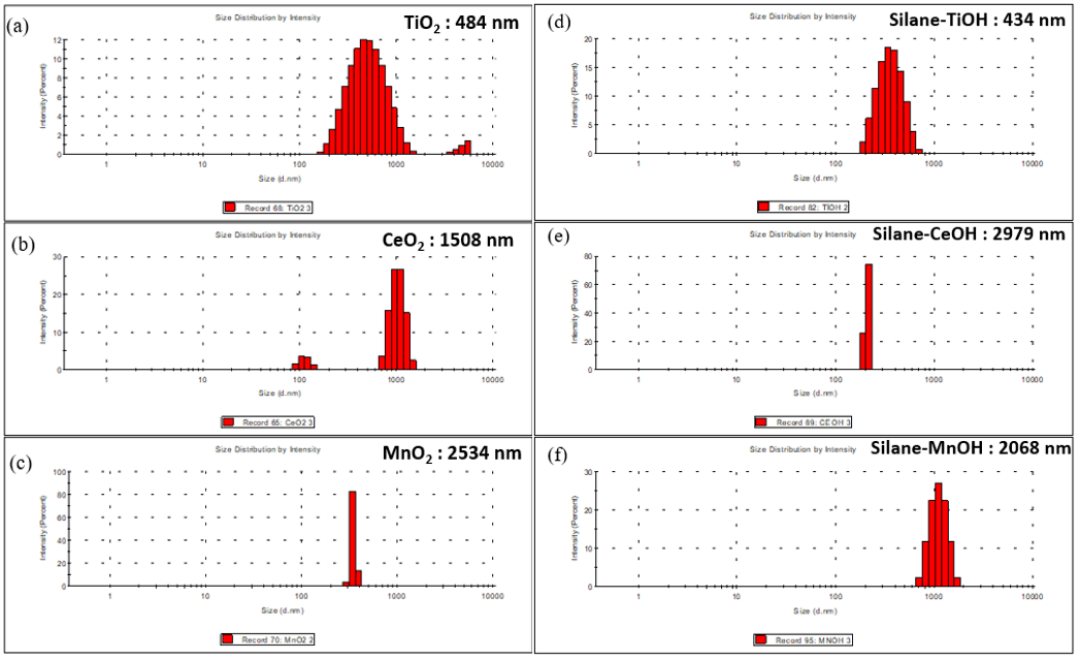

Figure 3.19. Intensity size distributions of Intensity size distributions of metal oxides a) TiO_2 b) CeO_2 c) MnO_2 d) Silane –TiO_2 e) Silane –CeO_2 f) Silane –MnO_2.

3.2.5. Zeta Potential Measurement

In the Table 3.6, zeta potential values of powder metal oxide particles and silane-modified metal oxide particles were given. The zeta potential value of powder TiO_2 was -3.39 mV, when it was modified with silane, there was a slight decrease in the negative charge. Powder CeO_2 has 1.77 mV zeta potential value, then this value has decreased to the -10.0 mV. The zeta potential value of powder MnO_2 was 6.31 mV, the silane-modified MnO_2 was 3.26 mV with a slight decrease in the positive charge. The increment in the negative charge of the silane-modified metal oxide particles, may be caused by the unreacted OH groups of the silane material or the negatively charged oxygen in the silane structure.

Table 3.6. Zeta potential values of the powder metal oxides and silane modified metal oxide particles in water at room temperature.

Sample	Zeta Potential (mV)	Sample	Zeta Potential (mV)
Powder TiO_2	-3.39	Silane-TiO_2	-2.22
Powder CeO_2	1.77	Silane-CeO_2	-10.0
Powder MnO_2	6.31	Silane-MnO_2	3.26

3.2.6. SEM Images

The surface modification of metal oxide particles can be observed. Not surprisingly, there was a change on the surfaces of the metals oxide particles due to the silane (Figure 3.20, Figure 3.21, Figure 3.22).

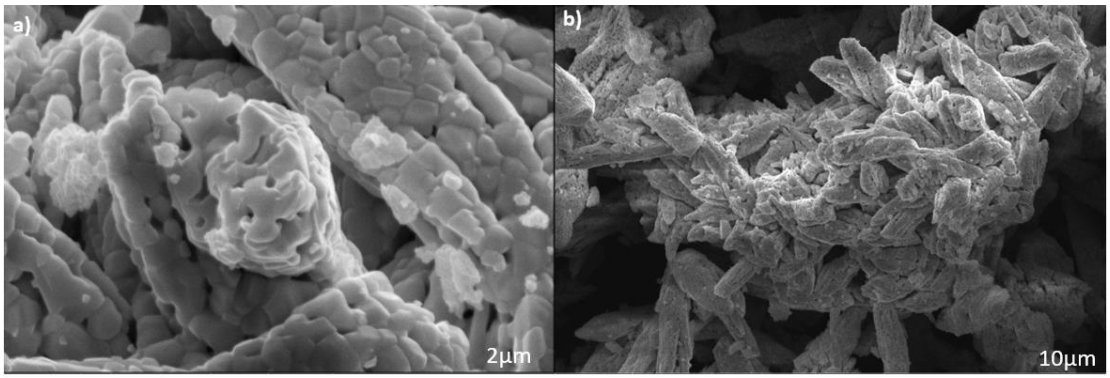

Figure 3.20. SEM images of the silane modified CeO_2 powder at a) 50k × and b) 10k × magnification.

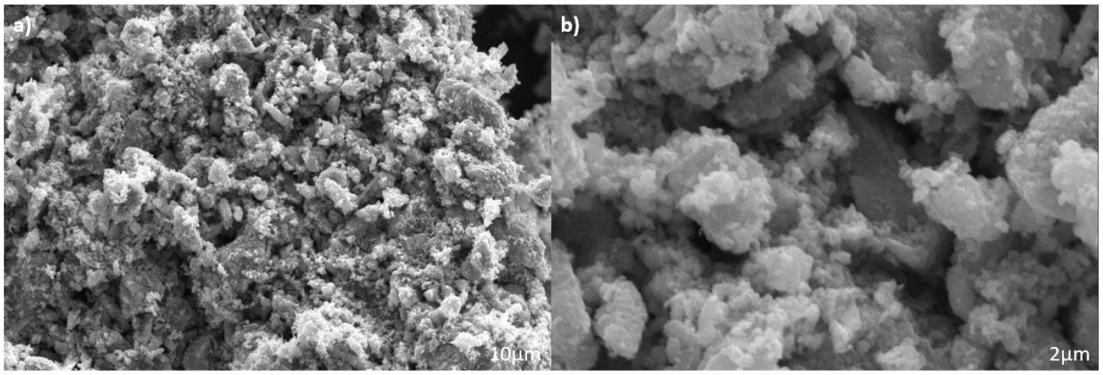

Figure 3.21. SEM images of the silane modified MnO_2 powder at a) 10k × and b) 50k × magnification.

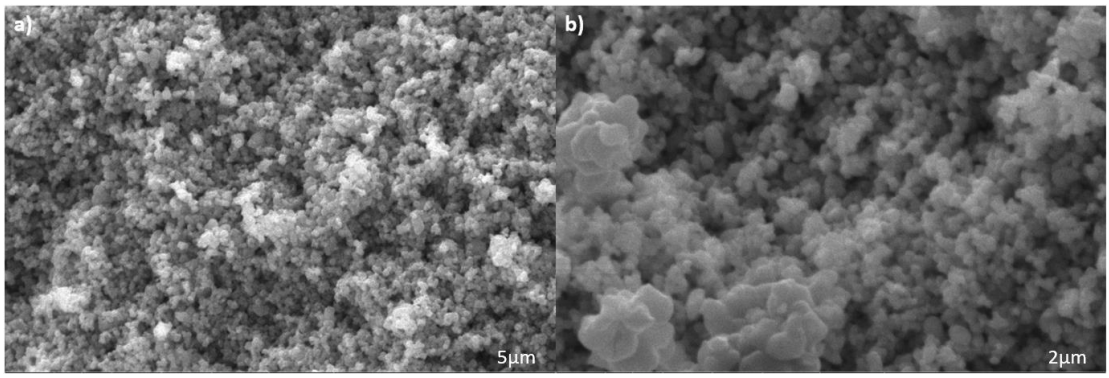

Figure 3.22. SEM images of the silane modified TiO_2 powder at a) 25k × and b) 50k × magnification.

3.3. Characterizations of metal oxide particle included PAE resins

3.3.1. FTIR Analysis

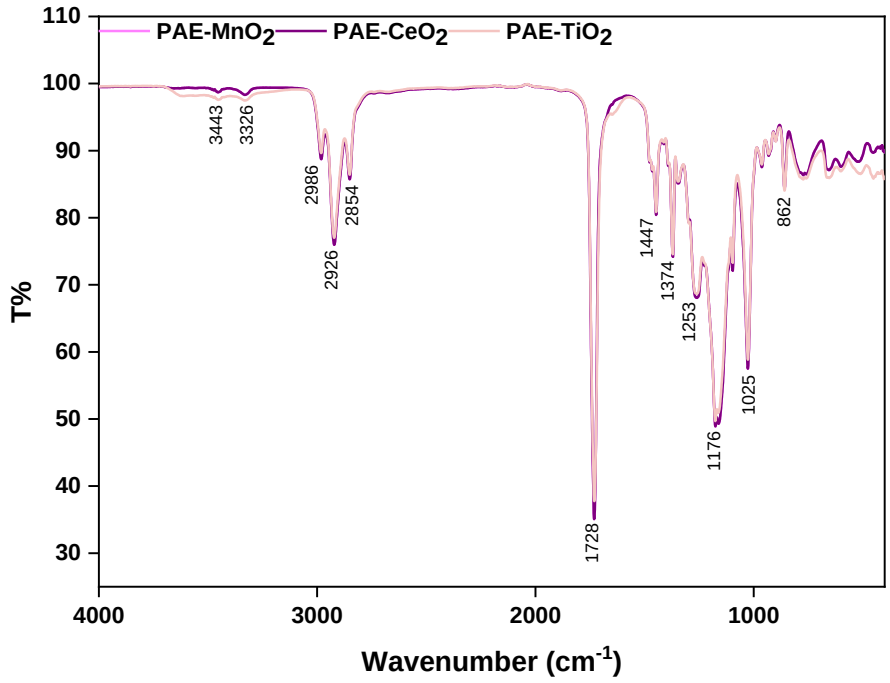

Figure 3.23. FTIR transmittance spectra of PAE Resin dispersions included metal oxides.

Figure 3.23 represents the signals, 3443 cm^{-1}: N-H stretching, primary amine, 3326 cm^{-1}: N-H stretching, secondary amine, 2986-2854 cm^{-1}: C-H stretching, alkane, 1728 cm^{-1}: C=O stretching, ester, 1447 cm^{-1}: C-H bending, alkane (methyl group), 1374 cm^{-1}: C-H bending, methylene group, 1253 cm^{-1}: C-N stretching, amine, 1176 cm^{-1}: C-O stretching, ester, 1025 cm^{-1}: C-O-C stretching, ester, 862 cm^{-1}: Si-H stretching.

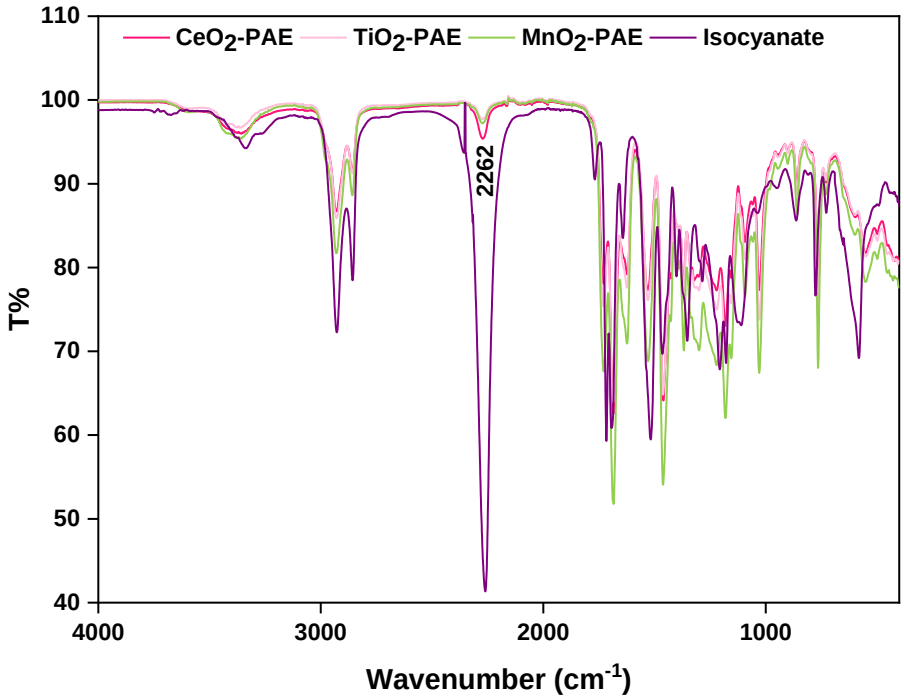

Figure 3.24. FTIR spectra of metal oxide particles included PAEPU film.

The intensity of N=C=O signal at the 2262 cm^{-1} was decreased significantly when reacted with the polyaspartic ester resin (Figure 3.24). This shows almost all reactive groups (N=C=O) were used to crosslinked with the PAE resin to form a film.

3.3.2. XRD

According to the XRD signals of the films, the TiO_2 and CeO_2 included PAE films showed crystallographic characters similar to TiO_2 and CeO_2 powder (Figure 3.26,Figure 3.27). However, the distinct XRD signals of MnO_2 have disappeared in the PAE film (Figure 3.25). The polymer matrix might encapsulate the γ-MnO_2 particles so thoroughly that the X-rays cannot effectively penetrate and interact with the crystalline regions, leading to reduced or absent diffraction signals. The γ-MnO_2 particles might be very well dispersed within the polymer matrix. This theory can be supported with intensity size distribution graph of MnO_2-PAE dispersion. According to the size intensity graph, the size value is 336 nm, which is smaller than the MnO_2 and silane-modified MnO_2 size values (Figure 3.28). The polymer matrix itself might contribute to a broad background

signal that can overshadow the peaks of γ-MnO_2, making them difficult to distinguish or there could be chemical interactions between the γ-MnO_2 and the polymer matrix that alter the crystal structure of the γ-MnO_2, potentially leading to changes in the diffraction pattern.

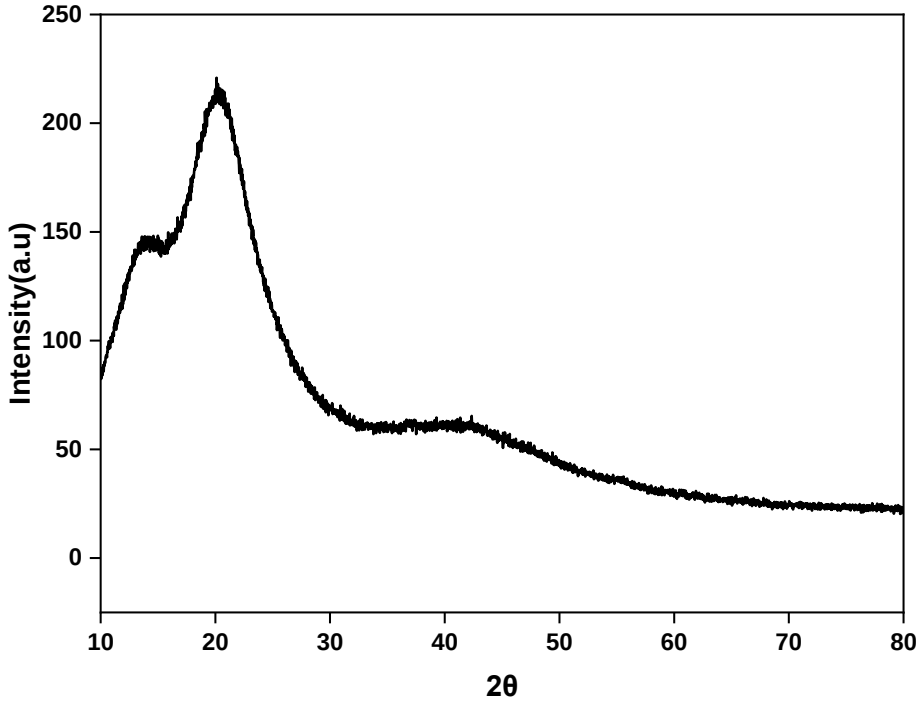

Figure 3.25.XRD of MnO_2 included PAE resin film.

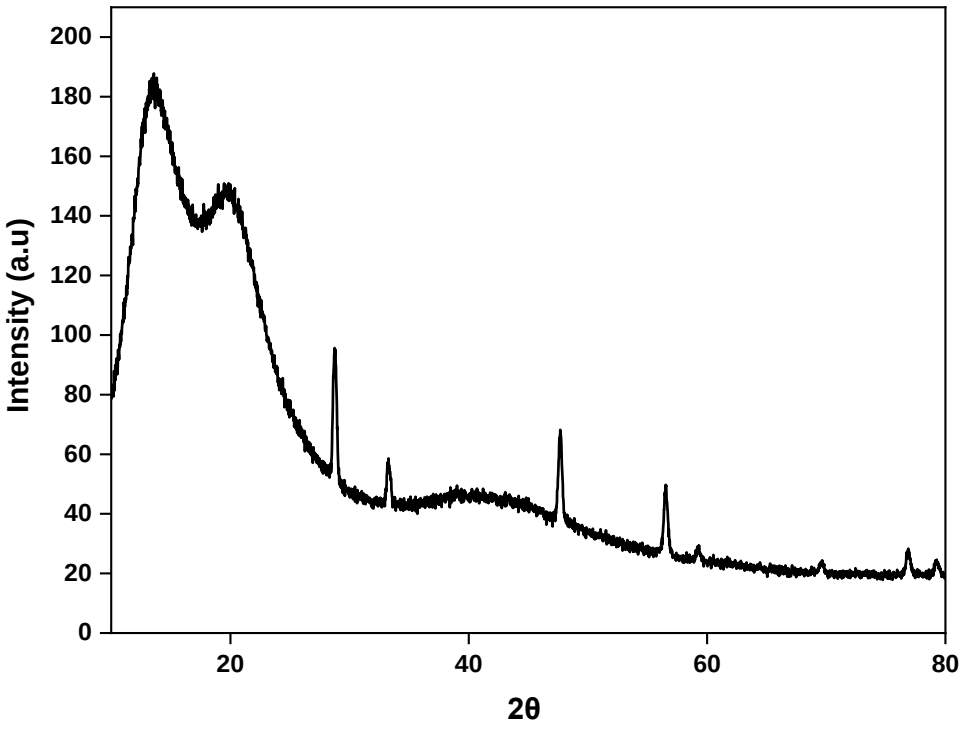

Figure 3.26.XRD of CeO_2 included PAE resin film.

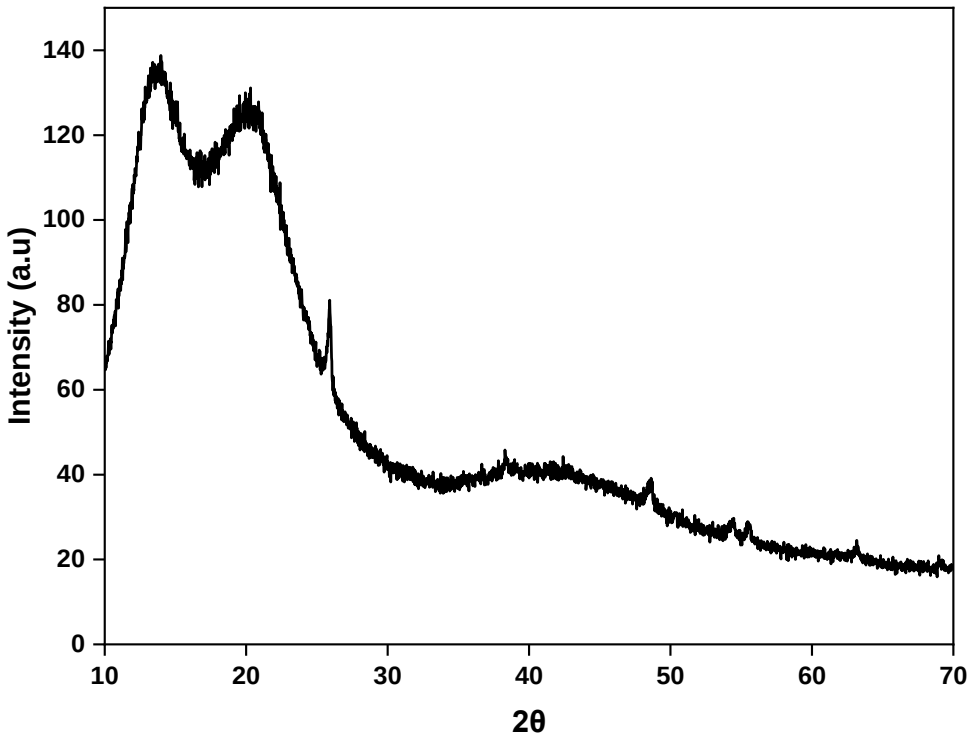

Figure 3.27.XRD of TiO_2 included PAE resin film.

3.3.3. BET Analysis

According to the Table 3.7, the BET surface area of PAEPU films were decreased to compared with the powder metal oxides and silane modified metal oxides. In the composite film, metal oxide particles are embedded within the polyaspartic ester polyurea matrix. This encapsulation can cover the surface of the particles, reducing the overall accessible surface area for gas adsorption during BET analysis.

Table 3.7. BET surface area, pore volume and pore size values of metal oxide particle included PAEPU resin film samples

Sample	BET Surface Area (m^2 /g)	Pore Size (Å)
PAE-TiO_2	0.6	14
PAE-CeO_2	0.5	11
PAE-MnO_2	0.5	2

3.3.4. DLS/Size Analysis

Silane modification can improve the compatibility of metal oxide particles with the resin matrix. The functional groups on the silane molecules can interact with the resin, leading to better dispersion. This improved compatibility can result in a more uniform distribution of particles within the resin. The silane layer provides steric hindrance and potentially electrostatic stabilization helps in preventing particle aggregation. As a result, the size distribution of the particles is narrower, with fewer large aggregates. The intensity size distribution graph of TiO_2 showed the size values were increased when the metal oxide particles were dispersed in the PAE resin (Figure 3.28). MnO_2 included PAE resin's size intensity distribution was wider than the non-modified and silane-modified form, with smaller size which means better dispersion.

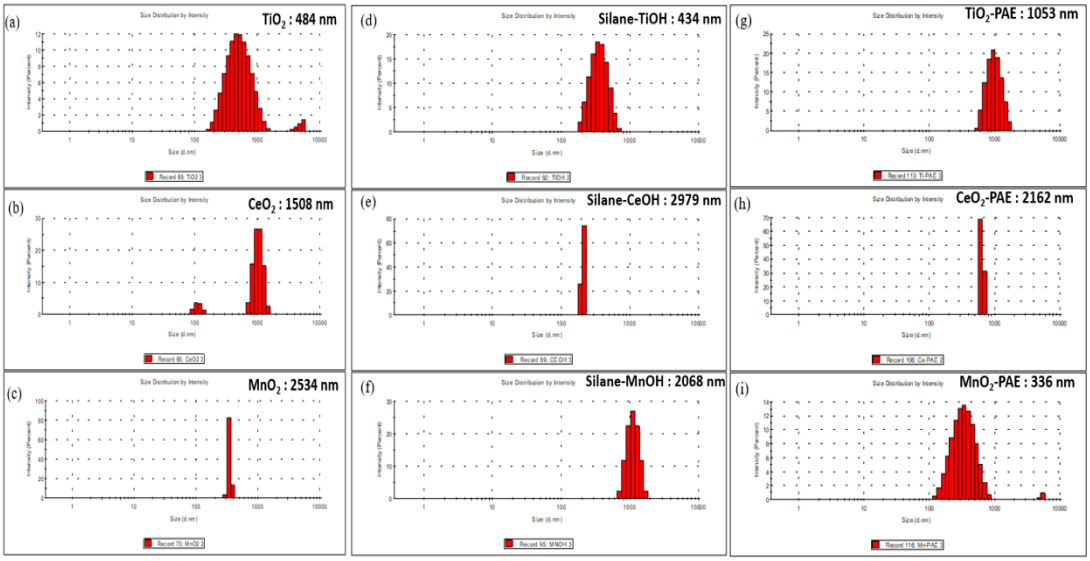

Figure 3.28. Intensity size distributions of a) TiO_2 b) CeO_2 c) MnO_2 d) Silane-TiO_2 e) Silane-CeO_2 f) Silane-MnO_2 g) PAE- TiO_2 h) PAE- CeO_2 i) PAE- MnO_2

3.3.5. SEM Images

SEM is used to study the distribution and morphology of metal oxide particles incorporated into a polyaspartic ester polyurea film, aiming to understand their impact on the composite material's properties. These are SEM images of the particles dispersed in the resin film. There are some agglomerates in the films that contain cerium and manganese oxides (Figure 3.29,Figure 3.30). In the images of PAE films containing titanium dioxide were distributed in smaller pieces and slightly more homogenous than the cerium oxide and manganese dioxide (Figure 3.31).

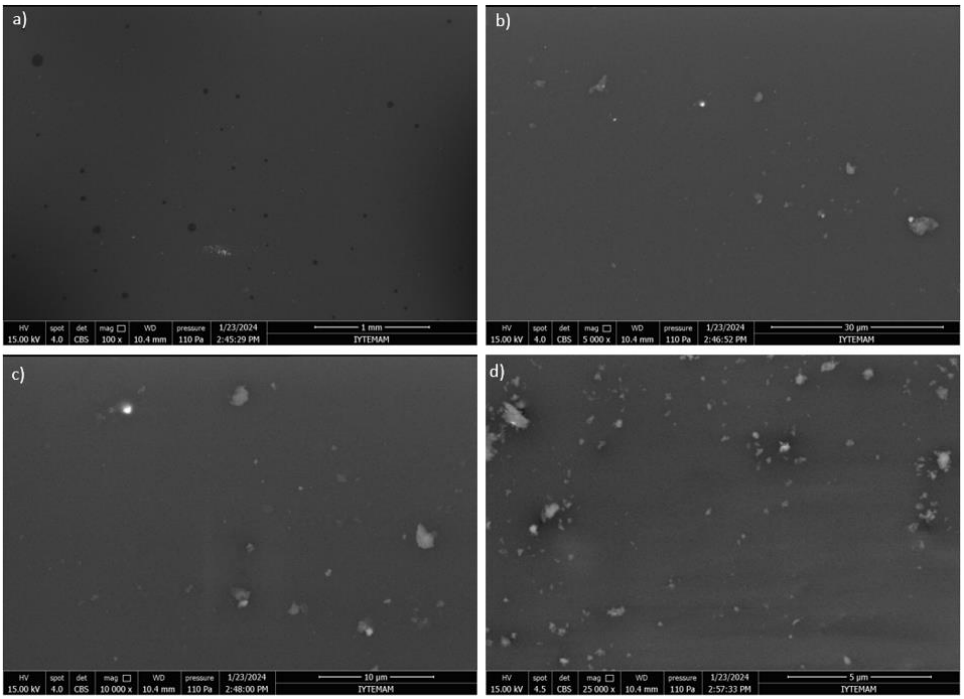

Figure 3.29. The SEM images of PAE film containing CeO_2 prepared with casted method a)100 x b) 5k x c) 10k x d) 25k x magnification.

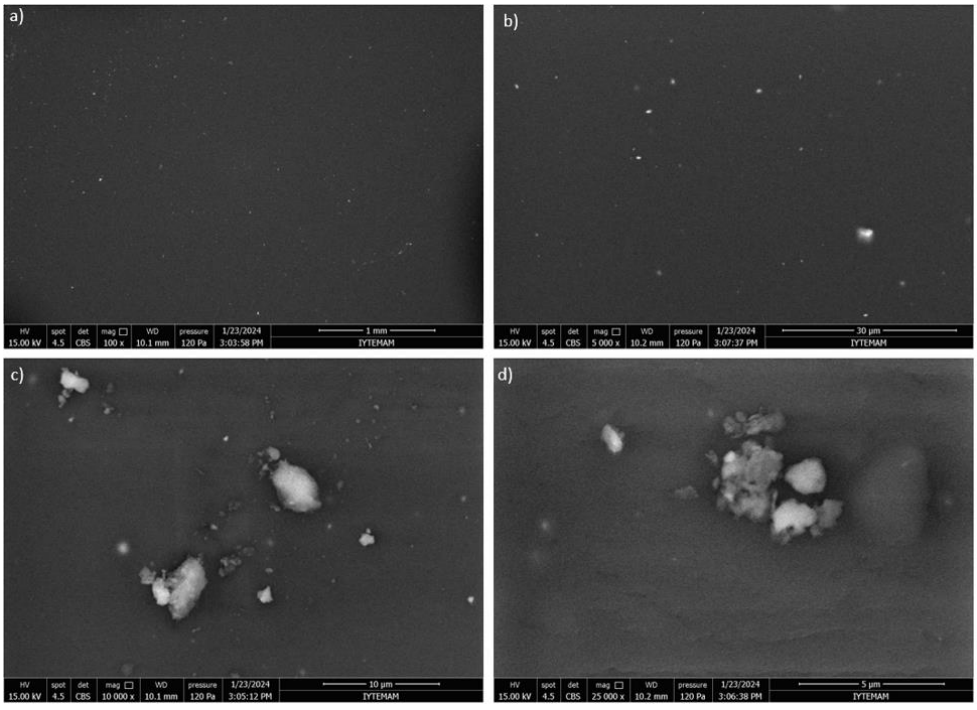

Figure 3.30. The SEM images of PAE film containing MnO_2 prepared with casted method a)100 x b) 5k x c) 10k x d) 25k x magnification.

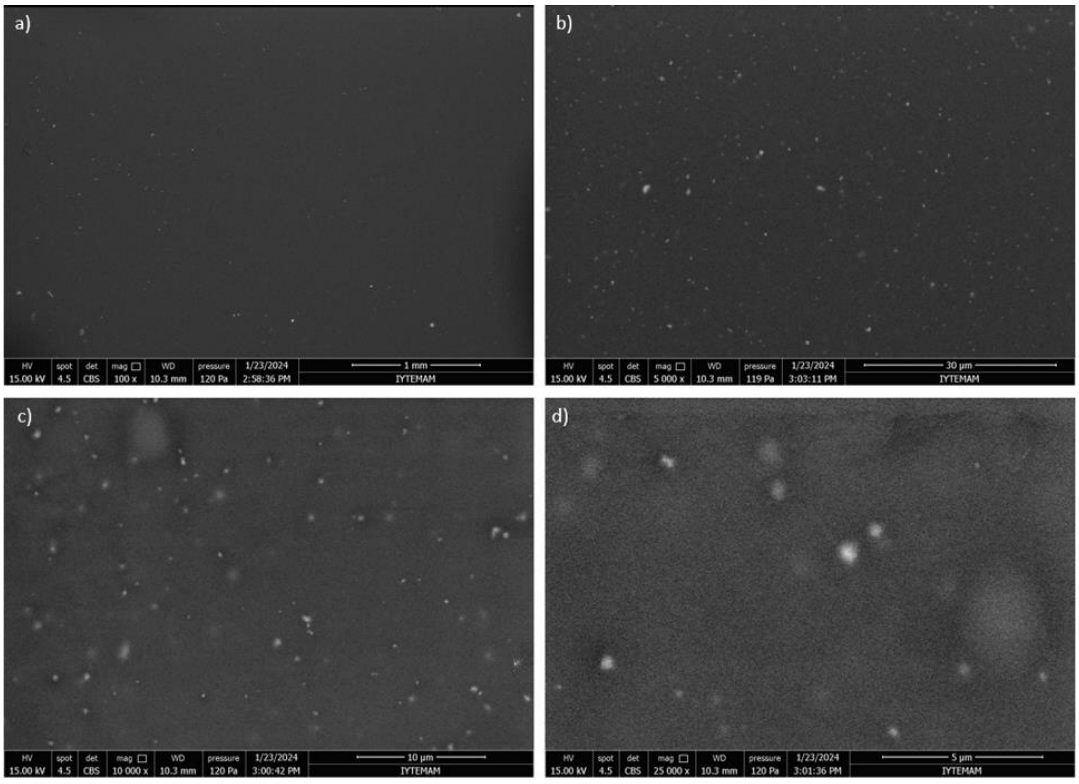

Figure 3.31. The SEM images of PAE film containing TiO_2 prepared with casted method a)100 x b) 5k x c) 10k x d) 25k x magnification.

3.3.6. AFM Images

AFM images provide high-resolution information about the surface morphology of the nanoparticles. By analyzing AFM images, it can be can measured the size and distribution of the metal oxide nanoparticles. Particle size analysis tools within AFM software allow for the quantification of particle dimensions, including diameter, height, and aspect ratio. According to the AFM images, the metal oxides were dispersed into the PAEPU resin film. The height of the cerium oxide particles in the PAEPU film (5μm), is about 13.3 nm (Figure 3.32b). The height of the titanium dioxide particles in the PAEPU film (10 μm), is about 32.5 nm (Figure 3.32f). The height of the manganese dioxide particles in the PAEPU film (10 μm), is about 33.9 nm (Figure 3.32e).

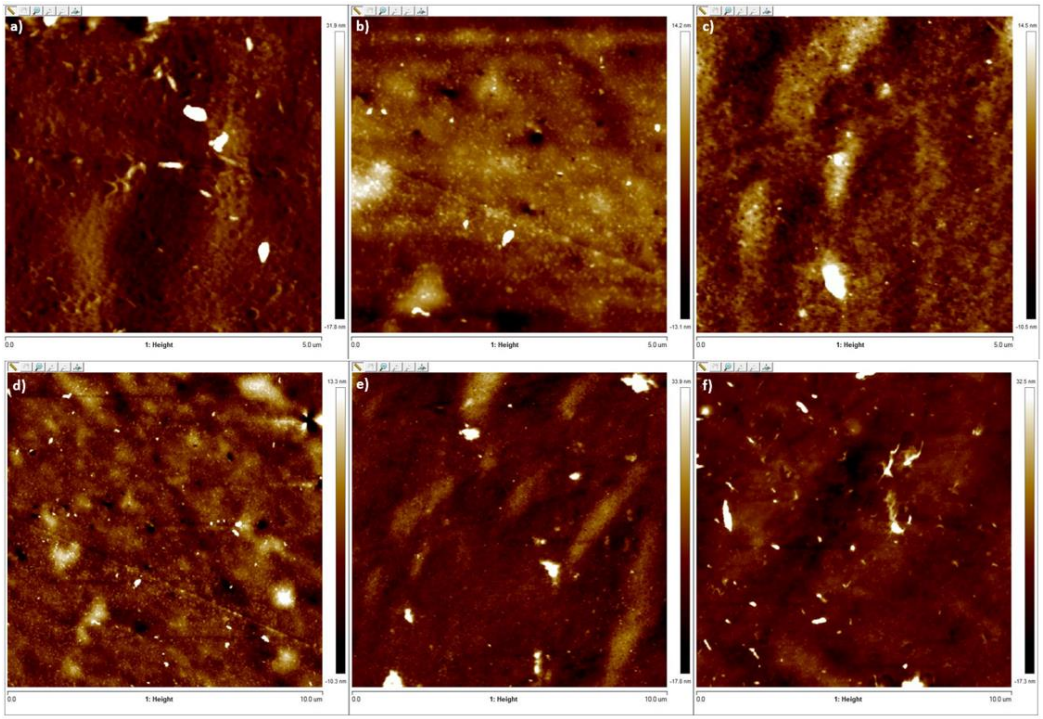

Figure 3.32. AFM images of PAE resin films includes metal oxides (casted samples) a) TiO_2 (5µm) b) CeO_2 (5µm) c) MnO_2 (5µm) d) CeO_2 (10µm) e) MnO_2 (10µm) f) TiO_2 (10µm).

3.3.7. UV-Vis Analysis

In the Figure 3.33, UV absorbance spectra of PAE resin, MnO_2 included PAE resin, TiO_2 included PAE resin and CeO_2 included PAE resin dispersions were demonstrated. The measurement was performed in in acetone with the concentration of 5×10^{-4} M. The metal oxide included PAE dispersions have absorption values (λ_{max}= 335 nm) in the ultraviolet region (UVA). The absorption value of the MnO_2-PAE dispersion was the highest among them. The absorption the of resin dispersions containing metal oxide particles increase as compared to pure PAE resin (Figure 3.33).

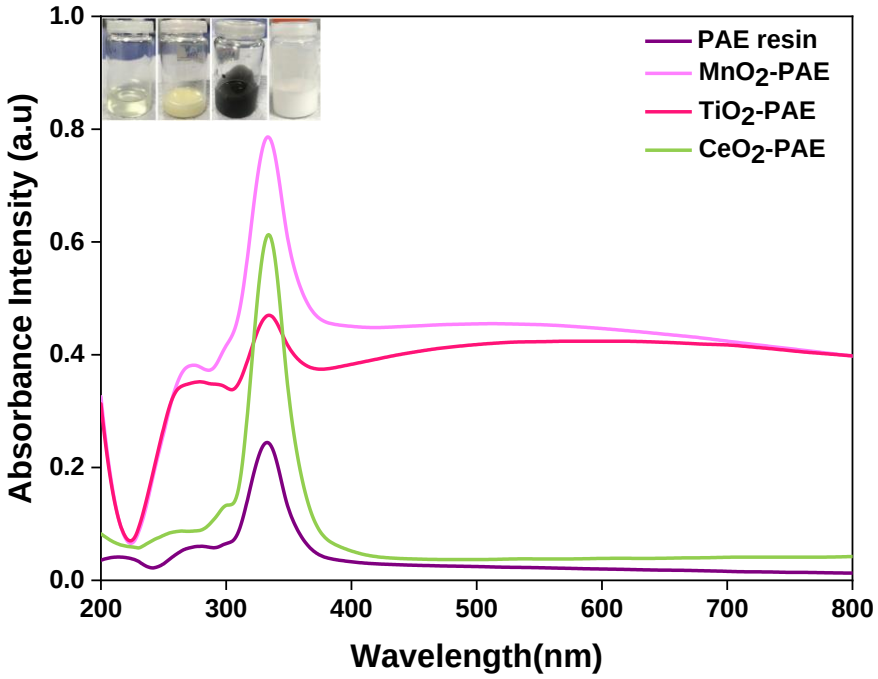

Figure 3.33.The UV absorbance spectra of PAE Resin, MnO_2 –PAE, TiO_2-PAE and CeO_2 –PAE dispersions.

After the reaction with the isocyanate and PAE resin, the films were prepared with different thickness and different ratios of metal oxides. The relation between the transmission (%) values and ratios of metal oxide particles included PAEPU films prepared with spin coating method, were investigated.

In the spin-coated polyaspartic ester polyurea film containing metal oxide as a UV absorber, having a thinner film thickness but showing higher UV transmission values compared to pure resin (Figure 3.34). Potential origins of this behavior as follows.

The acetone was used to facilitate the procedure since it is a fast-evaporating solvent. During the spin coating process, rapid evaporation can cause voids or irregularities within the film. This fast kinetic can hinder the homogeneous distribution of metal oxides and reduce UV absorption. Thus, a less dense film may form. Lower density allows UV light to pass through the film more easily, increasing the transmittance value. Thinner films may contain more defects (e.g., cracks, voids) compared to thicker films. These defects can become more pronounced with the effect of acetone, allowing more UV light to pass through and increasing the transmittance value. The interaction of acetone with metal oxide particles can affect their homogeneous distribution in the

solution. Inhomogeneous distribution can reduce UV absorption, leading to increased transmittance values (Figure 3.34). Also, below a certain thickness threshold, UV absorber particles in the film might not interact effectively. Films below this critical thickness absorb UV light less effectively.

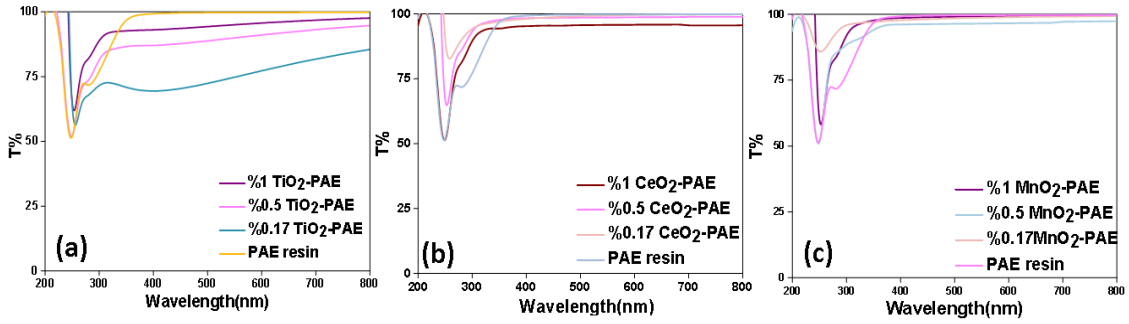

Figure 3.34. UV transmission (%) spectra of pure PAEPU film and different ratios of a) TiO_2 b) CeO_2 c) MnO_2 included PAEPU films prepared with spin coating method.

The relation between the transmission (%) values vs. different film thickness and ratios of metal oxide particles were investigated with the films prepared with Dr. Blade method, too. There is a decrease in transmittance value in the UV transmittance spectrum of polyaspartic ester polyurea resin containing metal oxide particles as a UV absorber, with increasing film thickness (Figure 3.35,Figure 3.36,Figure 3.37) and increasing amount of metal oxide (Figure 3.38). As the ratio of metal oxide increases, the likelihood of light encountering more metal oxide particles increases. This results in more UV light being absorbed and thus a decrease in transmittance (Figure 3.38). The amount of light reflected from the film surfaces and within the particles can increase. Moreover, light can be absorbed multiple times within a thick film, with each pass, light is absorbed a bit more and scattered, further reducing the transmittance (Figure 3.35,Figure 3.36,Figure 3.37). This reduces the net transmission. Moreover, as the film thickness increases, the dispersion of metal oxide particles becomes more uniform, resulting in a denser structure. This increases absorption and scattering, lowering transmittance values.

Additionally, in the visible region the PAE has no absorption and 100% transmission of the light. The metal oxide particle included PAE films have shown

absorption in the visible region and thus there is a decrease in the transmission values as compared to pure PAE film (Figure 3.38).

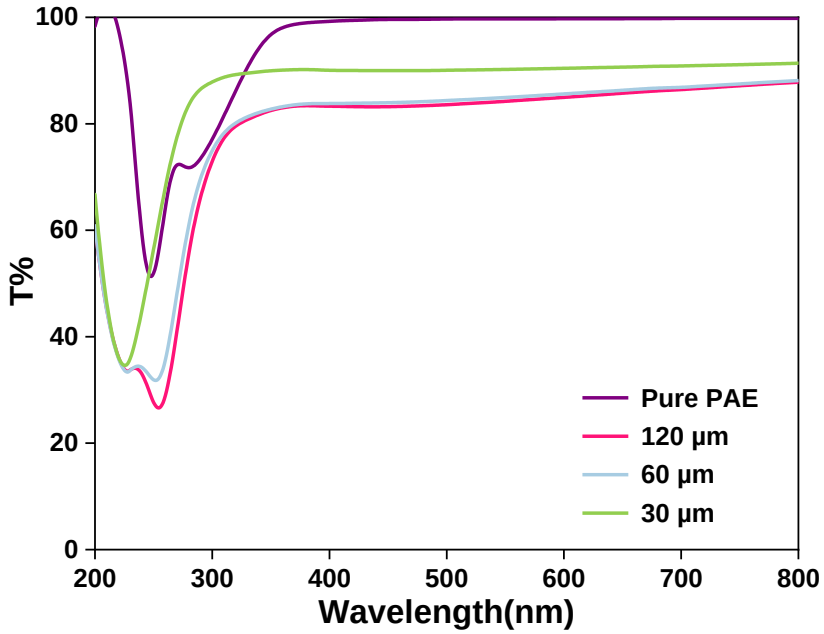

Figure 3.35. The UV transmittance (%) spectra of pure PAEPU film and 0.2 % TiO_2-PAEPU.

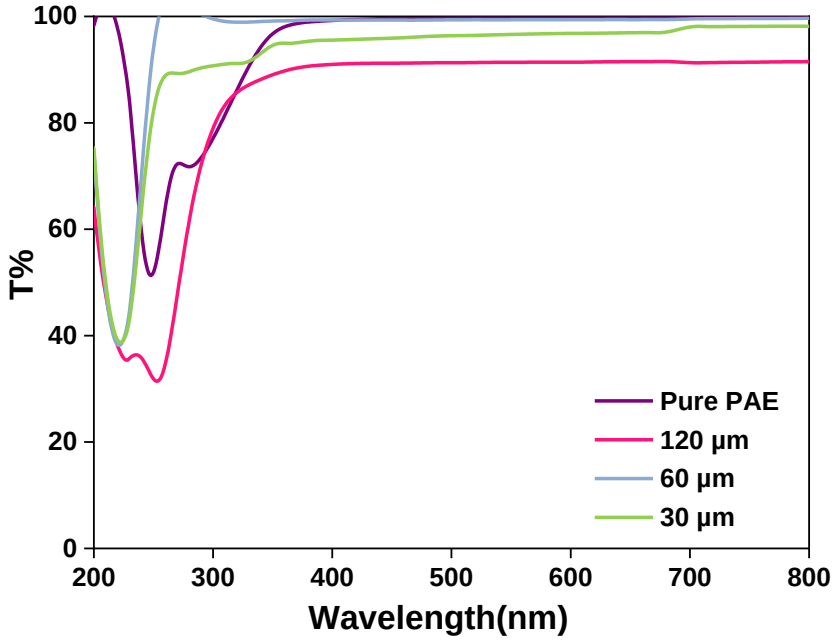

Figure 3.36. The UV transmittance (%) spectra of pure PAEPU film and 0.2 % CeO_2-PAEPU.

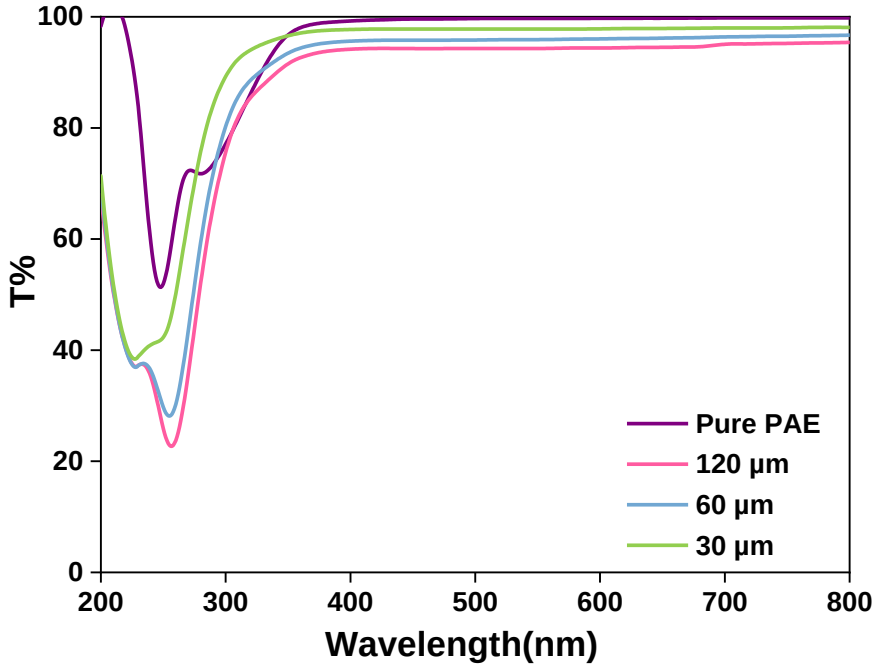

Figure 3.37. The UV transmittance (%) spectra of pure PAEPU film and 0.2 % MnO_2-PAEPU.

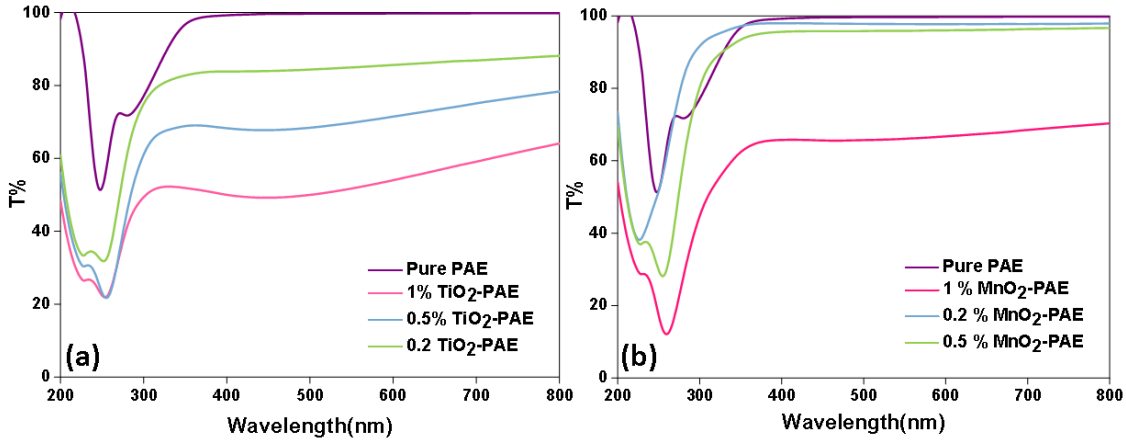

Figure 3.38. The UV transmittance (%) spectra of pure PAEPU film and different ratios of (a) TiO_2-PAEPU and (b) MnO_2-PAEPU with 60 µm film thickness prepared with Dr. Blade method.

The optical transmission of the films at visible and UV wavelengths (550 and 255 nm) is displayed based on metal oxide content (Figure 3.39,Figure 3.41,Figure 3.43). The wavelength 255 nm (UV Region) lies in the UV-C region and is generally strongly absorbed by metal oxides.[45] The tendency of metal oxides to absorb high-energy UV light

results in low transmission values at this wavelength. The wavelength 550 nm (Visible Light Region) is in the middle of the visible light spectrum. Metal oxides usually transparent in this region, optical scattering may decrease transmission of the films and resulting translucent/opaque material. Increasing the amount of metal oxides increases the density and thickness of the film, making it more difficult for light to pass through the material. This effect can be especially pronounced in the UV region due to the higher absorption in this region. In the visible light region (550 nm), the absorption properties of metal oxides are lower, allowing more light to pass through. However, as the amount of metal oxides increases, light transmission decreases even in this region. In the UV-C region (255 nm), metal oxides strongly absorb UV light, resulting in lower transmission values (Figure 3.39,Figure 3.41,Figure 3.43). As the amount of metal oxides increases, this absorption becomes more significant, further reducing transmission.

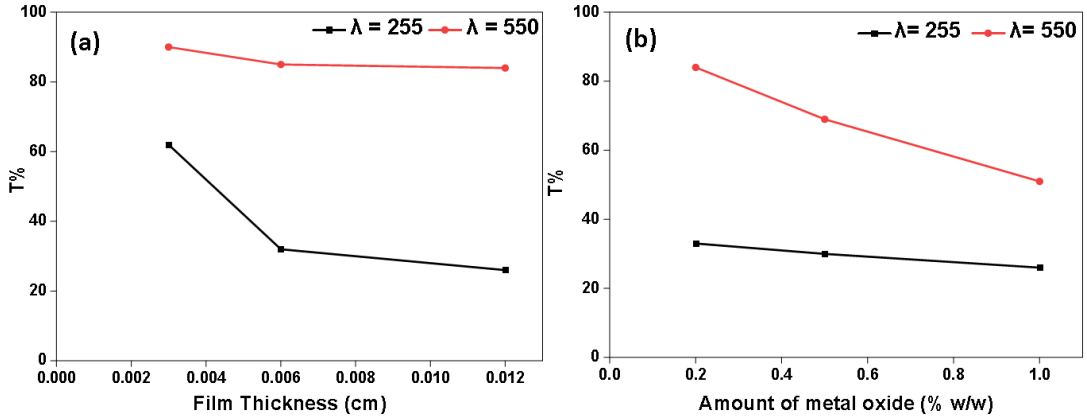

Figure 3.39. The UV transmittance (%) spectra of TiO_2-PAEPU film with (a) different film thicknesses (0.2%) and (b) different amounts (120 μm) of TiO_2 at 255 and 550 nm.

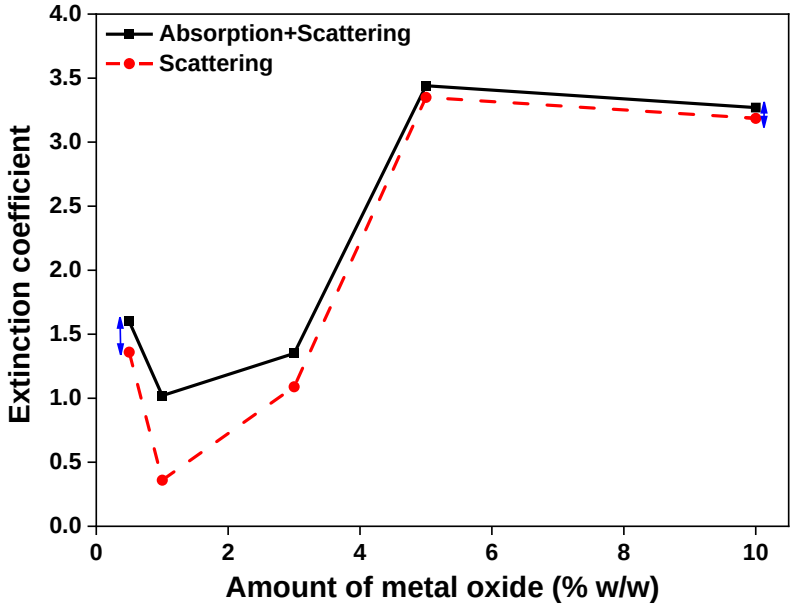

Figure 3.40. Extinction coefficient of TiO_2-PAEPU films at 255 nm (solid line shows absorption + scattering, dashed line represents scattering).

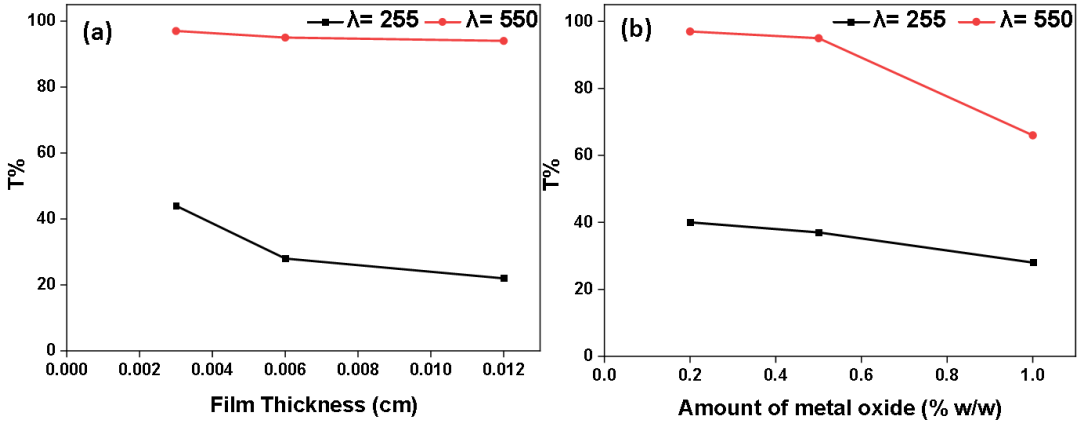

Figure 3.41. The UV transmittance (%) spectra of MnO_2-PAEPU film with (a) different film thicknesses (0.2%) and (b) different amounts (120 μm) of MnO2 at 255 and 550 nm.

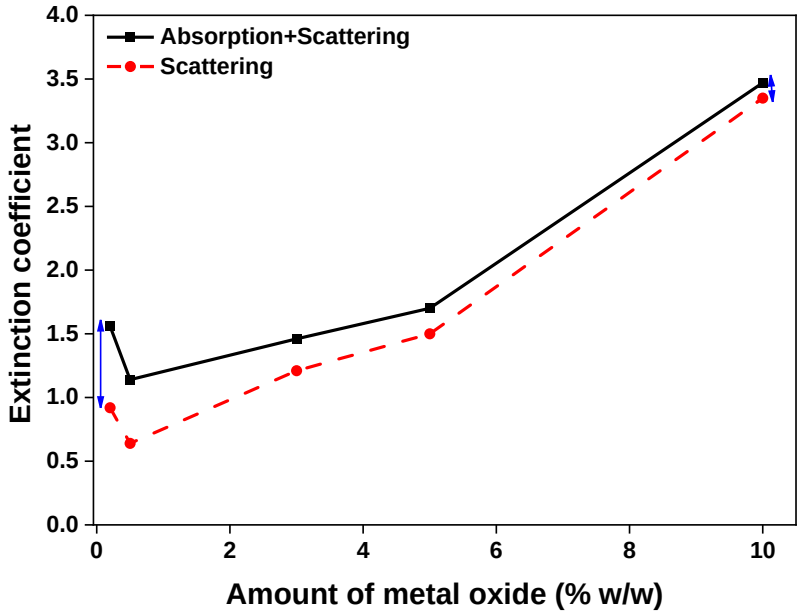

Figure 3.42. Extinction coefficient of MnO_2-PAEPU films at 255 nm (solid line shows absorption + scattering, dashed line represents scattering).

The total attenuation coefficient (μ_t) is a measure of how much the intensity of a wave decreases as it travels through a material. It encompasses all mechanisms that contribute to the reduction of intensity, including absorption, scattering, and any other processes that result in the attenuation of the wave. Absorption coefficient ($\mu\alpha$) represents the loss of intensity due to the absorption of energy by the material. Scattering coefficient (μs) represents the loss of intensity due to scattering, where the wave is deflected from its original path by interactions with particles or irregularities in the material.[45] The scattering coefficient is influenced by factors such as particle size, shape, and refractive index differences between the particles and the surrounding medium.

$$\mu t = \mu a + \mu s \qquad (3.1)$$

The extinction coefficient (k) is a part of the complex refractive index and represents the imaginary component.[47] It describes how much a material attenuates the amplitude of light as it propagates through it. The absorption coefficient directly measures absorption, while the extinction coefficient considers both absorption and scattering.

$$\mu a = 4\pi k/\lambda \qquad (3.2)$$

The difference between the two lines actually represents the absorption coefficient (blue arrow) and as the as the amount of metal oxide increased, the scattering and

absorption coefficient values increased (Figure 3.40,Figure 3.42,Figure 3.44). For the small amounts of metal oxides, the absorption is greater. However, increment in the amount of metal oxide causes the increment in the scattering values and smaller absorption values than scattering. Increasing the amount of metal oxides affects the material's density and internal structure. A denser structure allows for multiple scattering.

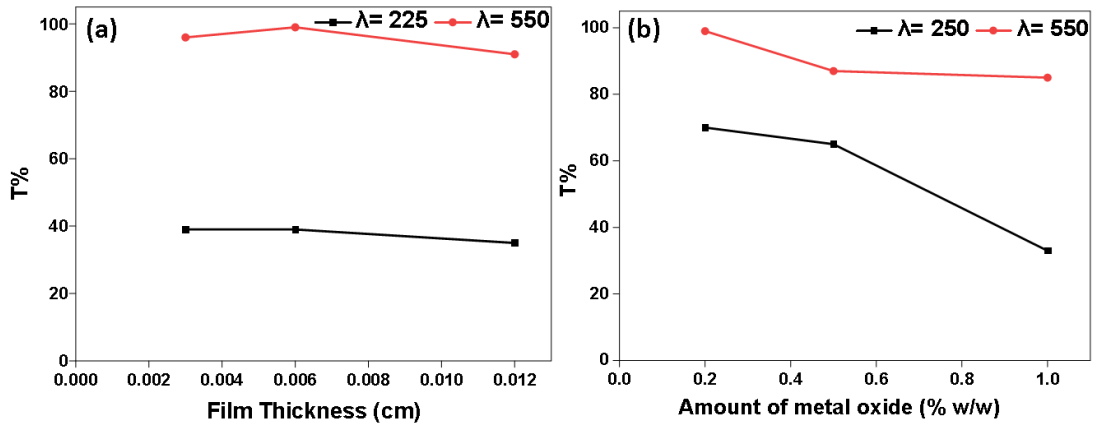

Figure 3.43. The UV transmittance (%) spectra of CeO_2-PAEPU film with (a) different film thicknesses (0.2%) and (b) different amounts (120 µm) of CeO_2 at 250 and 550 nm.

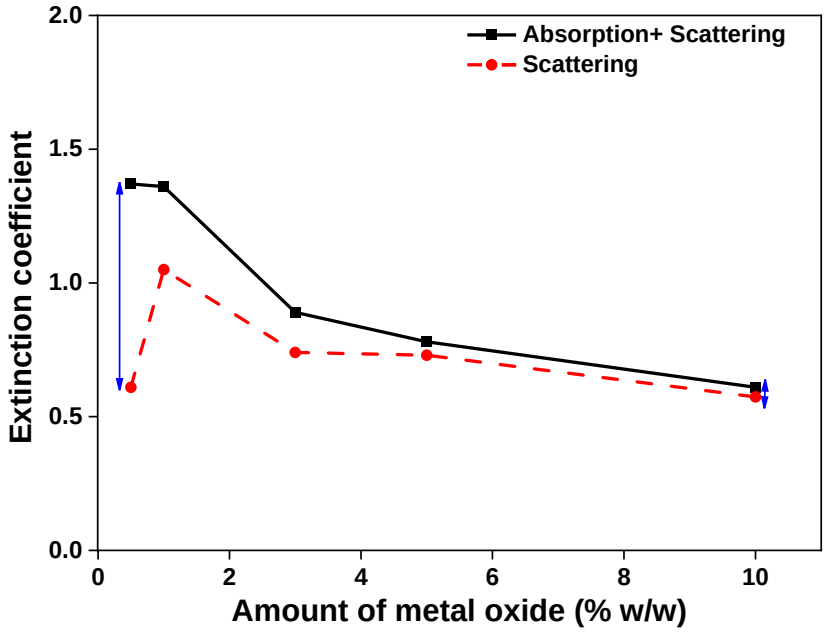

Figure 3.44. Extinction coefficient of CeO_2-PAEPU films at 255 nm (solid line shows absorption + scattering, dashed line represents scattering).

As the amount of metal oxide increased, scattering arises and absorption also decreases (Figure 3.44). For the smaller amounts of the CeO_2, the absorption values greater. Cerium oxide may have different optical properties compared to titanium and manganese oxides. CeO_2 might have different band structures and energy levels, leading to different UV light absorption characteristics. It typically has a higher scattering coefficient under UV light, which can dominate the total energy loss, resulting in lower absorption values. We are allowed to make speculation on these results, differences in crystal structure may affect photon absorption efficiency.

3.3.8. UV Weathering Test of PAE films

The magnitude of the ΔE value (equation 3.3)[46] indicates the degree of color change that has occurred. A larger ΔE value corresponds to a greater color difference between the pre-exposure and post-exposure measurements, indicating more significant color change or fading (Figure 3.45).

Figure 3.45. PAEPU panels after the UV weathering test.

The Figure 3.46 shows the graph of gloss change vs. different ratios of metal oxides. According to the specifications in the coating field, the gloss change should be in the range of minus three and plus three. Therefore, the 0.5 % CeO_2, 1 % CeO_2, 2 % CeO_2, 0.2 % TiO_2, 1 % TiO_2 ,0.2 % MnO_2 ,0.5 % MnO_2 and 1 % MnO_2 meet this requirement. Moreover, PAE film has a gloss change 2.97 almost 3. The mentioned specific ratio of metal oxide containing PAE films have shown better performance for the gloss change than the Pure PAE film.

Table 3.8. Delta E values and Gloss Loss Values of PAEPU films after 360 h. UV exposure.

Sample Name	Test Time (h)	First Value			Last Value			First Gloss			Last Gloss			Gloss Loss			Delta E
		(L)	(a)	(b)	(L)	(a)	(b)	20°C	60°C	85°C	20°C	60°C	85°C	20% Loss	60% Loss	85% Loss	
1% Ce	360	94.99	-1.49	1.43	94.34	-1.4	2.3	87.2	94.5	97.3	88.3	95.1	99.5	-1.26	-0.63	-2.26	1.09
2% Mn	360	48.74	1.67	4.47	63.22	2.79	9.13	79.3	88.9	95.8	84.3	92.2	98.8	-6.31	-3.71	-3.13	15.25
0.5% Mn	360	73.11	0.72	3.98	84.48	0.77	5.78	88	93.6	98.4	89.3	94.7	99.3	-1.48	-1.18	-0.91	11.51
0.2% Mn	360	83.86	-0.04	2.89	90.4	-0.32	3.41	87.7	95	99.3	88.1	95.5	100	-0.46	-0.53	-0.70	6.57
1% Mn	360	61.18	1.27	4.13	73.68	1.98	7.67	85.6	92.5	97.4	87.6	94	99.6	-2.34	-1.62	-2.26	13.01
2% Ti	360	95.33	-1.24	1.02	94.21	-1.43	4.1	86	93.6	95.9	64.4	83.3	98.7	25.12	11.00	-2.92	3.28
1% Ti	360	96.14	-1.1	1.09	95.65	-1.31	3.19	87.9	94.6	98.1	78.8	91.9	99.7	10.35	2.85	-1.63	2.17
0.5% Ti	360	96.01	-1.07	1.22	95.51	-1.2	3.02	89.4	96.4	91	86	95.2	91.9	3.80	1.24	-0.99	1.87
0.2% Ti	360	95.45	-1.29	1.2	94.99	-1.3	2.33	88	95.2	98	87.9	95.2	100	0.11	0.00	-2.04	1.22
2% Ce	360	95.83	-1.46	2.23	94.21	-1.33	3.33	85	94.6	98.4	87.2	95.2	99.6	-2.59	-0.63	-1.22	1.96
0.5% Ce	360	95.18	-1.18	0.88	94.8	-1.14	1.56	89.1	95.3	98.1	88.9	96	100	0.22	-0.73	-1.94	0.78

$$\Delta E^*_{ab} = \sqrt{(L^*_2 - L^*_1)^2 + (a^*_2 - a^*_1)^2 + (b^*_2 - b^*_1)^2} \quad (3.3)$$

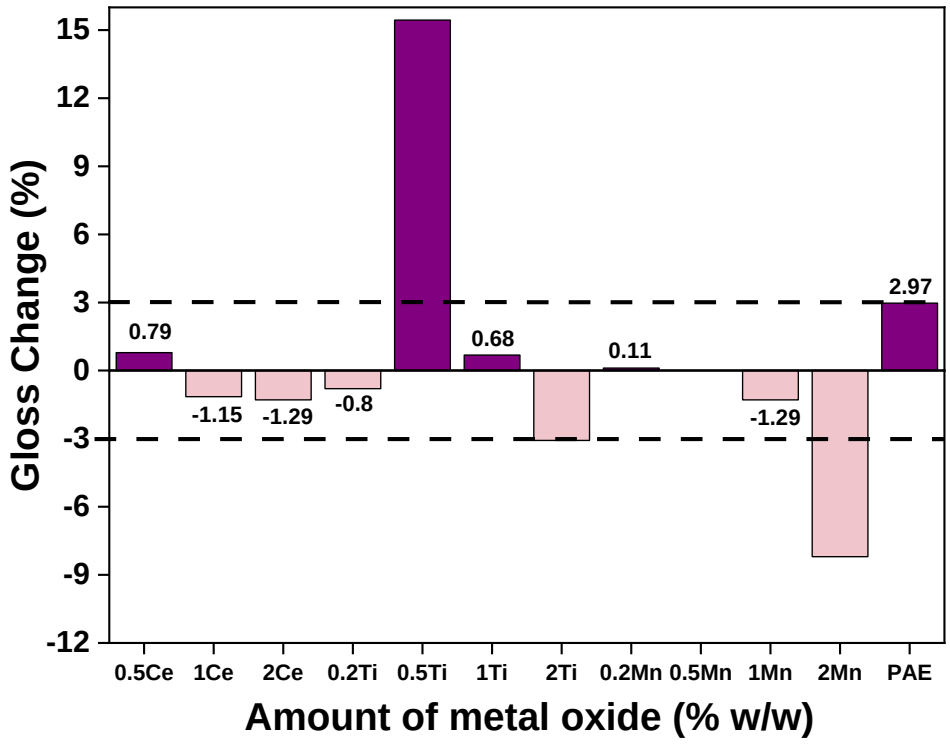

Figure 3.46. Graph of gloss change vs. different ratios of metal oxides.

The delta E values of the PAEPU films generally increases as amount of metal oxide particles increase. TiO_2 and CeO_2 included PAE resin has smaller delta E values. However, MnO_2 included PAE resin have greater delta E values. The results showed that the best UV resistant metal oxide particle was CeO_2 and TiO_2 according to the UV exposure test. (Figure 3.47)

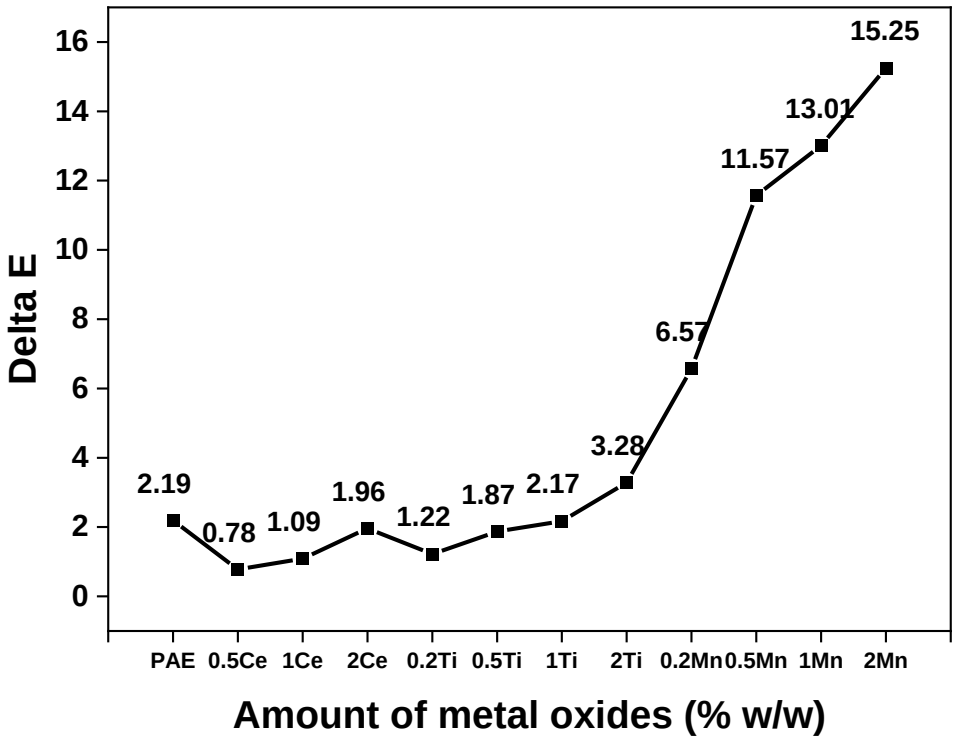

Figure 3.47. Graph of delta E vs. different ratios of metal oxides after 360 h of UV exposure.

The relationship between absorption and delta E values can be attributed to the different physical and chemical properties of metal oxides. Each metal oxide has distinct electronic structures, band structures, and surface properties, leading to varying absorption and energy difference (delta E) behaviors. Both cerium oxide and titanium dioxide are wide-bandgap semiconductors. In such materials, as absorption increases, more photons are absorbed, leading to the excitation of energy levels corresponding to the bandgap. Increased amounts of metal oxide result in more surface area and thus more light absorption. This excites the material's energy levels, leading to an increase in delta E (Figure 3.48).

The different crystal structure and surface properties of manganese dioxide can create a different relationship between absorption and energy difference. The electronic structure and energy levels of MnO_2 can cause delta E to increase even when absorption decreases. This can result in changes in energy levels even in situations where MnO_2 absorption is reduced. (Figure 3.48)

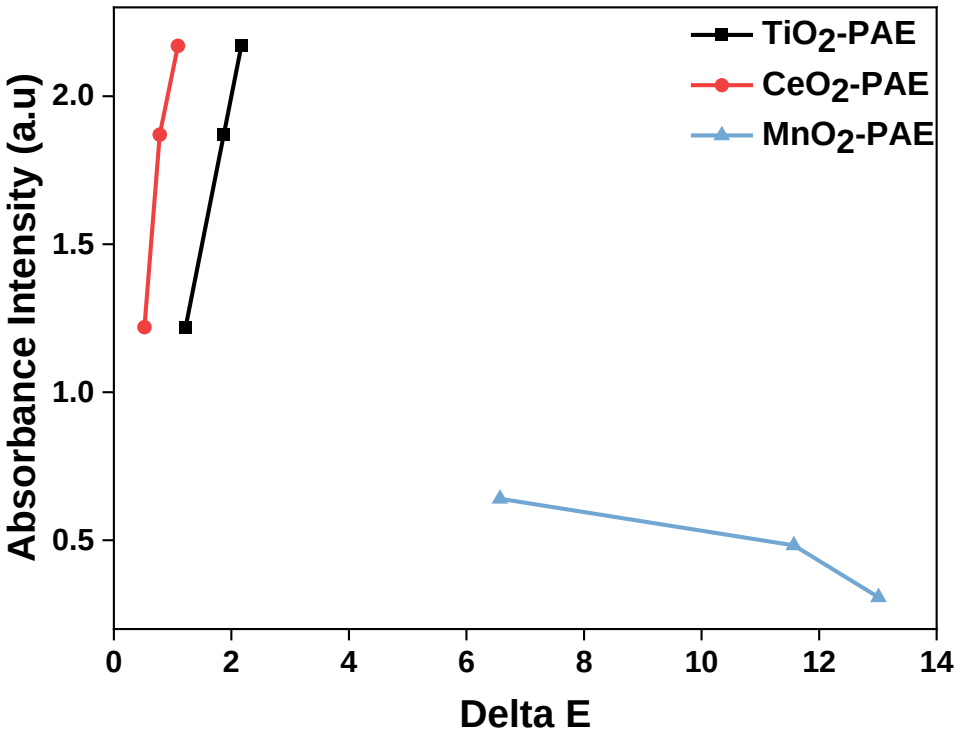

Figure 3.48. Graph of Delta E and absorption values of metal oxide included PAEPU films.

CHAPTER 4

CONCLUSIONS

In this thesis, the UV absorption characteristic of polyaspartics composite films including inorganic oxide particles was studied. The submicron diameter of UV-absorbing particles (MnO_2, CeO_2, and TiO_2) were modified with silane- based surfactant (3-(methacryloxy)propyltrimethoxy silane) to achieve compatibility with the PAE resin. The modified particles were dispersed into the PAE resin. PAE dispersions containing metal oxides, exhibit absorption at UVA region (λ_{max} = 335). The maximum absorption value was found in the MnO_2-PAE dispersion. The absorption values of resin dispersions including metal oxide particles, increased as compared to pure PAE resin. PAEPU film was prepared with the help of the isocyanate. The UV transmittance spectrum of PAEPU films including metal oxide particles showed a reduction in transmittance value as film thickness and metal oxide ratio increase. The metal oxide amount increment causes the absorption and scattering coefficient increment for the films that contain titanium and manganese, but less absorption more scattering. The metal oxide included PAEPU films were exposed to UV weathering for 72 and 360 h to observe UV degradation (color change, gloss retention). The ratio of the 0.5 % CeO_2, 1.0 % CeO_2, 2.0 % CeO_2, 0.2 % TiO_2, 1.0 % TiO_2 , 0.2 % MnO_2 , 0.5 % MnO_2 and 1.0 % MnO_2 are in the desired range of gloss change and have less gloss change than the PAEPU. The delta E values of PAEPU films were usually increased with the number of metal oxide particles. CeO_2-containing PAEPU films were exhibit lowest delta E values that means minimum color change. In addition, the delta E values of PAEPU films containing TiO_2 were lower. However, MnO_2-containing PAEPU films have higher delta E values. Overall, the incorporation of metal oxide particles into polyaspartic ester has been shown to be an effective strategy for enhancing their UV resistance. The results demonstrate that carefully selected and optimally dispersed metal oxide particles can significantly improve the UV protective properties of PAE resins, making them more suitable for applications requiring prolonged UV exposure. Further research could explore the long-term stability of these enhancements and the potential impacts on other mechanical and physical properties of the resin.

REFERENCES

1. *Coatings Technology Handbook*; Tracton, A. A., Ed.; CRC Press, 2005. https://doi.org/10.1201/9781420027327.

2. Sørensen, P. A.; Kiil, S.; Dam-Johansen, K.; Weinell, C. E. Anticorrosive Coatings: A Review. *J Coat Technol Res* **2009**, *6* (2), 135–176. https://doi.org/10.1007/s11998-008-9144-2.

3. Gärtner, M. Historical Pigments, Dyes and Binders. *Physical Sciences Reviews* **2021**, *6* (9), 419–476. https://doi.org/10.1515/psr-2020-0176.

4. Maile, F. J. Colorants in Coatings. *Physical Sciences Reviews* **2021**, *6* (11), 707–789. https://doi.org/10.1515/psr-2020-0160.

5. *Coatings Technology Handbook*; Tracton, A. A., Ed.; CRC Press, 2005. https://doi.org/10.1201/9781420027327.

6. Akafuah, N.; Poozesh, S.; Salaimeh, A.; Patrick, G.; Lawler, K.; Saito, K. Evolution of the Automotive Body Coating Process—A Review. *Coatings* **2016**, *6* (2), 24. https://doi.org/10.3390/coatings6020024.

7. Baij, L.; Hermans, J.; Ormsby, B.; Noble, P.; Iedema, P.; Keune, K. A Review of Solvent Action on Oil Paint. *Herit Sci* **2020**, *8* (1), 43. https://doi.org/10.1186/s40494-020-00388-x.

8. Americus. Coatings Update: Scientific Studies. *Pigment & Resin Technology* **1979**, *8* (10), 9–16. https://doi.org/10.1108/eb041521.

9. Tunçgenç, M. Boya Teknolojisine Giriş. **2004**.

10. Palaniandy, K.; Auckloo, S. A. B.; Chan, E.-S.; Pasbakhsh, P. Formulations and Properties. In *Polyurea*; Elsevier, 2023; pp 3–15. https://doi.org/10.1016/B978-0-323-99450-7.00011-3.

11. Golling, F. E.; Pires, R.; Hecking, A.; Weikard, J.; Richter, F.; Danielmeier, K.; Dijkstra, D. Polyurethanes for Coatings and Adhesives – Chemistry and Applications. *Polym Int* **2019**, *68* (5), 848–855. https://doi.org/10.1002/pi.5665.

12. Chattopadhyay, D. K.; Raju, K. V. S. N. Structural Engineering of Polyurethane Coatings for High Performance Applications. *Prog Polym Sci* **2007**, *32* (3), 352–418. https://doi.org/10.1016/j.progpolymsci.2006.05.003.

13. Engels, H.; Pirkl, H.; Albers, R.; Albach, R. W.; Krause, J.; Hoffmann, A.; Casselmann, H.; Dormish, J. Polyurethanes: Versatile Materials and Sustainable Problem Solvers for Today's Challenges. *Angewandte Chemie International Edition* **2013**, *52* (36), 9422–9441. https://doi.org/10.1002/anie.201302766.

14. Howarth, G. Polyurethanes, Polyurethane Dispersions and Polyureas: Past, Present and Future. *Surface Coatings International Part B: Coatings Transactions* **2003**, *86* (2), 111–118. https://doi.org/10.1007/BF02699621.

15. Pivec, T.; Sfiligoj Smole, M.; Gašparič, P.; Stana Kleinschek, K. Polyurethanes for Medical Use. *TEKSTILEC* **2017**, *60* (3), 182–197. https://doi.org/10.14502/Tekstilec2017.60.182-197.

16. Shojaei, B.; Najafi, M.; Yazdanbakhsh, A.; Abtahi, M.; Zhang, C. A Review on the Applications of Polyurea in the Construction Industry. *Polym Adv Technol* **2021**, *32* (8), 2797–2812. https://doi.org/10.1002/pat.5277.

17. Virt, I. Special Issue: Recent Advances in Semiconducting Thin Films. *Coatings* **2023**, *13* (1), 79. https://doi.org/10.3390/coatings13010079.

18. Primeaux, D. , & D. J. Polyurea vs. Polyurethane & Polyurethane/Polyurea: What's the Difference? *In Proceedings of the Polyurea Linings Annual Conference, Polyurea Development Assocaition (PDA)* **2004**.

19. Pospíšil, J.; Nešpurek, S. Photostabilization of Coatings. Mechanisms and Performance. *Prog Polym Sci* **2000**, *25* (9), 1261–1335. https://doi.org/10.1016/S0079-6700(00)00029-0.

20. Gao, Q.; Wang, L.; Luo, H.; Fan, H.; Xiang, J.; Yan, J.; Li, C.; Chen, Z. Photodegradation Behavior and Blocking Strategy of Waterborne Polyurethane under UV and Xenon Irradiation. *Mater Today Commun* **2023**, *34*, 105212. https://doi.org/10.1016/j.mtcomm.2022.105212.

21. Zayat, M.; Garcia-Parejo, P.; Levy, D. Preventing UV-Light Damage of Light Sensitive Materials Using a Highly Protective UV-Absorbing Coating. *Chem Soc Rev* **2007**, *36* (8), 1270. https://doi.org/10.1039/b608888k.

22. Andrady, A. L.; Hamid, S. H.; Hu, X.; Torikai, A. Effects of Increased Solar Ultraviolet Radiation on Materials. *J Photochem Photobiol B* **1998**, *46* (1–3), 96–103. https://doi.org/10.1016/S1011-1344(98)00188-2.

23. Ibrahim, A. M. Plastics: Photodegradations and Mechanisms. In *Microplastics and Pollutants*; Springer Nature Switzerland: Cham, 2024; pp 25–49. https://doi.org/10.1007/978-3-031-54565-8_2.

24. Yousif, E.; Haddad, R. Photodegradation and Photostabilization of Polymers, Especially Polystyrene: Review. *Springerplus* **2013**, *2* (1), 398. https://doi.org/10.1186/2193-1801-2-398.

25. Gijsman, P. A Review on the Mechanism of Action and Applicability of Hindered Amine Stabilizers. *Polym Degrad Stab* **2017**, *145*, 2–10. https://doi.org/10.1016/j.polymdegradstab.2017.05.012.

26. Ma, B. C.; Ghasimi, S.; Landfester, K.; Zhang, K. A. I. Enhanced Visible Light Promoted Antibacterial Efficiency of Conjugated Microporous Polymer Nanoparticles via Molecular Doping. *J Mater Chem B* **2016**, *4* (30), 5112–5118. https://doi.org/10.1039/C6TB00943C.

27. Butt, M. A. Thin-Film Coating Methods: A Successful Marriage of High-Quality and Cost-Effectiveness—A Brief Exploration. *Coatings* **2022**, *12* (8), 1115. https://doi.org/10.3390/coatings12081115.

28. Azani, M.; Hassanpour, A. Nanotechnology in the Fabrication of Advanced Paints and Coatings: Dispersion and Stabilization Mechanisms for Enhanced Performance. *ChemistrySelect* **2024**, *9* (19). https://doi.org/10.1002/slct.202400844.

29. Yabe, S.; Sato, T. Cerium Oxide for Sunscreen Cosmetics. *J Solid State Chem* **2003**, *171* (1–2), 7–11. https://doi.org/10.1016/S0022-4596(02)00139-1.

30. Ma, S.; Shi, L.; Feng, X.; Yu, W.; Lu, B. Graft Modification of ZnO Nanoparticles with Silane Coupling Agent KH570 in Mixed Solvent. *Journal of Shanghai University (English Edition)* **2008**, *12* (3), 278–282. https://doi.org/10.1007/s11741-008-0316-1.

31. Nguyen, T.-C.; Nguyen, T.-D.; Vu, D.-T.; Dinh, D.-P.; Nguyen, A.-H.; Ly, T.-N.-L.; Dao, P.-H.; Nguyen, T.-L.; Bach, L.-G.; Thai, H. Modification of Titanium Dioxide Nanoparticles with 3-(Trimethoxysilyl)Propyl Methacrylate Silane Coupling Agent. *J Chem* **2020**, *2020*, 1–10. https://doi.org/10.1155/2020/1381407.

32. Hang, T. T. X.; Dung, N. T.; Truc, T. A.; Duong, N. T.; Van Truoc, B.; Vu, P. G.; Hoang, T.; Thanh, D. T. M.; Olivier, M.-G. Effect of Silane Modified Nano ZnO on UV Degradation of Polyurethane Coatings. *Prog Org Coat* **2015**, *79*, 68–74. https://doi.org/10.1016/j.porgcoat.2014.11.008.

33. Roy, H. S.; Mollah, M. Y. A.; Islam, Md. M.; Susan, Md. A. B. H. Poly(Vinyl Alcohol)–MnO2 Nanocomposite Films as UV-Shielding Materials. *Polymer Bulletin* **2018**, *75* (12), 5629–5643. https://doi.org/10.1007/s00289-018-2355-5.

34. Tsunekawa, S.; Wang, J.-T.; Kawazoe, Y.; Kasuya, A. Blueshifts in the Ultraviolet Absorption Spectra of Cerium Oxide Nanocrystallites. *J Appl Phys* **2003**, *94* (5), 3654–3656. https://doi.org/10.1063/1.1600520.

35. Thill, A. S.; Lobato, F. O.; Vaz, M. O.; Fernandes, W. P.; Carvalho, V. E.; Soares, E. A.; Poletto, F.; Teixeira, S. R.; Bernardi, F. Shifting the Band Gap from UV to Visible Region in Cerium Oxide Nanoparticles. *Appl Surf Sci* **2020**, *528*, 146860. https://doi.org/10.1016/j.apsusc.2020.146860.

36. Chen, Y.; Liu, R.; Luo, J. Improvement of Anti-Aging Property of UV-Curable Coatings with Silica-Coated TiO2. *Prog Org Coat* **2023**, *179*, 107479. https://doi.org/10.1016/j.porgcoat.2023.107479.

37. Palliyaguru, L.; Kulathunga, U. S.; Jayarathna, L. I.; Jayaweera, C. D.; Jayaweera, P. M. A Simple and Novel Synthetic Route to Prepare Anatase TiO2 Nanopowders from Natural Ilmenite via the H3PO4/NH3 Process. *International Journal of Minerals, Metallurgy and Materials* **2020**, *27* (6), 846–855. https://doi.org/10.1007/s12613-020-2030-3.

38. Hatakeyama, T.; Okamoto, N. L.; Ichitsubo, T. Thermal Stability of MnO2 Polymorphs. *J Solid State Chem* **2022**, *305*, 122683. https://doi.org/10.1016/j.jssc.2021.122683.

39. Chabre, Y.; Pannetier, J. Structural and Electrochemical Properties of the Proton / γ-MnO2 System. *Progress in Solid State Chemistry* **1995**, *23* (1), 1–130. https://doi.org/10.1016/0079-6786(94)00005-2.

40. Wang, J.; Zhou, Y.; Lv, Y.; Feng, J.; Wang, Z.; Cai, G. A Reversible MnO_2 Deposition-Enabled Multicolor Electrochromic Device with Efficient Tunability

of Ultraviolet–Visible Light. *Small* **2024**, *20* (21). https://doi.org/10.1002/smll.202310229.

41. Ghosh, D.; Bhandari, S.; Khastgir, D. Synthesis of MnO_2 Nanoparticles and Their Effective Utilization as UV Protectors for Outdoor High Voltage Polymeric Insulators Used in Power Transmission Lines. *Physical Chemistry Chemical Physics* **2016**, *18* (48), 32876–32890. https://doi.org/10.1039/C6CP06611A.

42. Kim, C.-H.; Akase, Z.; Zhang, L.; Heuer, A. H.; Newman, A. E.; Hughes, P. J. The Structure and Ordering of ε-MnO2. *J Solid State Chem* **2006**, *179* (3), 753–774. https://doi.org/10.1016/j.jssc.2005.11.042.

43. Babitha, K. K. , S. A. , P. K. P. , S. B. , & V. T. Structural Characterization and Optical Studies of CeO 2 Nanoparticles Synthesized by Chemical Precipitation. **2015**.

44. Kumar, E. , S. P. , & B. K. Preparation and Studies of Cerium Dioxide (CeO2) Nanoparticles by Microwave-Assisted Solution Method. *Recent Research in Science and technology* **2010**.

45. Demir, M. M.; Koynov, K.; Akbey, Ü.; Bubeck, C.; Park, I.; Lieberwirth, I.; Wegner, G. Optical Properties of Composites of PMMA and Surface-Modified Zincite Nanoparticles. *Macromolecules* **2007**, *40* (4), 1089–1100. https://doi.org/10.1021/ma062184t.

46. Karabacak, S.; Qun, D. L. C.; Ammanath, G.; Yeasmin, S.; Yagmurcukardeş, M.; Alagappan, P.; Liedberg, B.; Yıldız, Ü. H. Polarity Induced Vapochromism and Vapoluminescence of Polythiophene Derivatives for Volatile Organic Compounds Classification. *Sens Actuators B Chem* **2023**, *389*, 133884. https://doi.org/10.1016/j.snb.2023.133884.

47. Ahmmad, S. K.; Samee, M. A.; Edukondalu, A.; Rahman, S. Physical and Optical Properties of Zinc Arsenic Tellurite Glasses. *Results in Physics* **2012**, *2*, 175-181. https://doi.org/10.1016/j.rinp.2012.10.002.